# STRUCTURAL FABRIC OF THE PALISADES MONOCLINE: A

# STUDY OF POSITIVE INVERSION, GRAND CANYON, ARIZONA

A Thesis

by

JAMES CORY OROFINO

Submitted to the Office of Graduate Studies of
Texas A&M University
in partial fulfillment of the requirements for the degree of

MASTER OF SCIENCE

May 2005

Major Subject: Geology

STRUCTURAL FABRIC OF THE PALISADES MONOCLINE: A

STUDY OF POSITIVE INVERSION, GRAND CANYON, ARIZONA


A Thesis

by

JAMES CORY OROFINO


Submitted to the Office of Graduate Studies of
Texas A&M University
in partial fulfillment of the requirements for the degree of

MASTER OF SCIENCE


Approved as to style and content by:


| _____ | _____ |
| Judith S. Chester | Brann Johnson |
| (Chair of Committee) | (Member) |
| | |
| _____ | _____ |
| William Sager | Rick Carlson |
| (Member) | (Head of Department) |


May 2005


Major Subject: Geology

ABSTRACT

Structural Fabric of the Palisades Monocline: A Study of

Positive Inversion, Grand Canyon, Arizona.

(May 2005)

James Cory Orofino, B.A., The Colorado College

Chair of Advisory Committee: Dr. Judith S. Chester

A field study of positive inversion is conducted to describe associated structural fabrics and to infer kinematic development of the Palisades Monocline, Grand Canyon, Arizona. These features are then compared to sand, clay and solid rock models of positive inversion to test model results and improve understanding of inversion processes. The N40W 90 oriented Palisades fault underlying the monocline has experienced northeast-southwest Precambrian extension and subsequent northeast-southwest Laramide contraction. The magnitude of inversion is estimated to be 25% based on vertical offset across the fault, although this does not account for flexure or horizontal shortening. The preferred N50W 90 joint and vein orientation and N50W 68 NE and SW conjugate normal faults are consistent with the Palisades fault and northeast-southwest extension. The N45E 90 joint orientation and approximately N40W 28 NE and SW conjugate thrust faults are consistent with northeast-southwest contraction. The deformation is characterized by three domains across the fault zone: 1) the hanging wall, 2) the footwall, and 3) an interior, fault-bounded zone between the hanging wall and footwall. Extensional features are preserved and dominate the hanging wall, contractional features define footwall deformation, and the interior, fault-bounded zone is marked by the co-existence of extensional and contractional features. Extension caused a master normal fault and hanging wall roll-over with distributed joints, veins

and normal faults.  During inversion, contraction induced reverse reactivation of existing hanging wall faults, footwall folding and footwall thrust-faulting.  Precambrian normal slip along the master normal fault and subsequent Laramide reverse slip along the new footwall bounding fault created an uplifted domain of relatively oldest strata between the hanging wall and footwall.  Physical models of co-axial inversion suggest consistent development of the three domains of deformation described at the Palisades fault, however the models often require magnitudes of inversion greater than 50%.  Although vertical block motion during horizontal compression is not predicted directly by the Mohr-Coulomb criterion, physical models and analytical solutions (incorporating Mohr-Coulomb criterion) suggest maximum stress trajectories and near vertical failure above high angle basement faults that compare favorably with the Palisades fault zone.

# ACKNOWLEDGEMENTS

vi

You withstood exhausting travel, arduous and painful hiking, short snowy days, long frigid nights, and too little time to do too much work. This thesis is a direct reflection of the work you did, the data you collected and recorded, the maps and sketches you made, and the thoughts and insights you provided. You deserve authorship more than acknowledgement. I thank you, and hope nature rewarded you with a moment from the Grand Canyon that you may keep forever.

Thank you to my Center for Tectonophysics colleagues: Pelin Cubik, Li Zhang, Jake Ramsey, Marty Finn, Pablo Cervantes, Nathan Davis, Mitchell Graff, Jessica Fallon, Jen Bobich, Erica Rodriguez, Taka Kanaya, Hiroko Kitajima, Steve Lenz, Clayton Powell, Evan Smith (honorary tectono member) and John Panian. You are the Pinnacle of Excellence, even if you never graduate on time, do not meet new department standards, and do not burn the midnight oil. I know your true spirit is represented by trips to Denver, Seattle, Big Bend, Guadalupe Mountains and to Dudley's. I know the pride you take in teaching and research, and that is reflected in the countless amount of help and discussions we have had with each other and all the (illegal) software we have shared. I know that a gray shirt, khaki shorts and white tennis shoes symbolize Tectonophysics. I know that without you, I would have skied a lot more, found a supported project, graduated sooner, and been less of a geologist, friend and person. Thank you.

# TABLE OF CONTENTS

# LIST OF TABLES

# LIST OF FIGURES

CHAPTER I

INTRODUCTION

**1. Introduction**

Positive inversion is the process of contracting a previously extended region. Positive inversion is associated with orogenic events around the world, including Laramide deformation and the Colorado Plateau. When the contraction direction during inversion is parallel to the preceding extension direction, the two phases of deformation are said to be co-axial. Depending on the magnitude of inversion, pressure and temperature conditions during deformation, and the mechanical properties of the deforming units, extensional features may be reactivated and/or overprinted during contraction. Positive, co-axial inversion may produce structures and geometries diagnostic of inversion, but may also produce structures that are indistinguishable from contraction-only or extension-only deformation (e.g. Koopman, 1987; McClay, 1995; Turner and Williams, 2004). Previous inversion studies (Koopman, 1987; McClay, 1995; Kuhle, 2001) warn against using the geometry of the reverse fault propagation fold and associated structures to identify inversion, as they may often resemble structures developed in other deformational settings.

Several physical models have investigated the kinematic development and deformation of co-axial, positive inversion using various materials and magnitudes of inversion (e.g. Koopman et al., 1987; Buchanan and McClay, 1991; Mitra, 1993; Eisenstadt and Withjack, 1995; McClay, 1995; Keller and McClay, 1995; Kuhle, 2001). Many physical models incorporate syn-extensional and syn-compressional deposition of sediment, which provide diagnostic wedge-shaped stratigraphic units to help identify inversion. Inversion has been recognized on basin-scale seismic profiles using wedged-shaped deposits (e.g. Lowell, 1995), but identification of inversion is more difficult

_____

This thesis follows the style and format of the Journal of Structural Geology.

when syn-tectonic deposits are not present, as often occurs in continental geologic settings (e.g. Holdsworth et al., 1997; Turner and Williams, 2004). While physical models provide valuable information about inversion processes, few detailed field studies of continental inversion have investigated diagnostic features of positive inversion (e.g. Nemcok et al., 1995; Dart et al., 1995).

Both physical models and basin-scale analysis suggest recognition of inversion is most favorable at intermediate or moderate magnitudes of inversion (e.g. Lowell, 1995), such as at the Palisades Monocline, Grand Canyon, Arizona (Fig. 1; e.g. Reches, 1978; Kuhle, 2001). Field studies in the Grand Canyon region document stratigraphic evidence for near co-axial, positive fault inversion (e.g. Walcott, 1889; Noble, 1914; Kelley, 1955a; Reches, 1978; Elston and McKee, 1982; Huntoon, 1993; 2003). The Precambrian Supergroup displays high angle, normal faults, but the overlying Paleozoic formations are deformed into contractional monocline folds (Fig. 2). The geometry and cross-cutting relations indicate initial normal faulting during and/or after Precambrian deposition, but prior to Paleozoic deposition and subsequent Laramide deformation. Recent studies suggest that the regional structural fabric developed during Precambrian accretionary events resulted in vertical zones of weakness (i.e. suture zones) that deeply penetrate the lithosphere (e.g. Bowring and Karlstrom, 1990; Marshak et al, 2000; Timmons et al, 2001). These weak zones may have developed into high angle normal faults during Proterozoic extension, and subsequently reactivated as reverse faults during phases of horizontal compression (e.g. Kelley, 1955a; Reches, 1978, Huntoon, 1993).

This thesis describes the structural fabric and kinematic interpretation of a natural inversion structure, the Palisades Monocline, Grand Canyon, Arizona (Fig. 1; Reches, 1978). Specifically, the mesoscopic structure and fabric are compared with physical model predictions in an effort to increase our understanding of the geometry and kinematics of inversion and improve identification of inversion in poorly constrained regions.

3
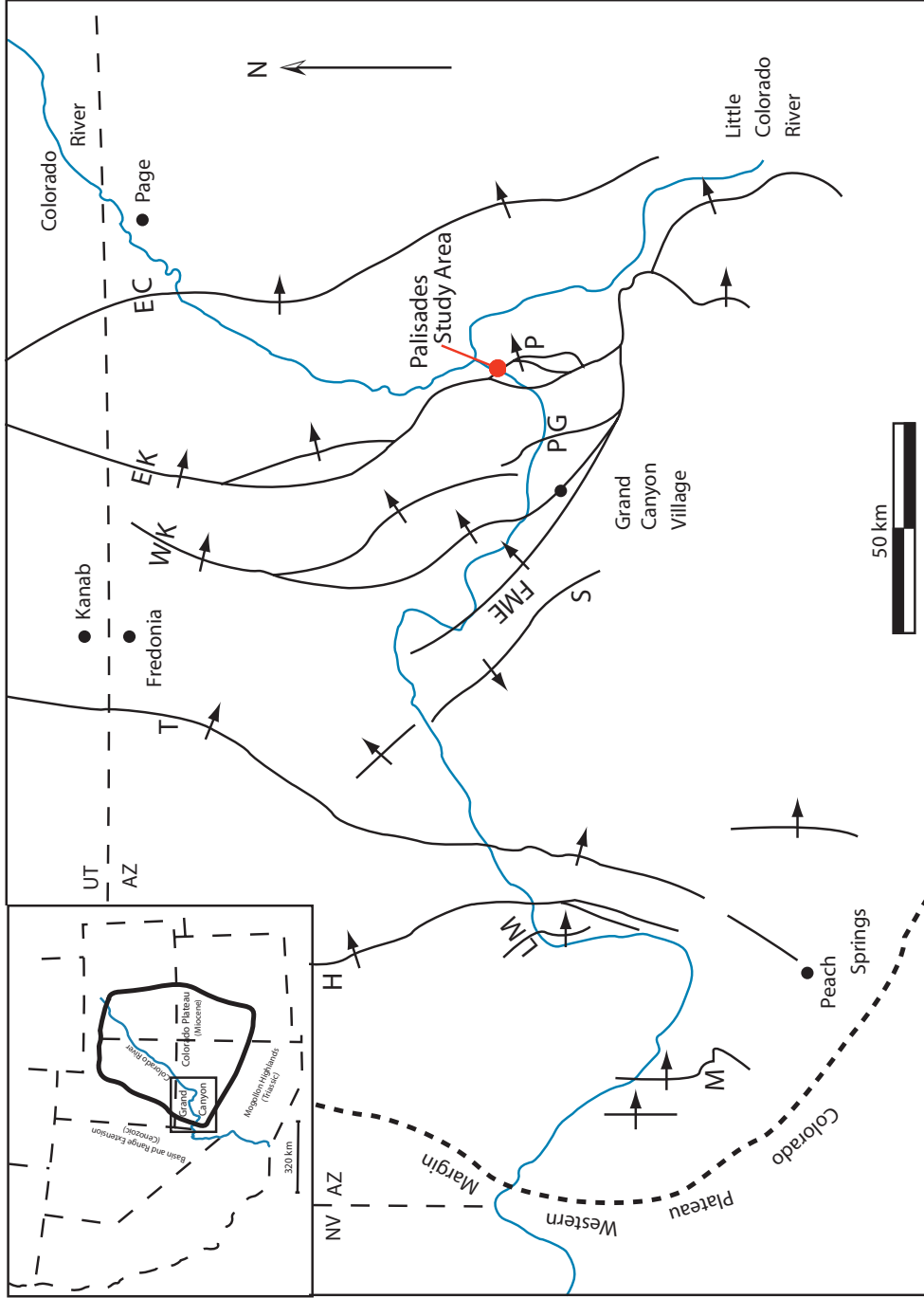


Fig. 1. Regional map of Grand Canyon monoclines. Inset is regional map of the western U. S., Colorado Plateau and Colorado River. Study area is the Palisades monocline (P), a branch of the East Kaibab (EK) monocline. Other monoclines shown are Meriwhitica (M), Lone Mountain (LM), Hurricane (H), Toroweap (T), Aubrey (A), Supai (S), Fossil-Monument-Eremita (FME), West Kaibab (WK), Phantom-Grandview (PG), East Kaibab (EK), Echo Cliffs (EC) (after Huntoon, 2003).
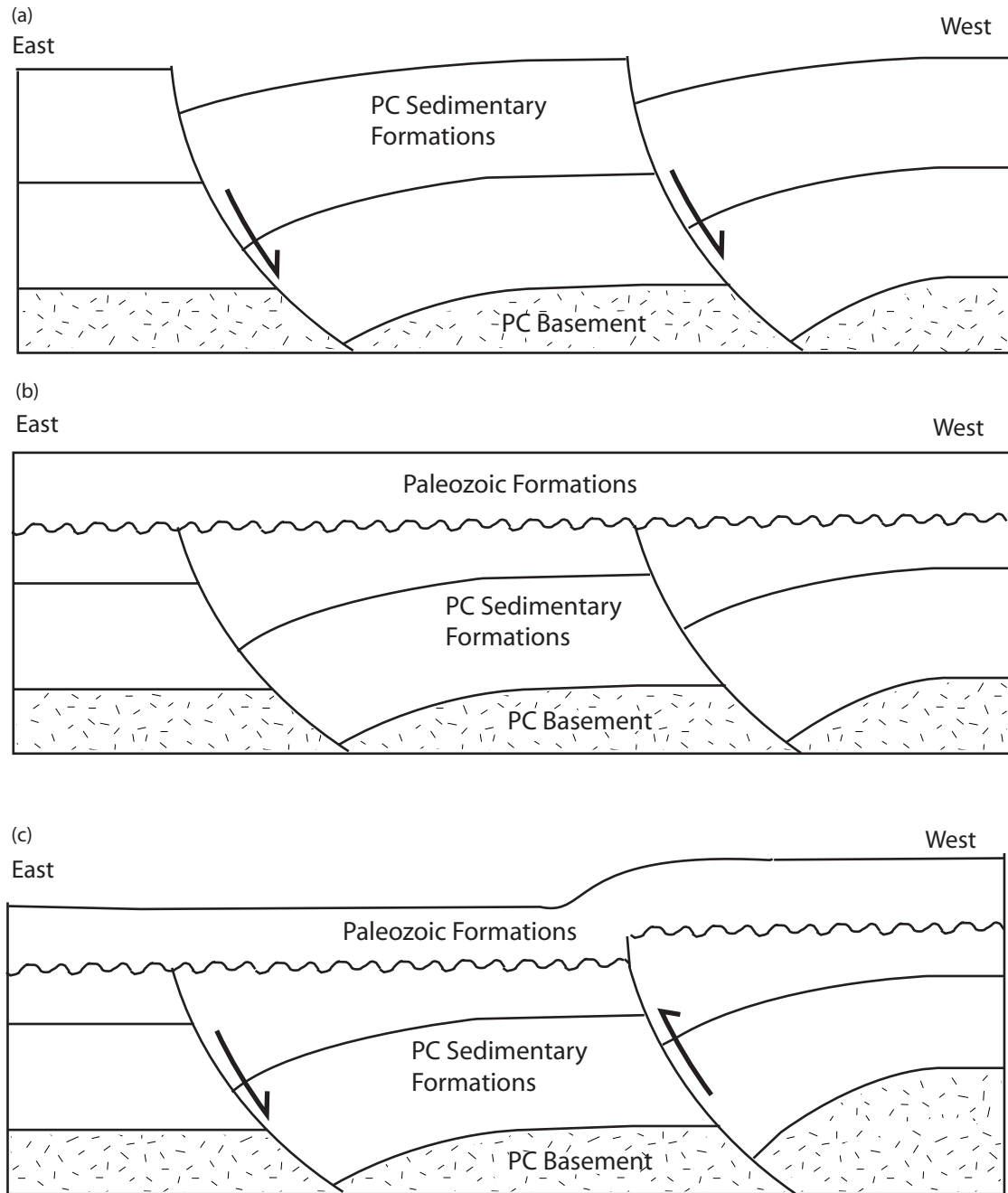
Fig. 2.  General structure and development of Grand Canyon monoclines. (a) Precambrian normal faulting offsets basement and Precambrian formations; (b) erosion of Precambrian formations followed by deposition of Paleozoic and subsequent formations; and (c) reverse reactivation of basement faults causing monocline flexure in Paleozoic formations but Precambrian formations display net normal offset. Note the curvature of faults is not to scale and the view is to the south to correspond with the outcrop exposure of this study (after Huntoon, 1993; 2003).

## 2. Implications of Physical Models of Positive Inversion

There are many published, physical models of positive inversion with different experimental apparatuses, different boundary conditions, and different model materials all with different mechanical properties (e.g. Koopman et al., 1987; Buchanan and McClay, 1991; Mitra and Islam, 1994; Eisenstadt and Withjack, 1995; McClay, 1995; Keller and McClay, 1995; Kuhle, 2001).

The rigid footwall, sandbox studies (e.g. Buchanan and McClay, 1991; Keller and McClay, 1995) provide useful insight into hanging wall deformation and faulting processes, as the cohesionless sand and mica layers do not allow for ductile deformation (Fig. 3). These models suggest reverse reactivation of high angle normal faults is plausible, and existing, weak planar features, such as bedding, can be activated as reverse faults if well oriented for shear during contraction.

Clay models (e.g. Eisenstadt and Withjack, 1995; Mitra, 1993; Mitra and Islam, 1991) allow for investigation of ductile deformation and the effects of layer cohesion in both the hanging wall and footwall. The clay models display isolated extensional faulting and deformation in the hanging wall and indicate reverse reactivation of hanging wall faults during contraction (Fig. 4). Additional contractional deformation includes formation of a footwall syncline, footwall-vergent thrusting and the formation of an up-thrusting wedge between the hanging wall and footwall. The relative timing and orientation of faulting with respect to folding determines if rotation of existing faults will allow for reactivation. The fault-fold timing relationship is particularly important within the footwall during contraction when both mechanisms are likely to occur.

Solid rock material may be deformed at confining pressure to investigate the effect of burial depth and lithostatic overburden during both initial extension and subsequent contraction. Solid rock experiments are most suitable for investigation of brittle faulting, fracture development and the dip angle of opening mode microfractures that may be used to interpret stress trajectories (Figs. 5 and 6; Kuhle, 2001). Extensional strain is accommodated through normal slip along a single, narrow zone of cataclasis

6
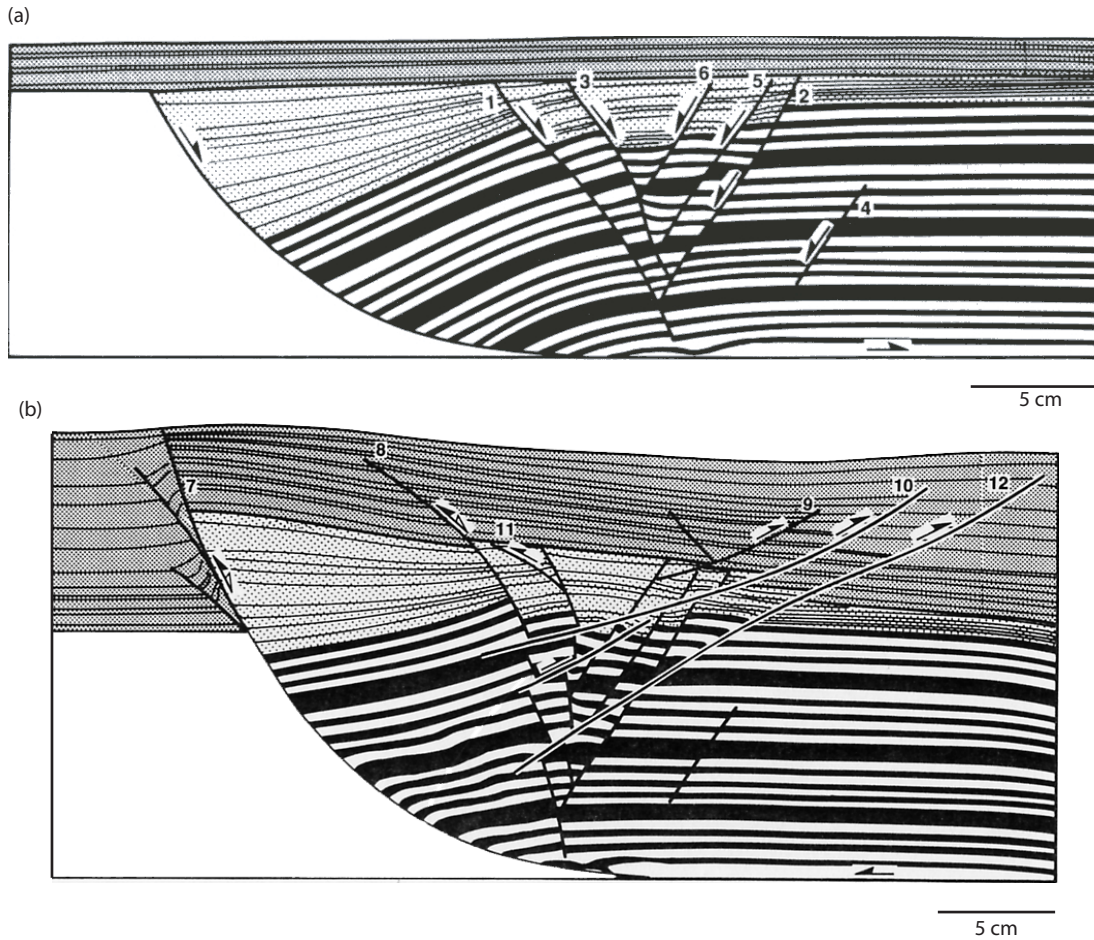


Fig. 3. Line drawing interpretation of a sandbox model of positive inversion. (a) Post-extension geometry (35% extension) with syn-extension and post-extension deposition. Faults are labeled in sequential formation. (b) Post-contraction geometry (30% shortening) causes reverse reactivation of master slip surface and existing normal faults, followed by low-angle back-thrusts which offset existing normal faults. Model from Buchanan and McClay (1991) and incorporates a rigid footwall and 60$^o$ listric fault surface.
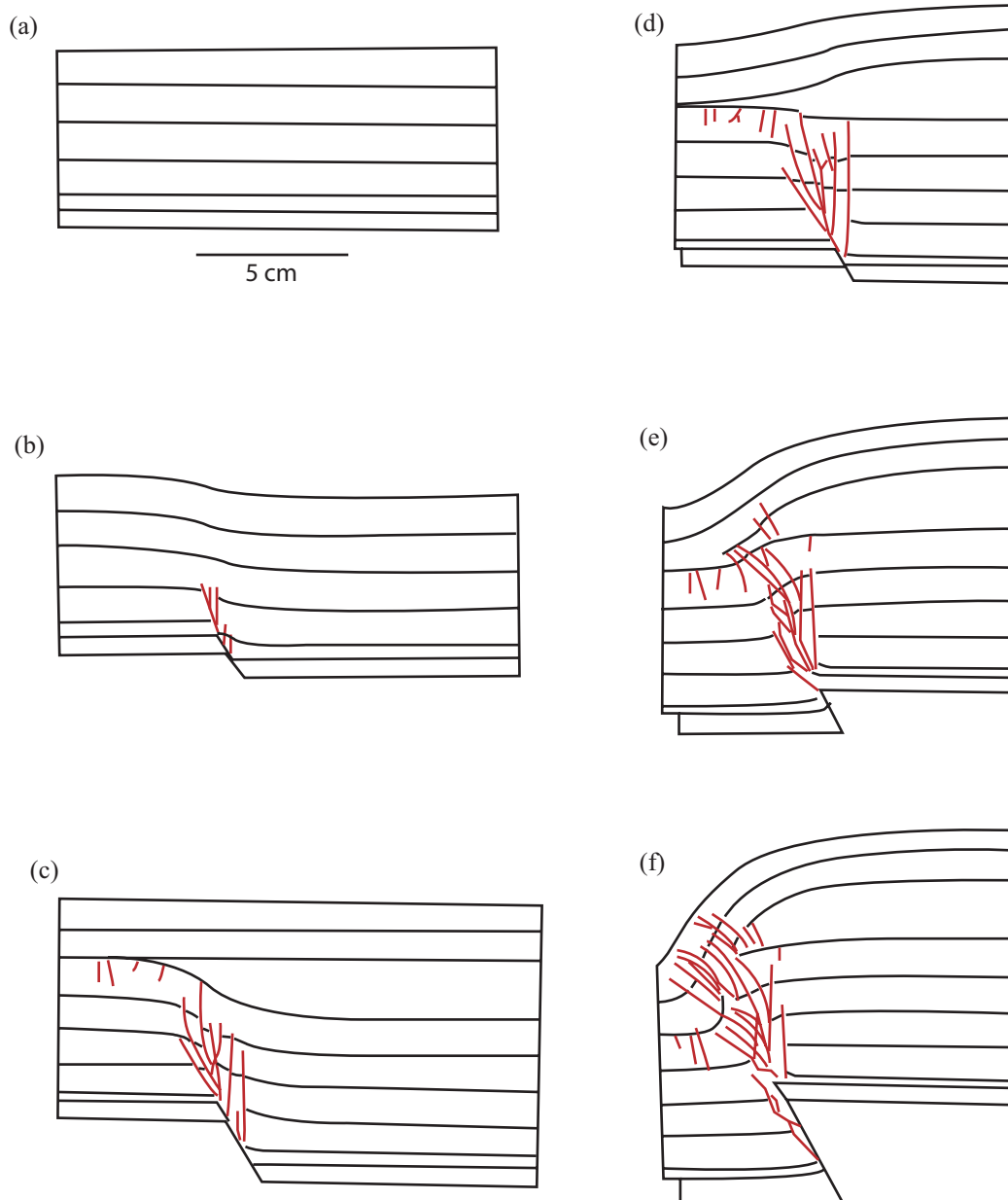
Fig. 4. Line drawing interpretation of clay layers above a planar fault. (a) Initial, undeformed model. (b) Deformation after 0.5 cm extension. (c) Deformation after 1 cm extension and syn-extensional and post-extensional depositional units. (d), (e) and (f) Deformation after 1, 2, and 3 cm of contraction. Forcing fault dips at $60^{o}$, and red lines indicate faults (after Mitra, 1993).

(master fault), but there are also sub-vertical microfractures evenly distributed throughout the hanging wall and footwall. During the contraction phase there is initial reverse-reactivation and upward widening of the master fault zone, followed by synthetic footwall reverse faulting and the development of an uplifted footwall wedge in the fault zone. Contraction also increases sub-vertical microfracture intensity in the hanging wall and super-imposes low angle, synthetic microfractures over the existing extensional, sub-vertical microfractures.

The physical models of inversion suggest common deformation features and kinematic development independent of the material properties and deformation conditions of the models: 1) extensional deformation is constrained to the hanging wall and contractional deformation is most intense in the footwall; 2) high angle faults will be reactivated in a reverse sense during horizontal contraction; 3) contractional folding may rotate existing planar features (e.g. bedding and faults) into an orientation that allows for reactivation as reverse faults; 4) formation of an uplifted wedge in the fault zone that is bounded by normal displacement against the hanging wall and reverse displacement against the footwall. The results of these models are to be compared with the structural fabric of the Palisades Monocline, and to help interpret the kinematic development of the monocline and underlying fault. Structural features with kinematic development found in both the physical models and at the Palisades Monocline may be used to help identify positive inversion in unconstrained tectonic settings.
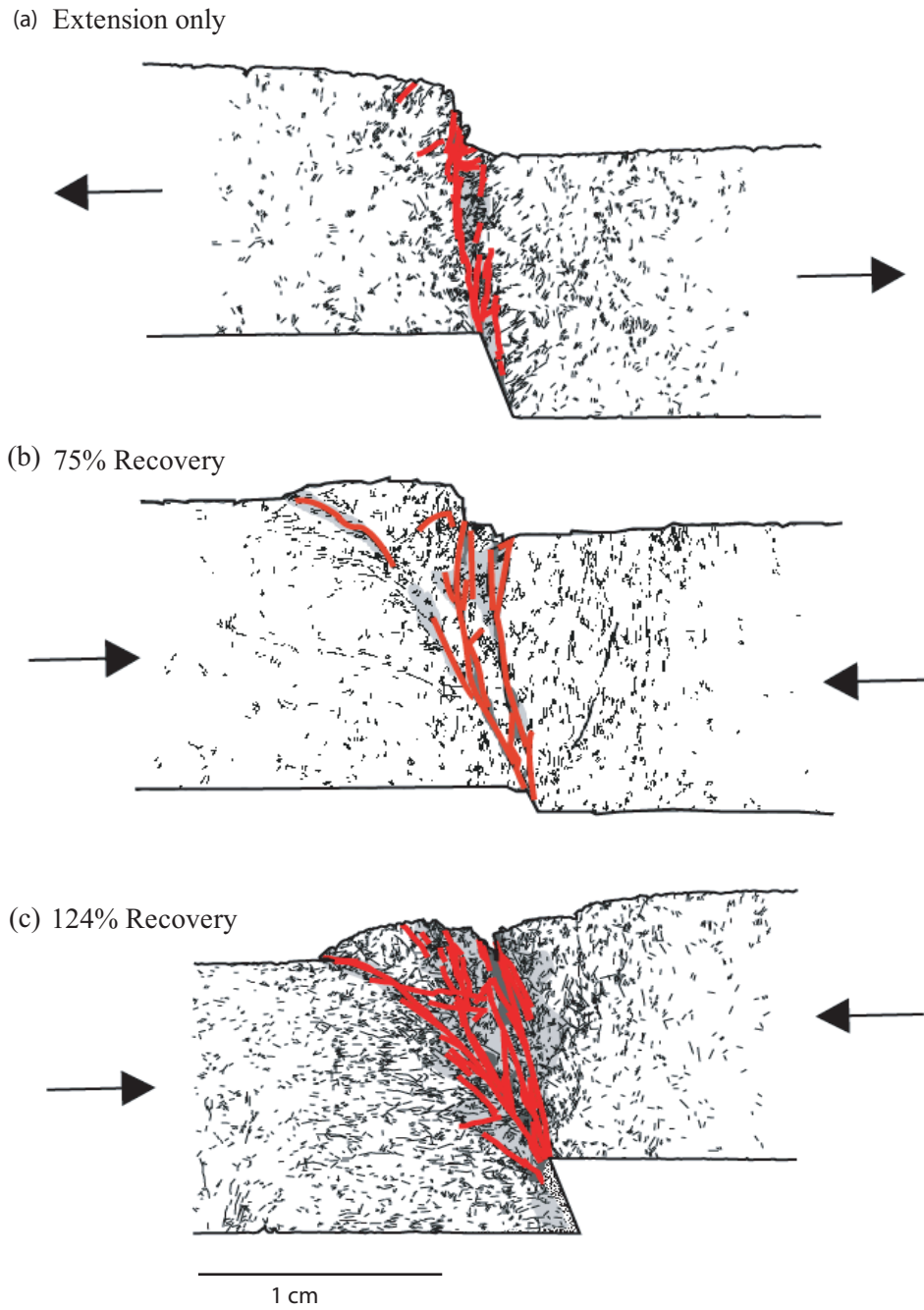
Fig. 5. Digitized photomicrographs of solid rock model experiments of positive inversion deformed at confining pressure. (a) Post-extension at 100 MPa. (b) 75% inversion at 25 Mpa. (c) 124% inversion at 25 MPa. Red lines indicate faults (after Kuhle, 2001).

|  | Footwall | Fault zone | Hanging wall |
|---|---|---|---|



Extension Only — Footwall: 408 Pts; Fault zone: Non-existent; Hanging wall: 311 Pts

38% Inversion — Footwall: 403 Pts; Fault zone: Non-existent; Hanging wall: 287 Pts

113% Inversion — Footwall: 696 Pts; Fault zone: 360 Pts; Hanging wall: 699 Pts

Contraction Only — Footwall: 288 Pts; Fault zone: Non-existent; Hanging wall: 291 Pts
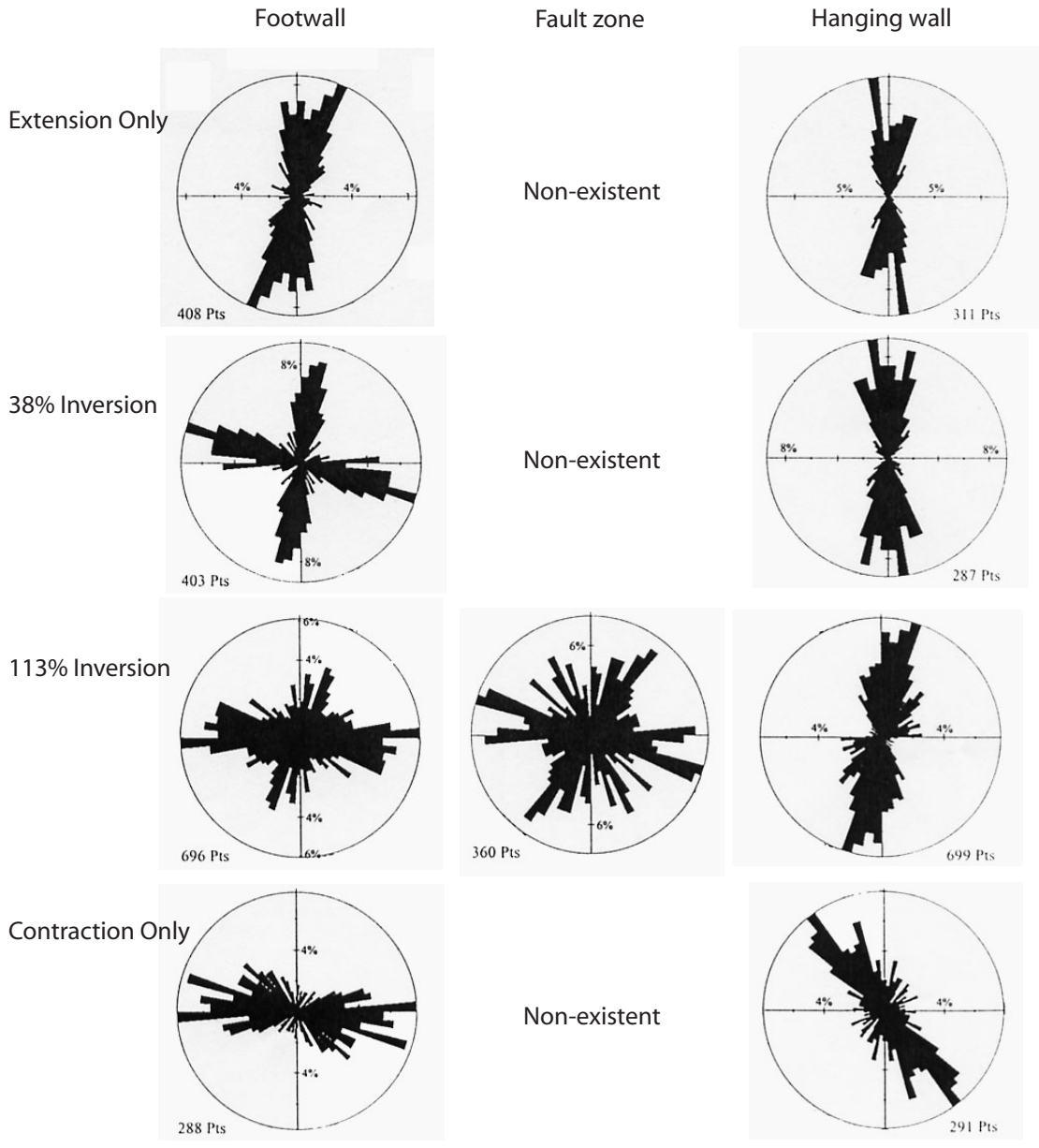
Fig. 6.  Rose diagrams of microfracture dip angles for solid rock models inversion experiments deformed at confining pressure. 100 MPa confining pressure used during extension and 25 MPa confining pressure during contraction (after Kuhle, 2001).

CHAPTER II

GEOLOGY OF THE GRAND CANYON REGION AND THE

PALISADES MONOCLINE

**1. Regional Tectonic History**

The deeply eroded Grand Canyon of Arizona provides rare exposure of deformed Precambrian and Phanerozoic rocks associated with deep-seated structures within the crust. Many early studies of the Grand Canyon region recognized multiple episodes of deformation, and the importance of Precambrian faults that controlled subsequent deformation (e.g. Powell, 1873; Gilbert; 1876; Dutton, 1882; Walcott, 1889; Noble, 1914; Maxson and Campbell, 1933). Walcott (1889) was the first to describe Precambrian faults with opposite senses of displacement in the Precambrian and Phanerozoic epochs. Noble (1914) documented other post-Paleozoic faulting events that occurred along Precambrian faults and had generally smaller and opposite displacements than the Precambrian faults they reactivated. Maxson and Campbell (1933) described faults with multiple episodes of activity within Precambrian time. More recently, the network of Precambrian basement faults and associated unconformities along with eustatically driven disconformities has been examined and re-examined by a host of researchers (e.g. Kelly, 1955a; Sears, 1973; Reches, 1978; Davis 1978; Shoemaker et al., 1974; Huntoon, 1981; 1993; 2003; Elston and McKee, 1982; Timmons et al., 2001; 2003 Karlstrom et al., 2003).

*1.1 Precambrian Tectonics*

The crystalline basement Proterozoic rocks of the Grand Canyon (e.g. Granite Gorge Metamorphic Suite, Vishnu Schist, Brama Schist) reveal a long history of crust formation, continental accretion, deformation, metamorphism and reactivation of crustal suture zones. These basement rocks formed along volcanic arcs from 1.84 to 1.71 b.y.

and collided and accreted onto the North American continent between 1.74 to 1.68 b.y. (Karlstrom et al., 2003).  The accretionary sutures may represent vertical zones of weakness that penetrate deep into the lithosphere, controlling and localizing subsequent deformation (e.g. Bowring and Karlstrom, 1990; Marshak et al., 2000; Timmons et al., 2001).  Many of these basement structures have been reactivated multiple times throughout Precambrian contraction and extension, Laramide contraction, and Cenozoic extension (e.g. Noble, 1914; Maxson and Campbell, 1933; Shoemaker et al., 1974; Huntoon, 1993; 2003).

At 1.4 b.y., possible magmatism drove uplift and erosion of about 10 km of crust, creating the nonconformable surface upon which Proterozoic and Phanerozoic sediments were deposited (Karlstrom et al., 2003).  In the eastern Grand Canyon, tilted middle and late Proterozoic formations overly the basement, and most commonly outcrop in the hanging wall of Precambrian normal faults.  The middle and late Proterozoic records a minimum of 5 km of sediment deposition on top of the basement, but the absolute thickness is unknown due to pre-Paleozoic erosion.  The Precambrian sedimentary formations are collectively known as the Grand Canyon Supergroup, which includes the basal Unkar Group (1.4-1.1 b.y.), Nankoweap Formation (1.0 b.y.), Chuar Group (0.8-0.7 b.y.) and Sixtymile Formation (0.7 b.y.), each separated by unconformities (Fig. 7).

The Supergroup records Precambrian tectonic events from 1.4 b.y. to 700 m.y., which were associated with the formation and break up of the supercontinent Rodinia (Fig. 8).  These events include northwest-directed, Grenville contraction (1.2-1.1 b.y.) and concurrent magmatism (1.1 b.y.), followed by general east-west extension during break-up of Rodinia.  Northwest Grenville contraction was concurrent with northeast extension as identified by syn-depositional faulting of northeast trending reverse faults (Grenville) and northwest trending normal faults in the Unkar Group (Timmons et al., 2001; Karlstrom et al., 2003).  It is suggested that the northeast extension and northwest trending normal faults resulted from far field extension and failed 1.1 b.y. rifting of Rodinia to the east, which may have been initiated by the Grenville collision (Karlstrom
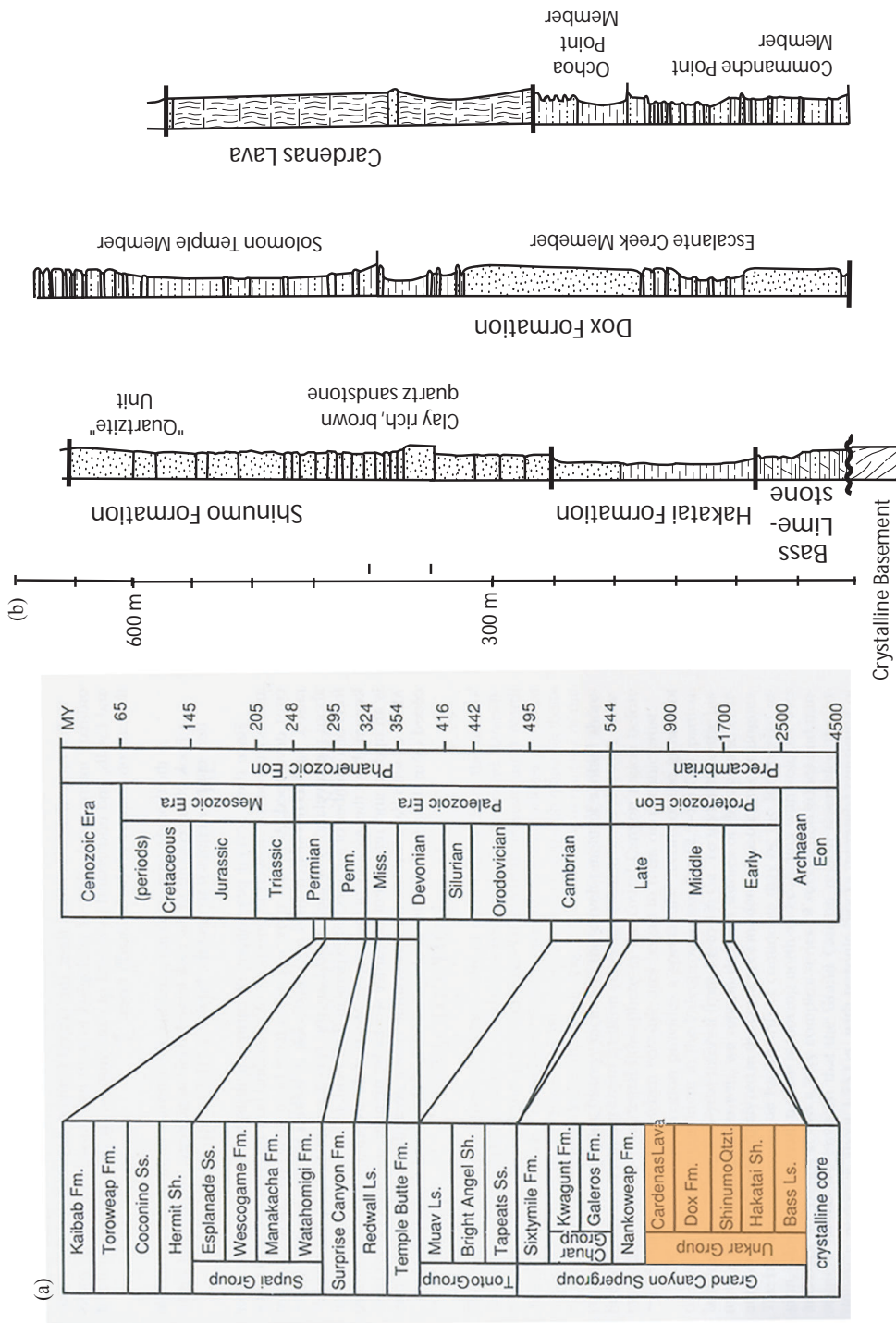
Fig. 7. Geologic column of the Grand Canyon and stratigraphic section of the Unkar Group. (a) Complete geologic column of the Grand Canyon and associated ages (from Bues and Morales, 2003). Units found within the study area include the Shinumo Quartzite, Dox Formation, Cardenas Lava, Tapeats Sandstone and Bright Angle Shale. There is no occurence of the Nankoweap through Sixtymile Formations in the study area. (b) Stratigraphic section of the Shinumo Quartzite, Dox Formation and Cardenas Lava exposed across the Palisades Fault (after Hendricks and Stevenson, 2003).
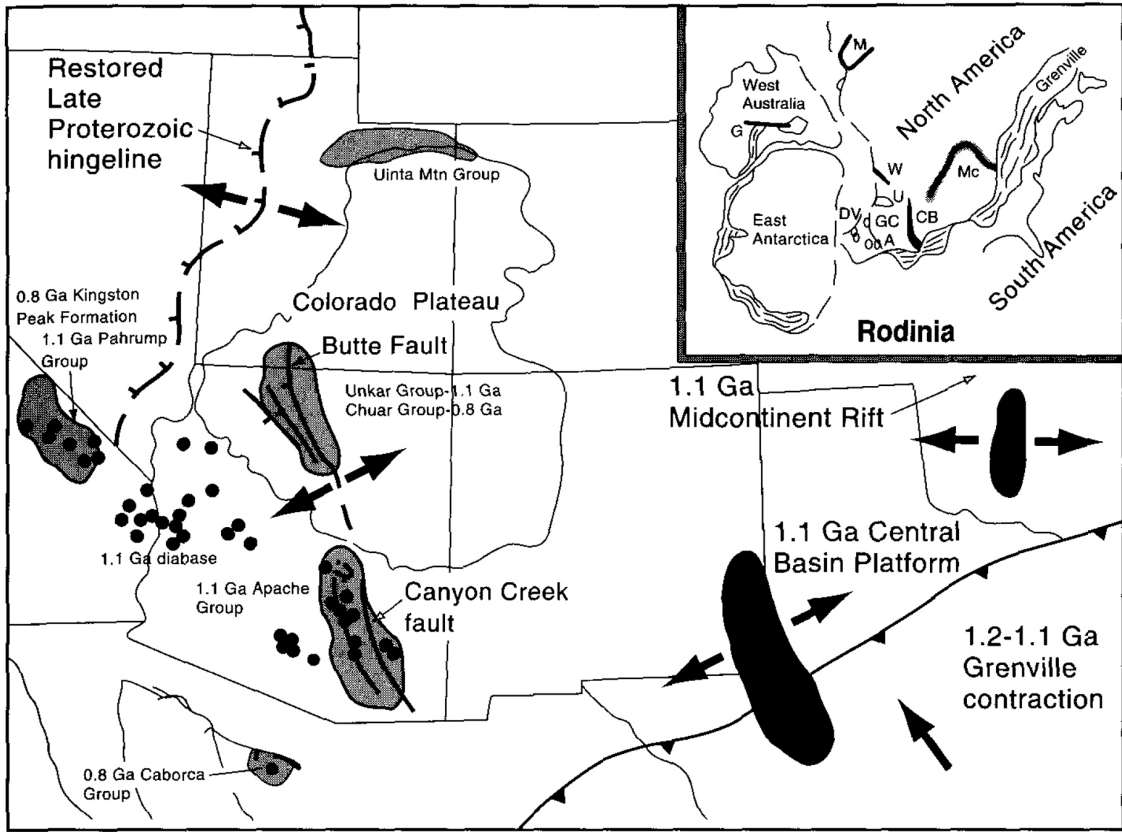
Fig. 8. Regional map of the Precambrian tectonic setting of the southwestern U. S. Intrusive bodies suggest two extensional events: 1.1 and 0.8 billion years ago (from Timmons et al., 2003).

et al., 2003).  Timmons et al. (2003) suggest a second distinct phase of extension during Chuar Group deposition at 0.8 b.y.  This phase is characterized as east-west extension with north-south normal faults displaying syn-faulting deposition in the Chuar Group. This extension phase is related to successful rifting of Rodinia initiated at 0.8 b.y. with continental separation somewhere between 700 to 550 m.y. (Karlstrom et al., 2003, and references therein).  The Precambrian extension and normal faulting tilted and offset Supergroup formations, which were then beveled by pre-Paleozoic erosion (Great Unconformity).  Due to Precambrian normal faulting, the Great Unconformity surface is much lower stratigraphically in the footwall than the hanging wall.  In many cases, the only outcrops of the Supergroup can be found in the tilted and down-dropped blocks of the hanging wall.  In the Palisades area, erosion has removed 2100 m of Sixtymile, Chuar and Nankoweap Formations prior to Phanerozoic deposition and deformation (Fig. 7).

*1.2 Phanerozoic Tectonics*

The Phanerozoic history of the Grand Canyon region includes 3000 m of sediment deposition, three regional tectonic events, 3 km of both regional subsidence and uplift, and over 3 km of lateral plate movement (e.g. Dutton, 1882; Noble 1914; Kelley, 1955b; Lucchitta, 1974; Middleton and Elliot, 2003; Huntoon, 2003). Throughout this Phanerozoic tectonic history, deformation has been limited to the margins of the craton and has not developed through-going failures within the interior of the craton.  Presently, there are just over 1200 m of overlying Paleozoic strata beginning with Cambrian Tapeats overlying the Great Unconformity erosional surface and ending with Permian Kaibab limestone outcropping along the rim of the canyon (Fig. 7).  The regionally extensive, but slightly discontinuous, rock record documents marginal marine depositional environments, and only minor epeirogenic unconformities during Paleozoic time.

Although much of the 1200 m of Mesozoic rock record of the Colorado Plateau is missing in the Grand Canyon region, the regional stratigraphic record indicates transgression-regression cycles followed by emergence and regional uplift of the Mogollon Highlands to the south and eastward Sevier thrusting to the north (e.g. Armstrong, 1968; Allmendinger and Jordan, 1981; Huntoon, 2003). The deformation was in response to subduction of the Pacific Ocean crust and accretionary events along the western margin of North America and opening of Atlantic Ocean along its eastern margin, but minimal deformation is recorded in the Paleozoic sequences of the Grand Canyon (Huntoon, 2003).

Late Cenozoic through Eocene Laramide orogenesis resulted from eastward (inward) propagation of Cordilleran margin deformation, causing widespread uplift of the Colorado Plateau (e.g. Dickinson, 1981). Laramide deformation is characterized by basement-controlled, east-verging reverse faults and folding of the overlying strata. In the western Colorado Plateau, the folds are typically monoclines (e.g. Kelly, 1955a; Davis, 1978; Anderson and Barnhard, 1986), as opposed to the anticline structures common in Wyoming (e.g. Stearns, 1978; Brown, 1993; Stone, 1993). Although near-surface fault movement was nearly vertical, the causative stress regime for Colorado Plateau and Grand Canyon monoclines involved a horizontal, northeast maximum compressive stress, often inferred from second order folds and conjugate faults, calcite twinning, kink bands and non-basement controlled monoclines (Reches, 1978; Huntoon, 1981; 1993; Anderson and Barnhard, 1986). Anderson and Barnhard (1986) determined a horizontal, N65E Laramide contraction axis for the major monoclines of the western Colorado Plateau. In many cases, monoclines are located over reactivated basement faults originally formed during Precambrian extension (e.g. Reches, 1978; Huntoon, 1993). Davis (1978) reports that total crustal shortening was less than one percent across the region, as a result of the large spacing between monoclines and the mostly vertical movement along high angle faults. The total stratigraphic thickness above the Great

Unconformity is unknown during Laramide deformation, but is estimated at over 3000 m assuming the presence of regional Mesozoic sediments (Huntoon, 2003).

The final phase of regional deformation includes late Cenozoic extension and volcanism associated with the Basin and Range province, resulting from subduction of Farallon-Pacific plate spreading ridge (e.g. Dickinson, 1981). Due to limited Cenozoic exposure in the Colorado Plateau, the timing of normal faulting is difficult to determine, but it appears that faulting is currently migrating eastward through the Grand Canyon and into the western Colorado Plateau (e.g. Sears, 1973; Shoemaker et al., 1974; Huntoon, 2003). Much as Laramide contraction led to reactivation of existing Precambrian faults, Cenozoic normal faulting often occured along the same Precambrian faults and offset the overlying, folded Paleozoic units. Cenozoic extension has not reactivated all Laramide structures, leaving some structures, such as the Palisades Monocline, as they were at the end of Laramide deformation (Reches, 1978; Huntoon, 2003).

## 2. Palisades Monocline

*2.1 Stratigraphic Section and Lithologic Description*

The Grand Canyon Supergroup is composed of Precambrian sedimentary formations that are found only in isolated wedges of sediment associated with Precambrian normal faults, and are exposed mostly in the eastern Grand Canyon (Fig. 7). These formations are easily recognized by their slope-forming character, their angular unconformable relations with overlying, horizontal Paleozoic formations in the canyon walls, and their contrasting dark red, brown, gray and purple colors. The Supergroup is subdivided into the basal Unkar Group, Nankoweap Formation and Chuar Group, each separated by disconformities. Due to late Precambrian erosion (Great Unconformity), neither the Nankoweap Formation nor the Chuar Group is found at the Palisades Monocline.

The Unkar formations are the oldest sedimentary units in the Grand Canyon region, and are unconformably deposited on 2.2 to 1.65 b.y. crystalline basement rocks (e.g. Granite Gorge Metamorphic Suite; Fig. 7). The Unkar group ranges in age from 1.25 to 1.07 b.y. with reported sedimentary thicknesses from 1525 to 1768 m, and an additional 300 m of basaltic lava overlying the sedimentary formations (Hendricks and Stevenson, 2003; Stevenson and Beus, 1982). The depositional environment was a marine basin along the southwestern edge of the North American craton, which records multiple transgression and regression episodes (Hendricks and Stevenson, 2003). The sequence is divided into four conformable sedimentary formations: Bass limestone, Hakatai shale, Shinumo Formation and Dox Formation, all of which are conformably overlain by the Cardenas lava and subsequently intruded by 800 m.y. diabase sills and dikes.

Formations exposed and mapped across the underlying basement fault of the Palisades Monocline are Shinumo Formation, Dox Formation, Cardenas lava, diabase intrusions and Tapeats sandstone (Fig. 9; Reches, 1978; Stevenson and Beus, 1982). The Precambrian-Paleozoic Great Unconformity occurs near the top of the Cardenas lava in the hangingwall, and in the lower Dox Formation in the footwall (Fig. 10). On both sides, the Cambrian Tapeats sandstone overlies the Precambrian formations. Paleozoic formations above the Tapeats sandstone were not mapped in this study because all Paleozoic formations post-date Precambrian deformation.

The Shinumo Formation is a massive, cliff forming series of sandstones and quartzites with a thickness in the eastern Grand Canyon of 345 m, which increases to 405 m towards the west (Hendricks and Stevenson, 2003). The Shinumo ranges in color from muted reds, browns and purples to white. Four (Hendricks and Stevenson, 2003) or five (Elston, 1989) members are defined: a basal conglomerate and submature sandstone, mature quartz sandstone (subdivided into two units by Elston (1989)), brown quartz sandstone with cross-bedding, clay galls and mudcracks, and a fine grained, well-sorted, rounded quartz sandstone with siliceous cement (i.e. the "quartzite"). The top
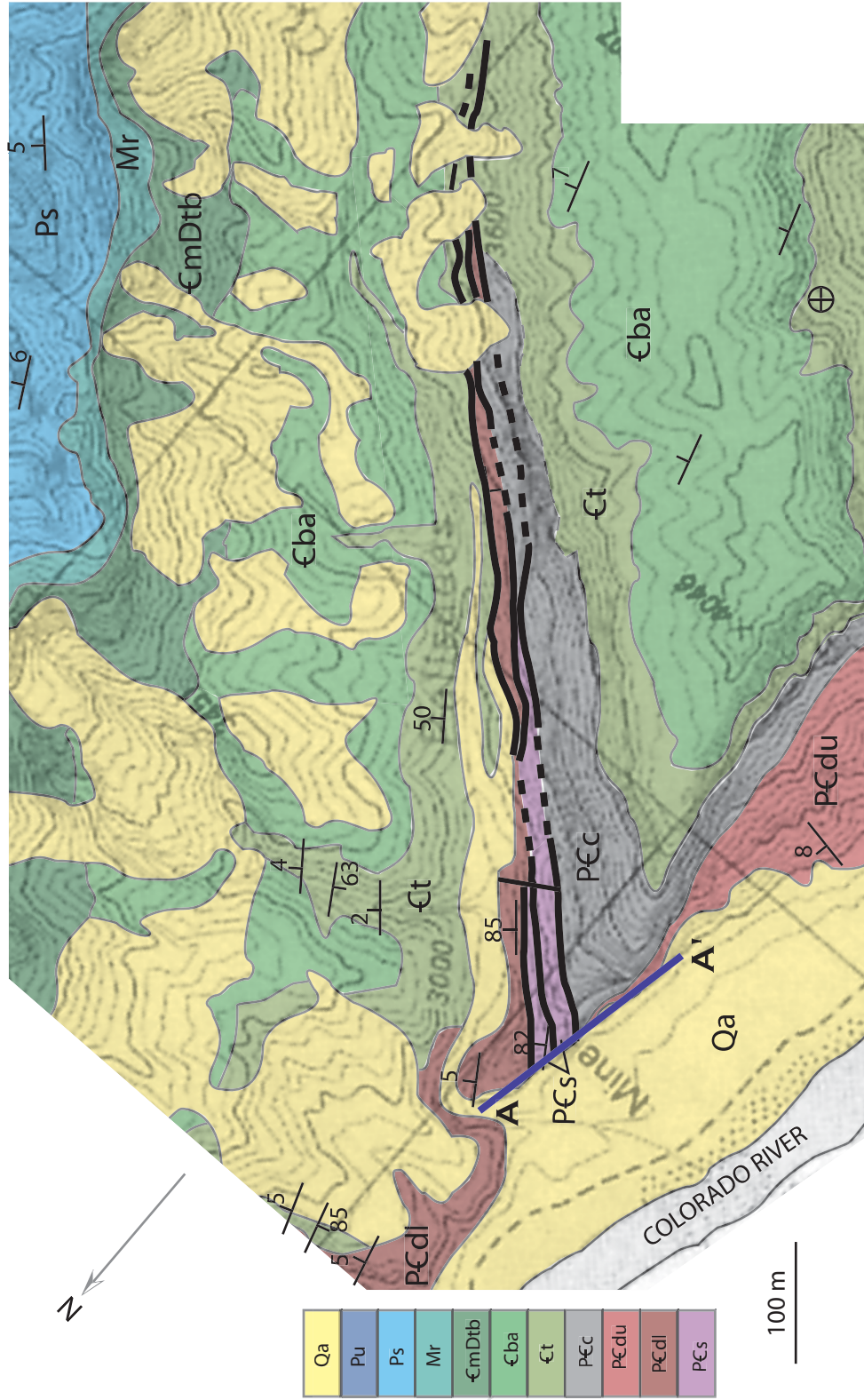
Fig. 9. Geological map with elevation contours of Palisades Creek canyon and monocline. Line A-A' is location of vertical outcrop exposure of underlying Palisades fault (after Reches, 1978). Formations: Shinumo (PCs), lower Dox (PCdl), upper Dox (PCdu), Cardenas Lava (PCc), Tapeats (Ct), Bright Angel (Cba), undifferentiated Muav and Temple Butte (CmDtb), Redwall (Mr), Supai (Ps), undifferentiated Hermit, Coconino, Toroweap and Kaibab (Pu), and alluvium (Qa).
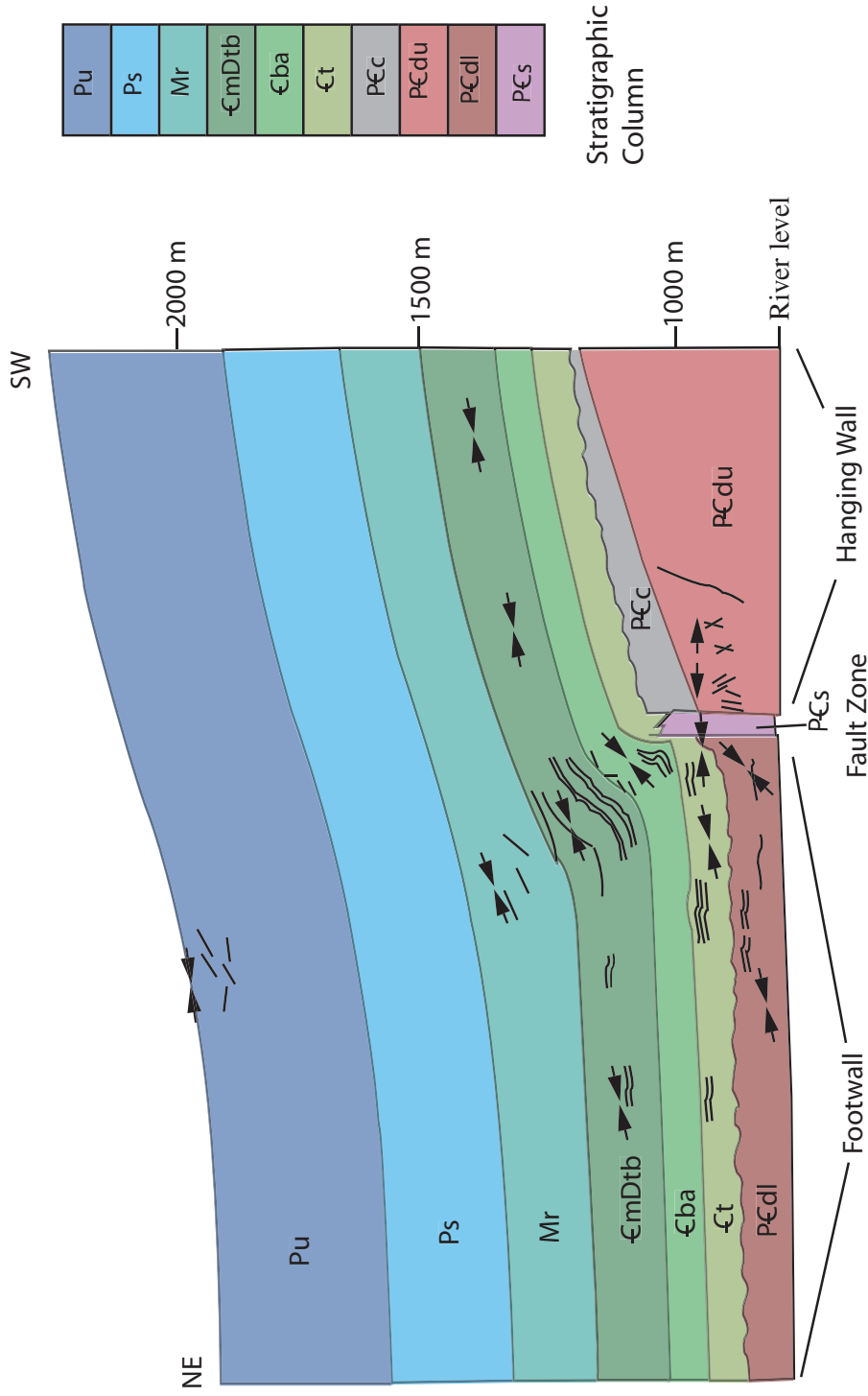
Fig. 10. Projected vertical cross-section across the Palisades Monocline. Vertical plane projection of the Palisades Monocline above outcropping Precambrian formations from Paleozoic exposures in the canyon walls without vertical exaggeration. The Precambrian formations display normal offset across the fault, while the overlying, folded, Paleozoic formations display reverse movement along the fault. The view is to the south, which is consistent with outcrop exposure. River level is at the base of the projection. Formations: Shinumo (PCs), lower Dox (PCdl), upper Dox (PCdu), Cardenas Lava (Cba), Bright Angel (Cba), undifferentiated Muav and Temple Butte (CmDtb), Redwall (Mr), Supai (Ps), undifferentiated Hermit, Coconino, Toroweap and Kaibab (Pu) (after Reches, 1978).

"quartzite" unit often has purple-speckles (reduction spots), and may include fluid evulsion or soft sediment deformation such as flame or dish and pillar structures (Elston, 1989). The depositional environment was a near shore, shallow, marginal marine setting with pulses of deltaic and fluvial sedimentation (Hendricks and Stevenson, 2003).

The Dox Formation is the thickest unit of the Unkar group at 920 to 984 m thick with complete exposure in eastern Grand Canyon (Hendricks and Stevenson, 2003; Stevenson and Beus, 1982). Four members of the Dox Formation are identified based mostly upon topographic and outcrop exression: 1) the Escalante Creek member is a 390 m thick, tan to brown, lithic and arkosic sandstone with a 122 m sequence of brown, purple and green shales and mudstones; 2) the Solomon Temple member is a 280 m thick, prominent slope forming red mudstone and sandstone with channel deposits; 3) the Commanche Point member is a 129 to 188 m thick, dominant slope forming mudstone and argillaceous siltstone with mudcracks, ripple marks and stromatolite layer; and 4) the Ochoa Point member is a 53 to 91 m thick, steep slope forming, red-brown mudstone that rarely exhibits bedding (Stevenson and Beus, 1982; Hendricks and Stevenson, 2003). The lower two members are referred to as the lower Dox Formation, and the top two members as the upper Dox Formation. The Dox Formation was deposited in a slowly filling, sub-aqueous delta that remained near the marine to sub-aerial transition, and included tidal flat and floodplain environments (Hendricks and Stevenson, 2003).

The Cardenas lava is a 239 to 305 m thick series of potassium-rich basaltic flows with sandstone interbeds (Hendricks, 1989; Hendricks and Stevenson, 2003). The Cardenas depositional thickness is unknown because the upper contact with the Nankoweap Formation is a Precambrian disconformity. In the Palisades study area (Figs. 1 and 9), the Cardenas lava is about 300 m thick and the Precambrian-Paleozoic Great Angular Unconformity erosional surface defines the upper contact with Paleozoic Tapeats sandstone (Reches, 1978). The basal contact with the Dox Formation is conformable and inter-fingering. Two members are indentified and separated by a 5 m

thick sandstone layer.  The lower "bottle green member" forms slopes relative to the upper cliff-forming unit.  The basal flows were deposited into a marine environment, and later flows were deposited sub aerially.  For detailed flow stratigraphy of the Cardenas lava, see Hendricks (1989).

There are diabase sills and dykes that intrude all Unkar formations.  Radiometric estimates have yielded an age range from 800 m.y. to 1.1 b.y. (Stevenson and Bues, 1982).  Paleomagnetic studies suggest intrusion occurred during Commanche Point depositon, approximately 1.1 b.y. (Elston, 1989).  The mineralogy is identical to the "bottle green member" of the Cardenas, but no contacts between intrusions and the Cardenas lava have been found and the parentage remains uncertain.

The Cambrian Tapeats sandstone is the lowermost and oldest formation of the classic Paleozoic sequence of cliff forming units that comprise the walls of the Grand Canyon.  It was deposited on top of the Great Unconformity erosional surface, and its typical 30 to 100 m (thinner to east) thickness may completely pinch out against erosional surface highs.  The basal member of the formation is a pebble conglomerate that grades upward into a coarse-grained, arkosic sandstone and finally into a quartz sandstone.  The Tapeats sandstone is easily identified by its cliff-forming outcrop and consistently thin bedding (less than 1 m).  The depositional environment was a transgressing, on-lapping to the east, beach-front (Middleton and Elliot, 2003).

*2.2 Fault-Fold Structure of Palisades Monocline*

In the eastern Grand Canyon, initial Precambrian extension tilted Precambrian strata along west-dipping normal faults (Fig. 2a), which was followed by erosion and subsequent Paleozoic and Mesozoic deposition (Fig. 2b).  Laramide contraction resulted in positive inversion of some Precambrian structures and developed east-facing, fault-cored monoclines in Paleozoic strata (Fig. 2c).  The Palisades Monocline is a southeast-trending splay of the East Kaibab monocline and underlying Butte Fault system, and is an excellent example of a fault-cored monocline common in the Colorado Plateau (Fig.

1).  The Palisades Monocline is an east-facing flexure and is well-exposed at all stratigraphic levels in Palisades Creek canyon, a 1,200 m deep tributary canyon of the Grand Canyon five miles downstream of the Little Colorado River confluence.  Both the Palisades Monocline and Palisades Creek canyon trend N40W, with the mouth of Palisades Creek located on the southeast side of the Colorado River (Fig. 9).

Reches (1978) provides the definitive study of the Palisades area, but focuses mostly on the style of deformation and relationship between faulting and monoclinal flexure in the overlying Paleozoic units (Fig. 10).  Reches (1978) divides the fault-monocline system into three structural levels based on styles of deformation and structural features such as joints, faults, breccia zones, tight to open folds, and steeply overturned to gently dipping layers.  The lower structural level includes the Precambrian formations and overlying Tapeats sandstone, and is deformed into a tight syncline fold with overturned to steeply dipping layers that is offset by the vertical Palisades fault.  Additionally, the lower structural level includes diabase intrusions, hydrothermal alteration, both open and tight small folds, and many small faults.  The intermediate structural level includes the Bright Angel shale, Muav and Temple Butte limestones, and lower Redwall limestone, which display steep monoclinal flexure, small folds and small faults within layers.  The upper structural level includes the upper Redwall limestone and all overlying units up to the Kaibab limestone, which display joints, small faults and open monocline flexure with layer dips less than $20^{\circ}$.

Reches (1978) determines the total Laramide-induced throw across the fault/ monocline is equal to fault displacement, flexural offset of the units and regional tilt, although the effect of regional tilt is not clear (Fig. 11).  Reches (1978) reports the total throw is dependent on structural level, and ranges from 250 m at the lower structural level to 150 m at the intermediate structural level and 111 m at the upper structural level.  Reches (1978) reports that 80 m of the total 250 m Laramide reverse throw of the lower structural level is accommodated through slip along the Palisades fault zone, while the remaining 170 m of reverse throw is accommodated through monocline flexure and

Upper Structural Level

Total throw = 311 m
(all flexure)

Lower Structural Level

$T_{HW\ flex/tilt}$ = 147m

$T_{fault}$ = 88 m

$T_{FW\ flex}$ = 71 m

Total throw = 306 m

500 m
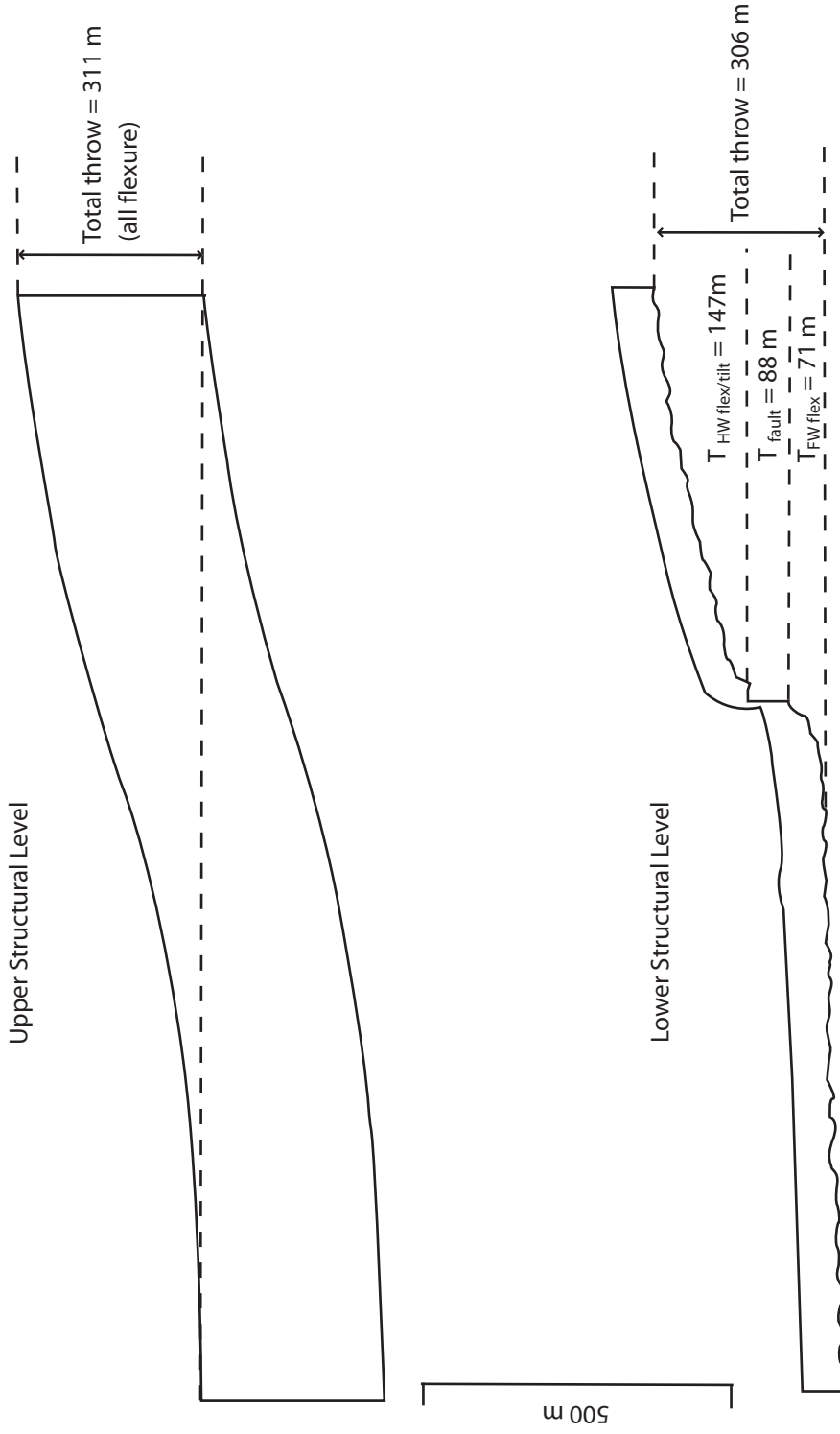
Fig. 11. Graphical estimate of the total reversere throw of the Palisades Monocline. Total throw for the lower and upper structural level estimated from the scaled vertical projection of Reches (1978) suggest reverse throw is vertically constant throughout the monocline, contrary to values reported by Reches (1978).

regional tilt rotation. The Palisades fault did not propagate into the intermediate or upper structural levels, where all of total throw across the monocline is the result of flexure and regional tilt.

It is also possible to estimate the total throw of the structural levels using Reches' (1978) vertical projection of the monocline (Fig. 10). Measurements of fault displacement and flexure taken from the vertical projection indicate the total throw across the monocline is consistent within all structural levels, which does not agree with the reported results from Reches (1978; Fig. 11). The vertical projection measurements discussed in this thesis use the largest possible total throw as measured from the lateral most extent of the projection, which may include a larger regional tilt value than those reported by Reches (1978). Measurements of the lower structural level taken at the Great Unconformity indicate 88 m of fault displacement, 71 m of footwall flexure and 147 m of hanging wall flexure and regional tilt combining for a total throw of 306 m. The fault displacement of the lower structural level is consistent with both the reported values and the vertical projection of Reches (1978). Measurement of the top of the upper structural level (Kaibab limestone) indicates a total throw of 311 m, all of which is due to flexure and regional tilt. The difference in total throw estimates of the upper structural level between the vertical projection and reported values of Reches (1978) is not clear, but appears to include more than measurement inconsistency of regional tilt.

At the Palisades study area the orientation of the underlying fault is N40W 90. The fault is assumed to flatten at depth towards the west as suggested by the 10 to 20 degree rotation of Precambrian units on the southwestern side of the fault (e.g. Reches, 1978; Huntoon, 1993). Assuming the fault dips to the southwest, the southwestern side of the Palisades Fault that had relative motion down during extension and up during contraction is identified as the hanging wall. The northeastern side that had relative motion up during extension and down during contraction is identified as the footwall. The reverse displacement during Laramide deformation was less than the Precambrian normal slip, thus there is a net normal separation of Precambrian formations but reverse

26
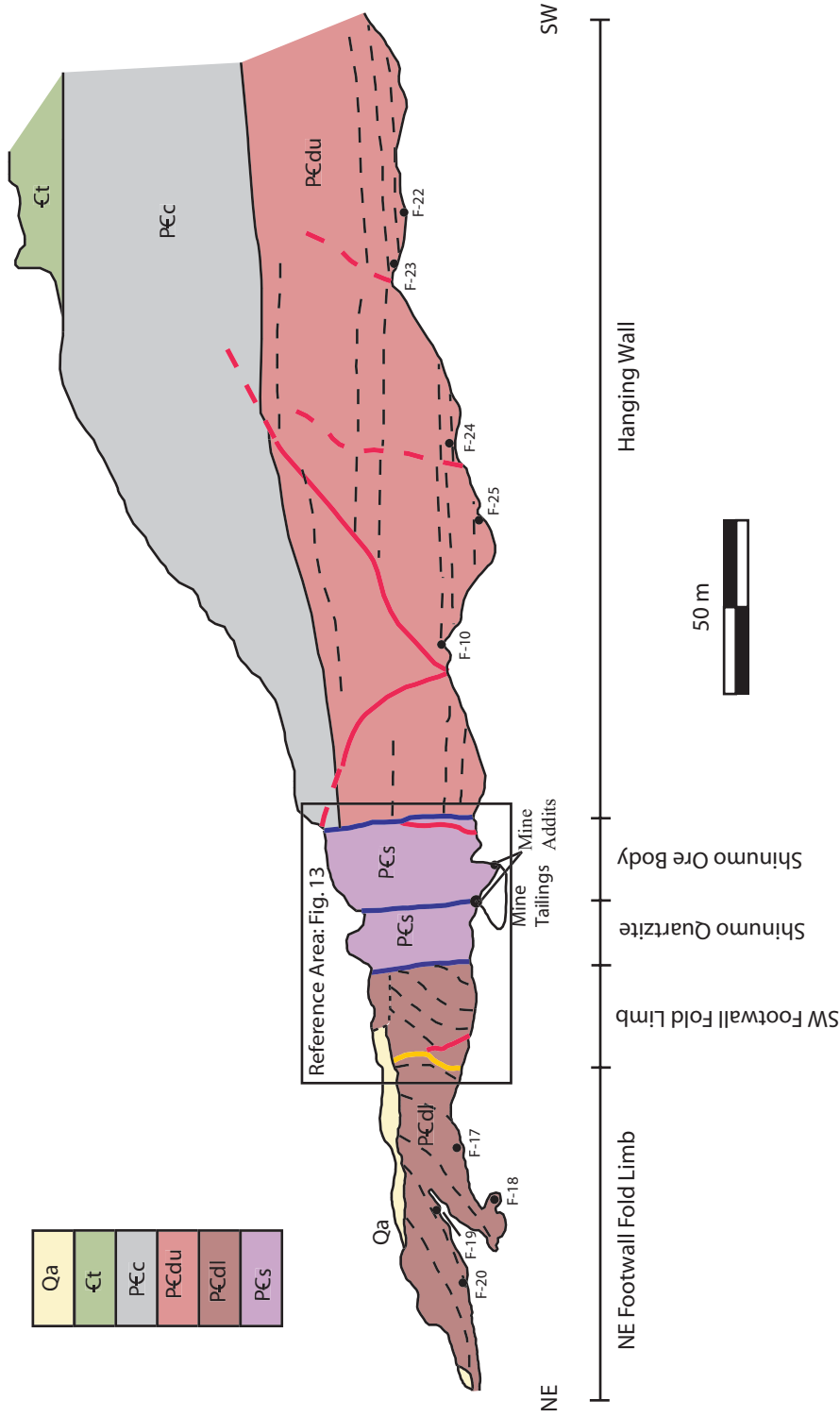


Fig. 12. Map of the vertical outcrop exposure of the Palisades fault. The three splays of the Palisades fault separate 4 structural domains: hanging wall, Shinumo ore body, Shinumo Quartzite, and the footwall, which may be divided into two fold limb domains. Upper Dox formation (PCdu) (Commanche Point and OchoaPoint members) Cardenas Lava (PCc) and Tapeats Sandstone (Ct) are exposed in the hanging wall, Shinumo Quartzite (PCs) is exposed within the fault zone, and Lower Dox (PCdl) formations (Escalante Creek meber) is exposed in the footwall (after Reches, 1978). Locations for collection of structual orientation data indicated by black circles.

(a)



(b)
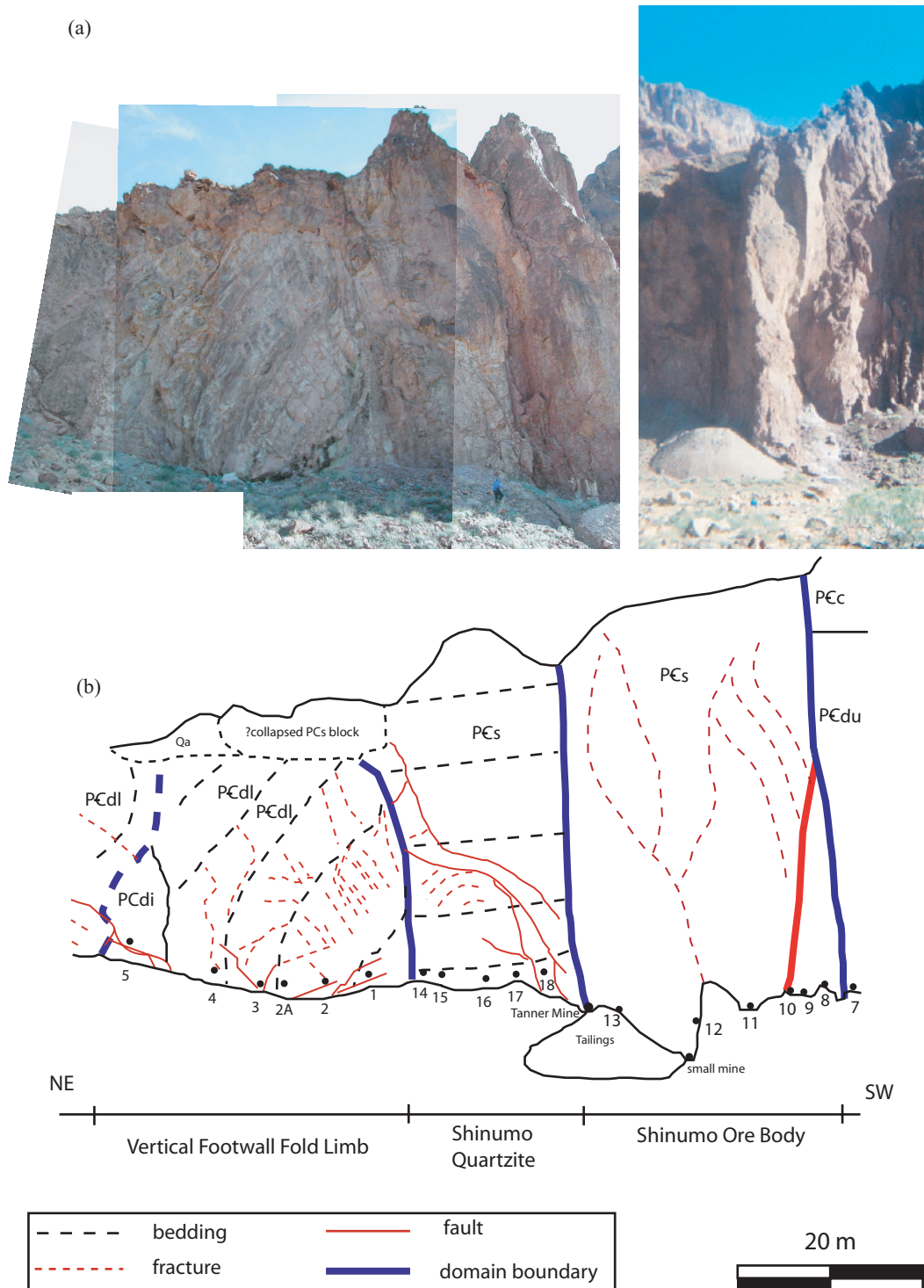


Fig. 13. Detailed map of the vertical exposure of the Palisades fault zone. (a) Photographs of the verical cliff exposure of the three Palisades fault splays and associated Shinumo ore body and quartzite domains and the near vertical footwall fold limb. (b) Sketch map of fault zone highlighting structural features and data collection locations for smaller structural features (see reference box on Fig. 12).

separation of the Paleozoic units.  Cross-sections of Reches (1978) suggest that there is approximately 700 m of normal separation of the Precambrian units across the fault zone, and approximately 250 m reverse separation of the Great Unconformity (Fig. 10).  This implies at least 950 m of initial Precambrian normal offset, followed by 250 m of post-Paleozoic reverse movement (Reches, 1978).

The underlying Palisades fault zone is exposed along the bottom of Palisades Creek with a 30 m high, cross-section exposure trending nearly perpendicular to the strike of the monocline at the mouth of Palisades Creek (Figs. 12 and 13).  At this location the fault zone consists of three sub-parallel fault surfaces, which can be traced to the southeast along Palisades Creek.  The three fault surfaces divide the fault zone into two vertical, 15 – 20 m wide, fault-bounded blocks between the hanging wall and footwall.  The two central, fault-bounded domains are comprised of Shinumo Formation (Reches, 1978), of which the southwestern domain is the location of copper mineralization and mining activity.  The Tanner mine addict is located at the base of the central fault boundary, and a smaller mine addict is located within the southwestern Shinumo block.  The hanging wall consists of gently northeast-dipping upper Dox Formation overlain by the Cardenas Lava, both of which are fractured and faulted.  The footwall consists of folded, faulted, fractured and altered lower Dox Formation with diabase intrusions.

Using faults, folds, calcite twins and unit thickness throughout the entire fault-fold structure, Reches (1978) concludes the Laramide contraction axis was nearly horizontal with a direction of N67E, which is about 70$^\circ$ to the normal to the fault.  Reches' (1978) Laramide contraction axis is consistent with the N65E, horizontal contraction axis inferred for the western Colorado Plateau region (Anderson and Barnhard, 1986).  These Laramide contraction axes, along with stratigraphic relations across the underlying fault, indicate the Palisades area underwent nearly co-axial, positive inversion (Figs. 10 and 12; e.g. Reches, 1978; Huntoon, 1993).  Reches (1978) notes the existence of conjugate, high angle normal faults in the hanging wall and

suggests that they formed during Precambrian extension, prior to Laramide deformation and monocline formation.

CHAPTER III

STRUCTURE AND FRACTURE FABRIC OF THE PALISADES FAULT

**1. Introduction**

      The mesoscale deformation features within the Precambrian units of the Palisades Monocline were mapped from a continuous vertical exposure perpendicular to the strike of the monocline and underlying fault zone.  Recorded features include bedding, intrusive bodies, fractures, veins, axial fold planes, hydrothermal alteration, locations of collected samples and locations of detailed structural data.  Fractures that displayed opening mode displacements are classified as joints, those with shear parallel to the fracture wall are classified as faults, and those in which displacement mode was not distinguishable are referred to as fractures.  When possible, the orientation, length, sense of shear and separation on joints and faults were recorded.  Joints were identified by the presence of plumose structure and lack of shear offset of bedding and veins.  Faults were distinguished by shear offset of bedding, veins, reduction bands and deformation bands, and the presence of polished or smooth slip surfaces with and without lineations or gouge.  Some faults are sealed by secondary cement that may resemble vein fill.

      The deformation data were collected at stations along the base of the outcrop exposure.  The measurement stations are located every 2 to 3 m within and immediately adjacent (up to 10 m) to the fault zone, with increased spacing of 8 to 10 m in the proximal (10 to 50 m from fault zone) footwall and hanging wall domains.  The distal locations (over 50 m from fault zone) were chosen to help define background fabric and are spaced over 10 m apart.  All structures features longer than 10 cm within a 1 m x 1 m area were recorded at each of the measurement stations.  The outcrop does not provide exposure parallel to the strike of the Palisades fault, which may cause under-sampling of features striking perpendicular to the Palisades fault.  All structural data were plotted using Allmendinger's Stereonet for Windows Version 1.1.6 (2002).

**2. Structure and Fabric of the Palisades Fault at Palisades Creek**

The Palisades fault zone in the Precambrian units is a 40 m wide zone defined by three sub-vertical, parallel faults that have average strikes of N40W, and are spaced approximately 20 m apart (Figs. 12 and 13; Reches, 1978). These three faults cut vertically through the entire outcrop, are three to five meters thick, and have been mapped to the southeast by Reches (1978) for a few hundred meters (Fig. 9). From the southwest to the northeast, the three faults are referred to as the: 1) hanging wall boundary fault, 2) central fault, and 3) the footwall boundary fault. The three faults define the boundaries of four of the five structural domains. From the southwest to the northeast, the structural domains are: 1) the hanging wall domain, 2) the Shinumo ore body domain, 3) the Shinumo quartzite domain, 4) the vertical footwall fold limb, and 5) the northeast-dipping footwall fold limb (Figs. 12 and 13). The boundary between the footwall fold limbs is not clearly visible or defined, but is inferred from discordant bedding and diabase intrusion. Exposures of the hanging wall domain are composed of the upper Dox Formation, Cardenas Lava, and Tapeats Sandstone, while those of footwall domains are composed the lower Dox Formation, and the two domains within the fault zone consist of Shinumo Formation (Figs. 7 and 12).

*2.1 Hanging Wall Domain*

The hanging wall is defined as the domain on the southwest side of the hanging wall boundary fault, including the southwest wall of the Palisades Creek canyon (Figs. 9 and 12). Joint, fault and fracture orientations are similar throughout the hanging wall domain (Fig. 14), but their intensity declines to apparent background level at approximately 30 m southwest of the fault zone. Separating out specific features, the fabric is characterized by joints oriented N56W 90 and N64E 90 joint orientations, and veins oriented N57W 90 (Figs. 14 and 15). Northwest-striking faults are most common in this domain, with 48 out of the 50 measured faults striking to the northwest (Fig. 14).
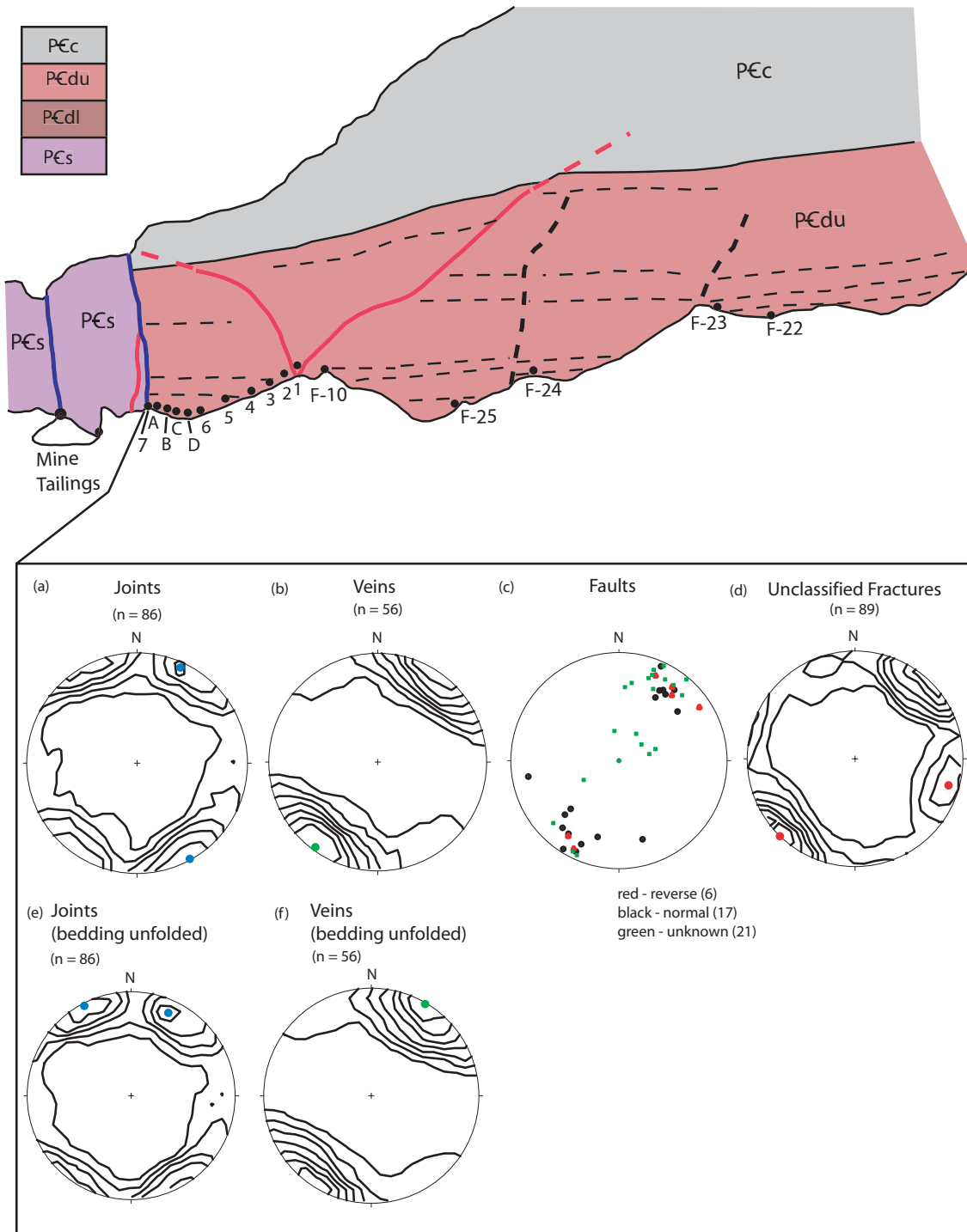
Fig. 14.  Structural features of the hanging wall domain. Sketch map shows orientation collection locations for small structures.  Stereonet plots display orientaions of (a) joints, (b) veins, (c) faults, (d) unclassified fractures, (e) joint orientation with bedding horizontal reference frame, (f) vein orientations with bedding horizontal reference frame. Stereonet plots are equal area, lower hemisphere projections, and best fit poles for Kamb contouring with contour interval of 2σ.
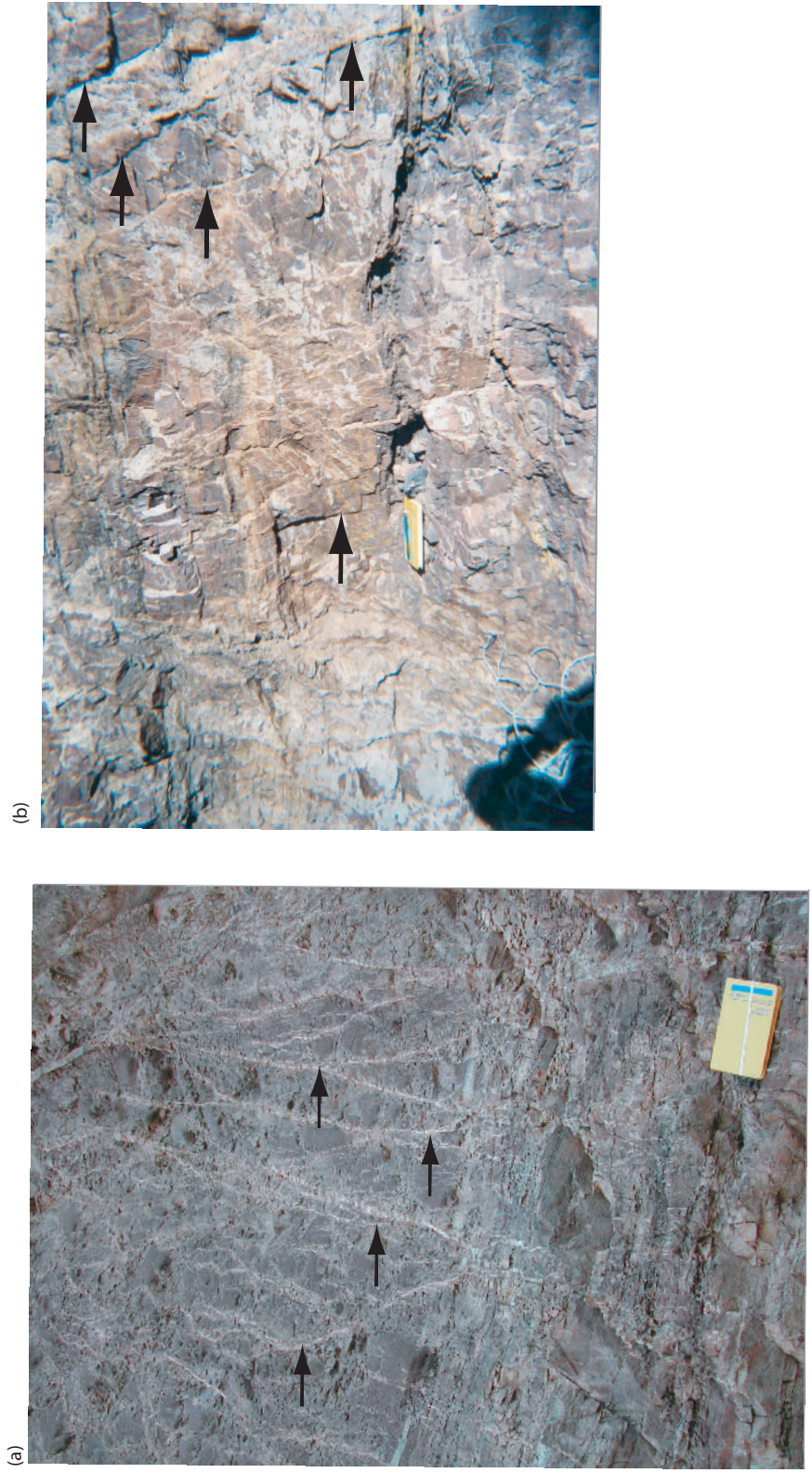
Fig. 15. Photographs of hanging wall deformation. (a) Vertical quartz veins, and (b) conjugate normal faults and dilational deformation bands.

The faults range from 1 m in length with centimeters of offset to hundreds of meters in length with meters of offset. Thirty-seven of the faults dip 75$^{\circ}$ to 80$^{\circ}$ to both the northeast and southwest with slip striations having rakes of 30$^{\circ}$ to 65$^{\circ}$. Of the 37 high angle faults in this domain, 17 have a net normal offset, 6 show net reverse offset, and 14 have unknown offset. There are thirteen faults with unknown slip indicators, seven of which are north-northwest striking faults with dips less than 20$^{\circ}$ and four which are northwest striking faults with high dip angles. The remaining fractures are characterized by a preferred orientation of N47W 90, and a secondary preferred orientation of N15E 78W (Fig. 15).

*2.2 Shinumo Ore Body Domain*

The hanging wall boundary is defined by a 3 to 5 m thick, vertical fault with normal separation. Fabric data collected within the fault boundary are from stations 8, 9, and 10 (Figs. 16 and 17). Micaceous, red siltstone blocks of the Dox Formation exist within this bounding fault zone and are located in between or are cross-cut by 8 to 30 cm thick Z-folded, approximately vertical, quartz veins (Fig. 16). Additionaly, there are anastamosing quartz veins less than 1 cm thick at stations 8 and 9 that contain minor amounts of copper and iron ore, whereas at station 10 the anastamosing veins contain significant copper and iron ore fill. Ore minerals occur in the center of the vein, with white quartz along the walls. The ore veins cross-cut the thick, vertical quartz veins, and they appear to have formed during a single event. Four measured faults in the boundary zone strike east-west and are vertical, while two faults strike northwest and dip 45 N (Fig 17). The two fractures in this boundary have similar orientations as the two northwest-striking faults, and dip 50 N. The nine measured veins in this zone all have strikes in the northwest quadrant, and dips ranging from 60 SW to 70 NE (Fig. 17).

The Shinumo ore body domain consists of a massive block of hydrothermally altered Shinumo formation containing the minor ore deposits and Tanner mine addicts. This domain forms a resistant protrusion on the cliff face, and a minor hogback in the
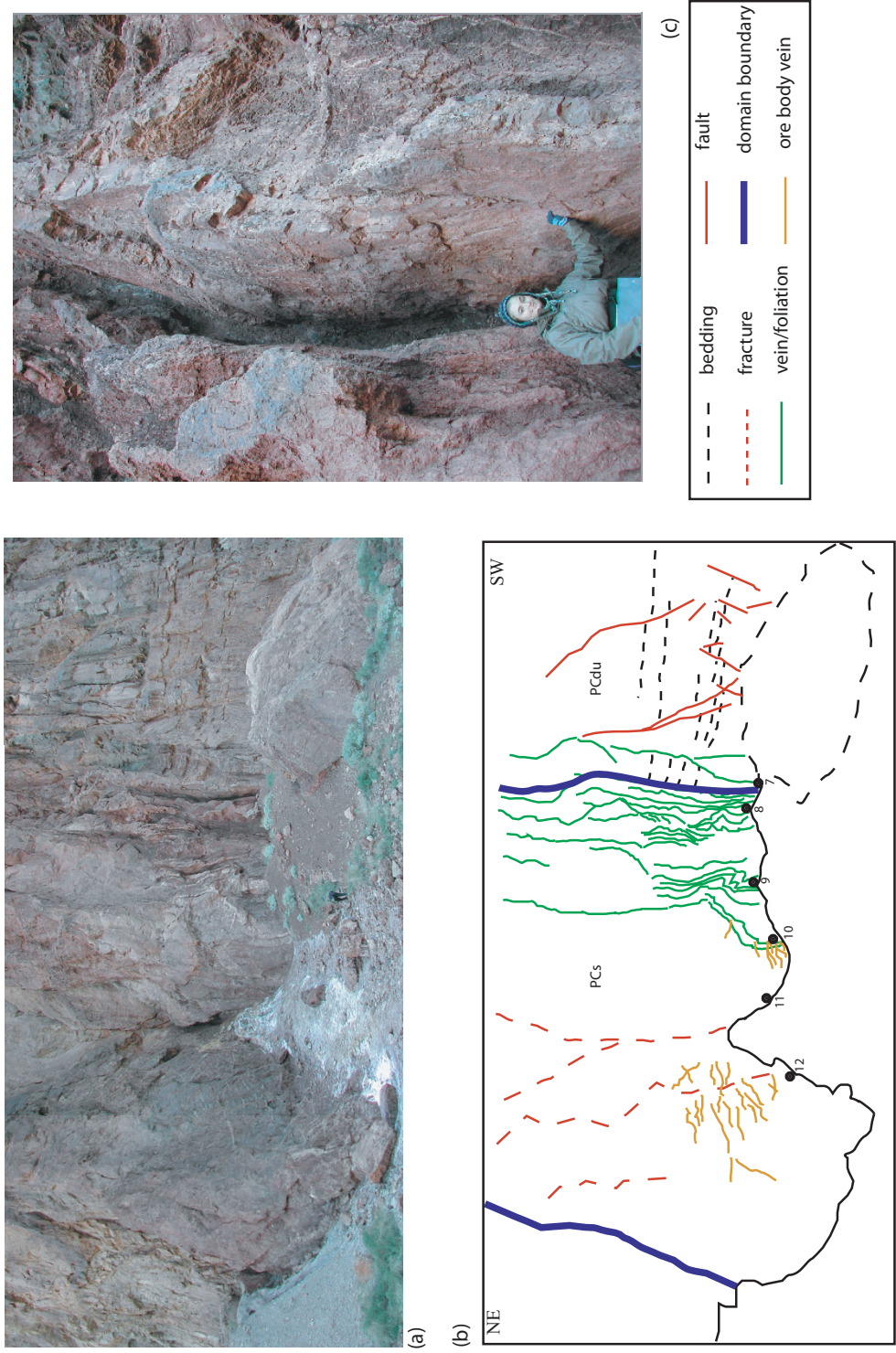
Fig. 16. Features of the hanging wall bounding normal fault. (a) Photograph and (b) sketch map of the hanging wall bounding normal fault with secondary "Z-folds" and adjacent Shinumo ore body veins. Small structure orientation data collected at numbered locations. (c) The undulating master slip surface of the bounding normal fault (near location 7) separating the hanging wall to the southwest from Shinumo formation to the northeast.
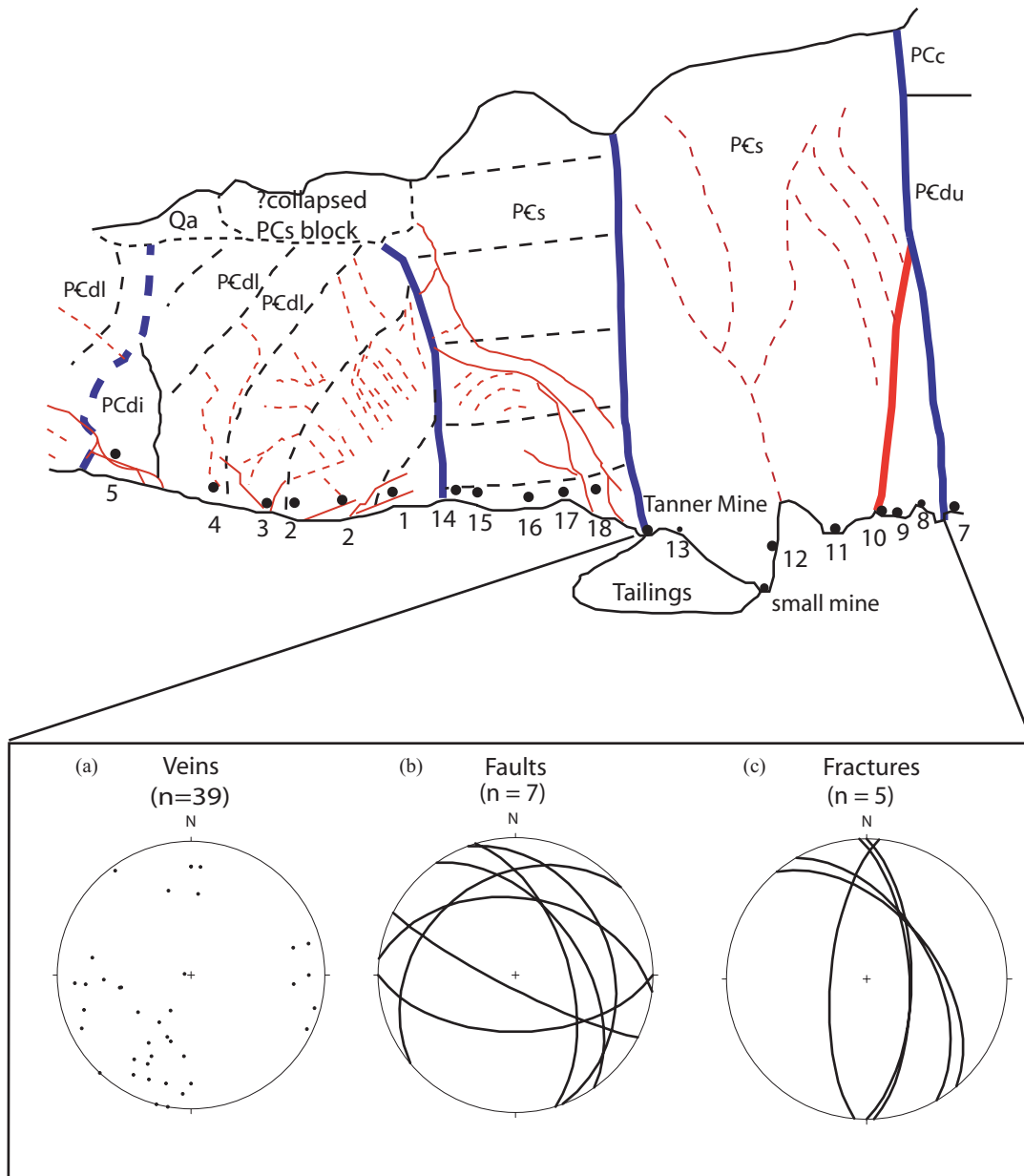
Fig. 17. Structural features of the Shinumo ore body domain. Sketch map (Fig. 8) indicates data collection locations for small structures. Stereonet plots display orientations of small structures. (a) Veins, (b) faults of unknown offset or slip, and (c) unclassified fractures. Stereonet plots are equal area, lower hemisphere projections.

Palisades Creek canyon. Fabric data collected within the fault boundary are from stations 11, 12 and 13 (Figs. 16 and 17). Compared to the stratigraphic description of Hendricks and Stevenson (2003), the domain lithology is consistent with the clay rich, brown quartz sandstone member of the Shinumo Formation that occurs directly below the top "quartzite" member (Figs. 7 and 13). Within this domain, no estimates of bedding orientation could be made due to the massive nature of the Shinumo Formation and presence of the ore mineralization and associated alteration.

Few open faults or fractures exist at the mesoscale, but the anastamosing ore veins also include secondary malachite and azurite within the protruding block of primary ore material (Fig. 18). All vein fill has identical mineralization, and does not display visible fibers or consistent cross-cutting relations, suggesting concurrent formation. Thirty-nine measured representative veins indicate a scattered set striking mostly fault parallel to the northwest with approximately $50^o$ dips to the north (Fig. 17).

This domain is bounded to the northeast by the central boundary fault, a 2 m thick, near vertical fault that separates the Shinumo ore body from the Shinumo quartzite domain. The central boundary fault contains a slip surface that is slightly undulatory and polished, and is often marked by blue azurite slip lineations in the Palisades Creek canyon that do not exist at the vertical outcrop. Measurements of the slip surface at the base of the vertical outcrop indicate a general orientation of N64W 86S.

*2.3 Shinumo Quartzite Domain*

On the basis of Hendricks and Stevenson's (2003) stratigraphic description of the Shinumo formation, this domain is identified to consist of the top "quartzite" member of the Shinumo formation (Figs. 7 and 13). The quartzite is massive, but occasionally displays very thin, lithic laminations, which yield poor bedding orientation estimates of N45W 20N along the cliff exposure (Fig. 19). Exposures to the southeast in the Palisades Creek canyon indicate near horizontal bedding orientation (Fig. 9). The

(a)

(b)
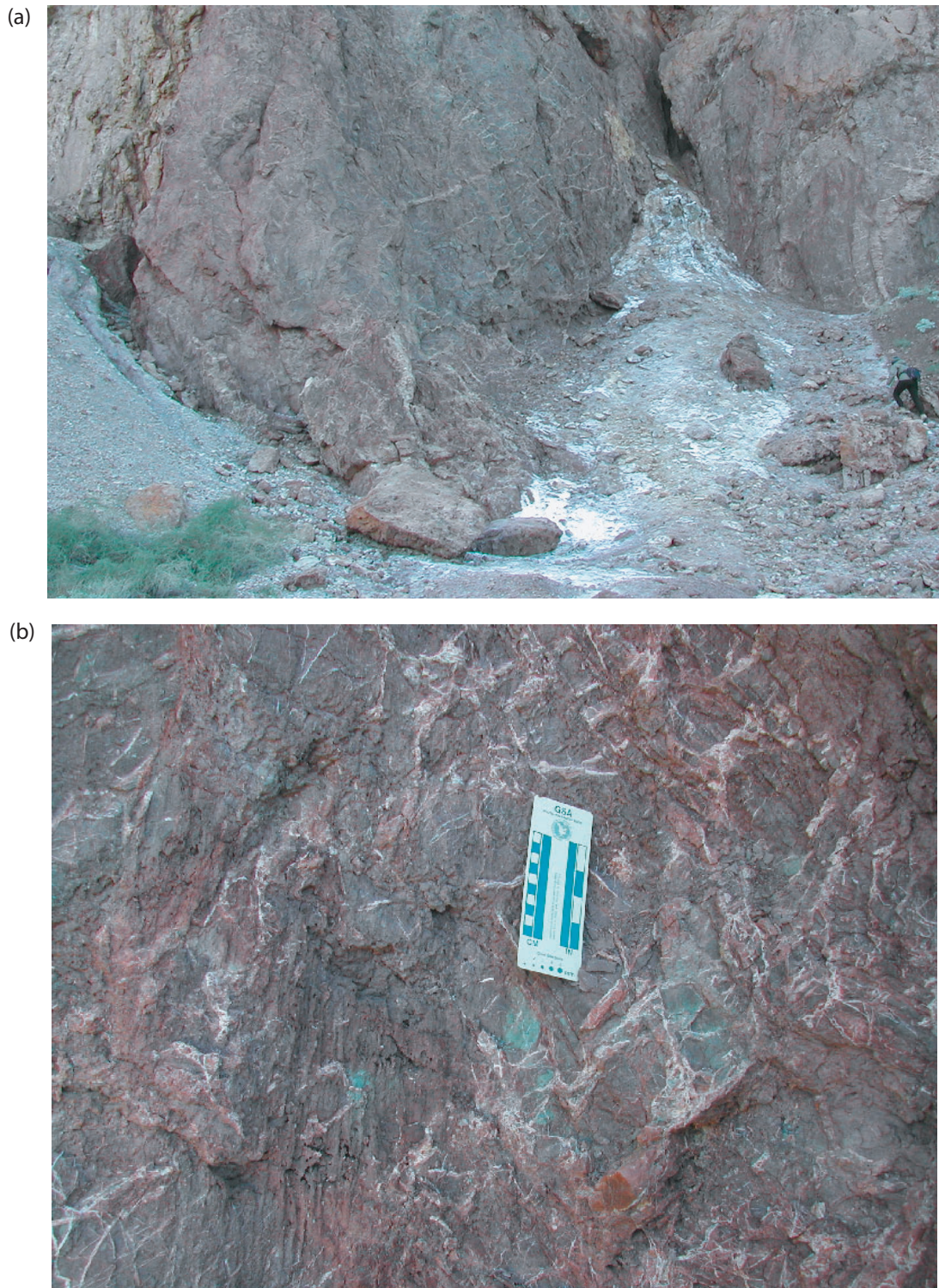
Fig. 18.  Photographs of the Shinumo ore body domain. (a) NW stiking, sub-vertical veins have horizontal traces on southwestern vertical cliff exposure. (b) Ore veins at station 10.
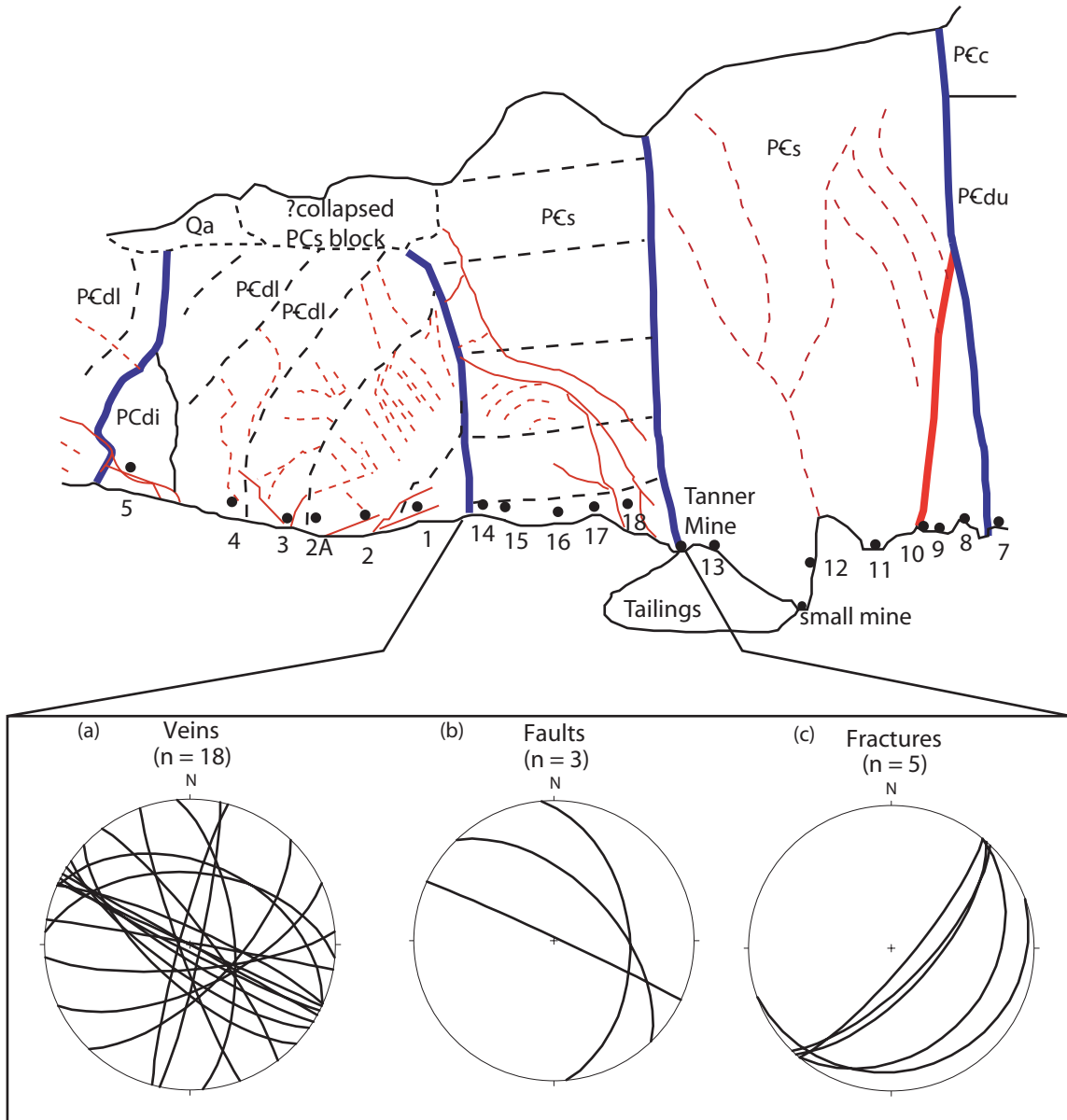
Fig. 19. Structural features of the Shinumo quartzite domain. Sketch map indicates sturctural features and data collection locations for small structures. Stereonet plots display orientations of (a) veins, (b) faults (unknown offset or slip) and c) unclassified fractures. Stereonet plots are lower hemisphere projections.

vertical face of this domain has very few open joints and fractures, and is coated with a 5 to 8 cm thick surface layer of secondary, calcite, travertine and possibly fluorite.

Structural data for this domain were collected at stations 14, 15, 16, 17 and 18 (Fig. 19). Veins are quartz filled, do not have visible copper ore, are less than 5 cm wide and often less than 0.5 cm wide. Many of the veins have a 1 mm wide ribbon of red fill material, inferred to be iron oxide, along the center of the vein. The veins have a preferred orientation of N60W 90, but there is a wide scatter in the strike of veins that dip greater than 45$^\circ$ (Fig. 19). The veins are not planar, often displaying open folds with inter-limb angles between 90$^\circ$ and 180$^\circ$.

The most distinct feature of this domain is the second order, synthetic fractures that cut diagonally up and across the block from southwest to northeast (Fig. 13). In vertical exposure, the fracture system can be traced diagonally upward from the basal southwest corner at the central fault boundary above Tanner mine to the footwall boundary fault. The fractures terminate within the central fault boundary, but no offset markers or slip indicators were apparent. The intersection of the fracture system with the footwall boundary fault is inaccessible and could not be investigated. Beneath the fracture system, there is crude bedding or curved fractures that resemble a small anticline fold (Fig. 13).

*2.4 Vertical Footwall Fold Limb Domain*

The vertical footwall fold limb consists of lower Dox Formation, as identified by Reches (1978). The domain is characterized by steeply dipping beds with a distinct, mottled green, yellow and purple-brown color that contrasts with the tan and brown colors of the rest of the outcrop (Figs. 20 and 21). The bedding along the base of the cliff ranges from N50W 60N at the southwest corner to N50W 79S overturned at the northeast corner. The fold curvature is less along the top of the cliff exposure and to the southeast along Palisades Creek, where the bedding dips at lower angles to the northeast (Fig. 9).
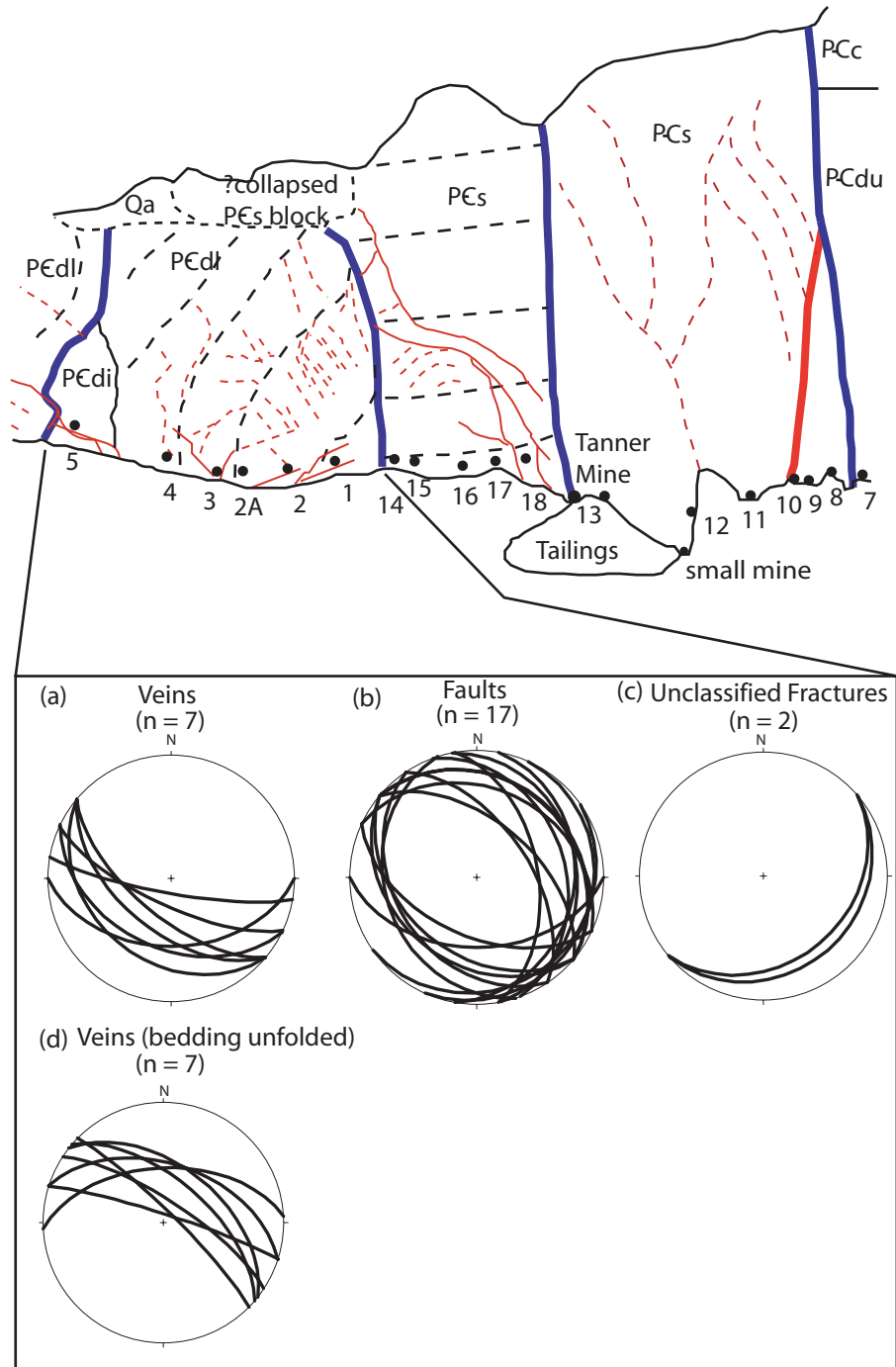
Fig. 20. Structural features of the vertical footwall fold limb. Sketch map indicates structural features and data collection stations for smalls structures. Stereonet plots display orientations of (a) veins, (b) faults (all reverse), (c) unclassified fractures and (d) veins rotated into horizontal reference frame. Stereonet plots are lower hemisphere projections.
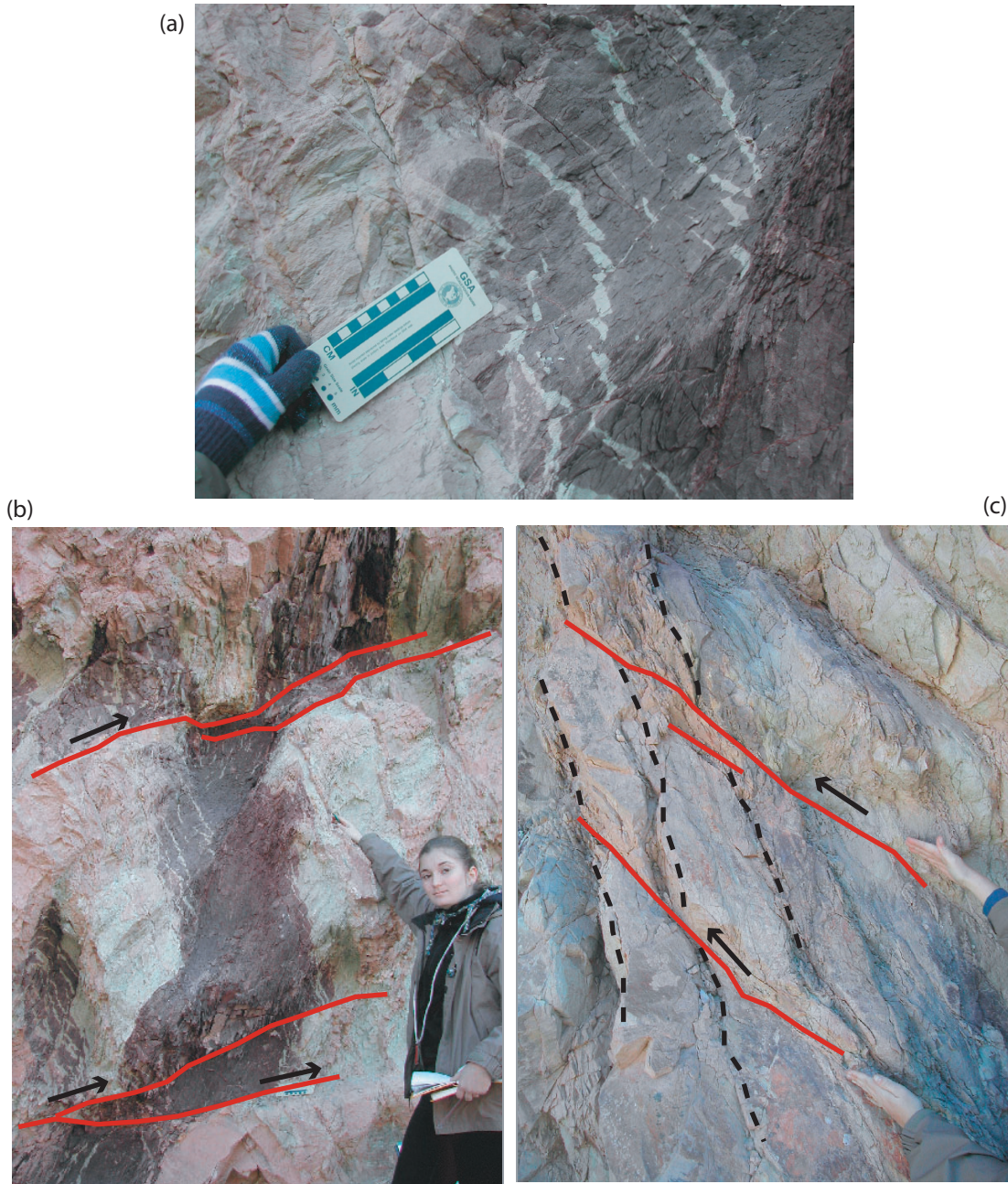
Fig. 21. Photographs of vertical footwall fold limb deformation. (a) and (b) Antithetic reverse faults cutting through bedding and offsetting green reduction bands. (c) Synthetic reverse faults cutting through vertical to slightly overturned bedding. Faults shown as solid red lines, bedding is dashed black lines.
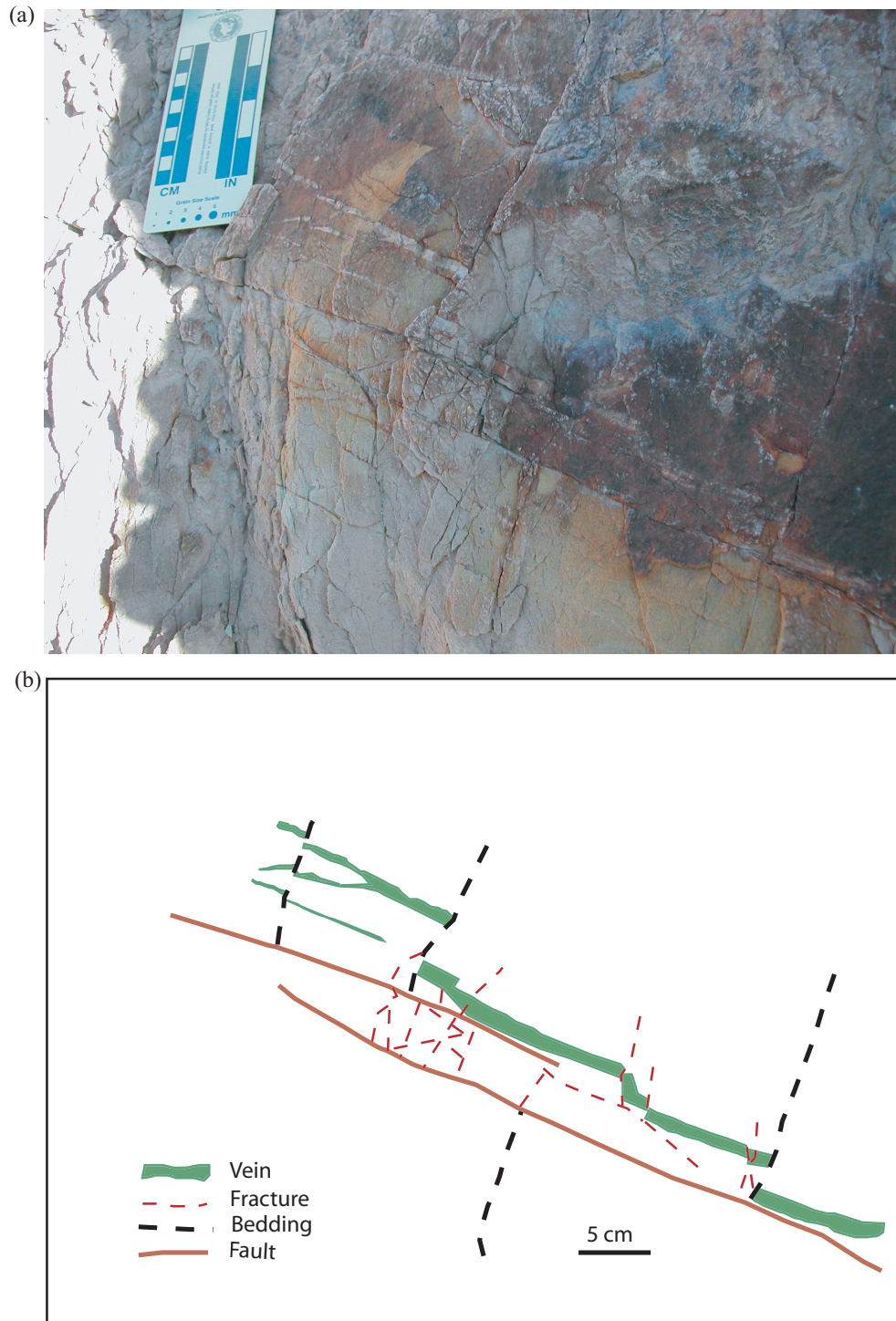
Fig. 22.  Footwall cross-cutting relationships at station 4. (a) Photograph and (b) sketch map of vertical exposure cross-cuting relationships in the footwall fold. Bedding perpendicular vein is offset by faults along bedding planes with synthetic fault offsetting bedding plane faults.  Slip movement and amount of offset is unknown, but thought to be 10 - 30 cm of reverse movement.

Structural data were collected from stations 1, 2, 2A, 3, 4 and 5 (Fig. 20). The lower Dox Formation is cut by parallel sets of joints and veins that are oriented roughly N70W 60S and are offset across or terminate at bedding layers (Figs. 20 and 22). Many of the joints in the brown, shale rich layers have ½ to 2 mm green reduction alteration in the surrounding host. The veins are typically ½ to 5 mm thick and filled with blocky quartz. The joints and veins are almost always perpendicular to the bedding throughout the fold, regardless of the bedding orientation.

There are two sets of faults that cut through bedding: a synthetic, southwest dipping set of reverse faults, and an antithetic, northeast dipping set of reverse faults (Figs. 20 and 21). The synthetic faults have a preferred orientation of N42W 34S, and is sub-parallel to the joints and veins cutting the steeply dipping beds. These faults are often located along vein walls and ramp upward linking into other vein walls (Figs. 22 and 23). Antithetic faults are found in the tightest portion of the fold (near stations 1 and 2), and offset veins and joints (Fig. 20). When beds dip steeply to the northeast, the antithetic faults are sub-parallel to bedding with ramps linking upward between bedding parallel segments (Fig. 21).

The domain boundary to the northeast is defined as the transition from the altered and steeply dipping beds to shallower and unaltered beds of the Dox Formation. The cause of alteration is unknown, and it is not clear if discordant bedding indicates a fault defines the boundary (Fig. 24). Bedding attitudes at the boundary cannot be determined due to the existence of a diabase sill and a meter wide, comminuted, finely laminated zone (Fig. 24). Bedding is generally estimated to be parallel to the sill and near vertical, but there is tight, isoclinal folding of less than a meter wavelength and amplitude (Fig. 24). The sill also marks the mottled color alteration boundary to the southeast in the Palisades Creek canyon.
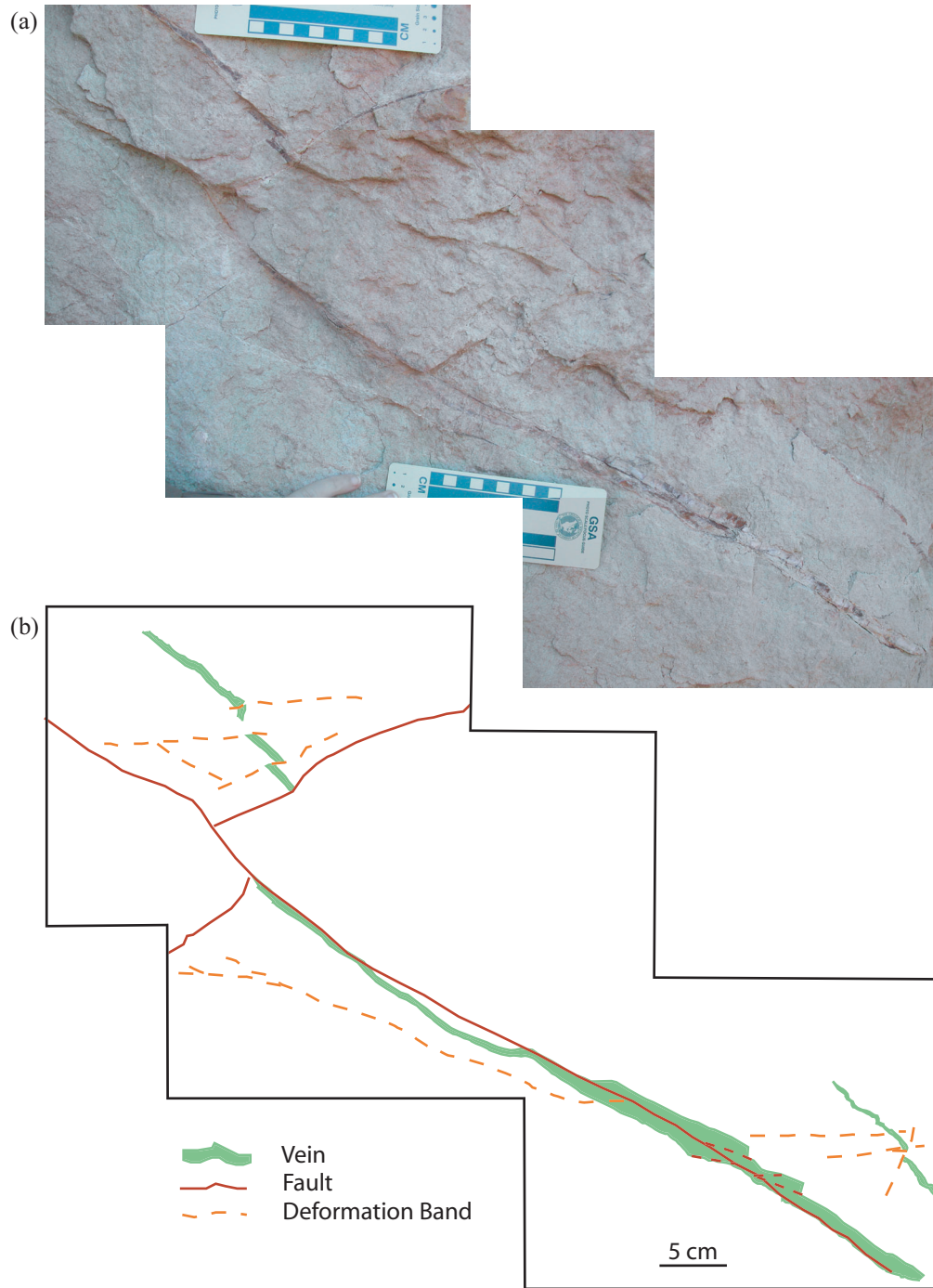
Fig. 23. Footwall cross-cutting relationships at station 2. (a) Photograph and (b) sketch map of vertical exposure cross-cutting relationships in footwall fold. Vein is offset by antithetic reverse fault, then both vein and antithetic fault are offset by synthetic thrust fault, which also overthrusts vein on itself. Deformation bands offset vein but timing with respect to faulting is unknown.
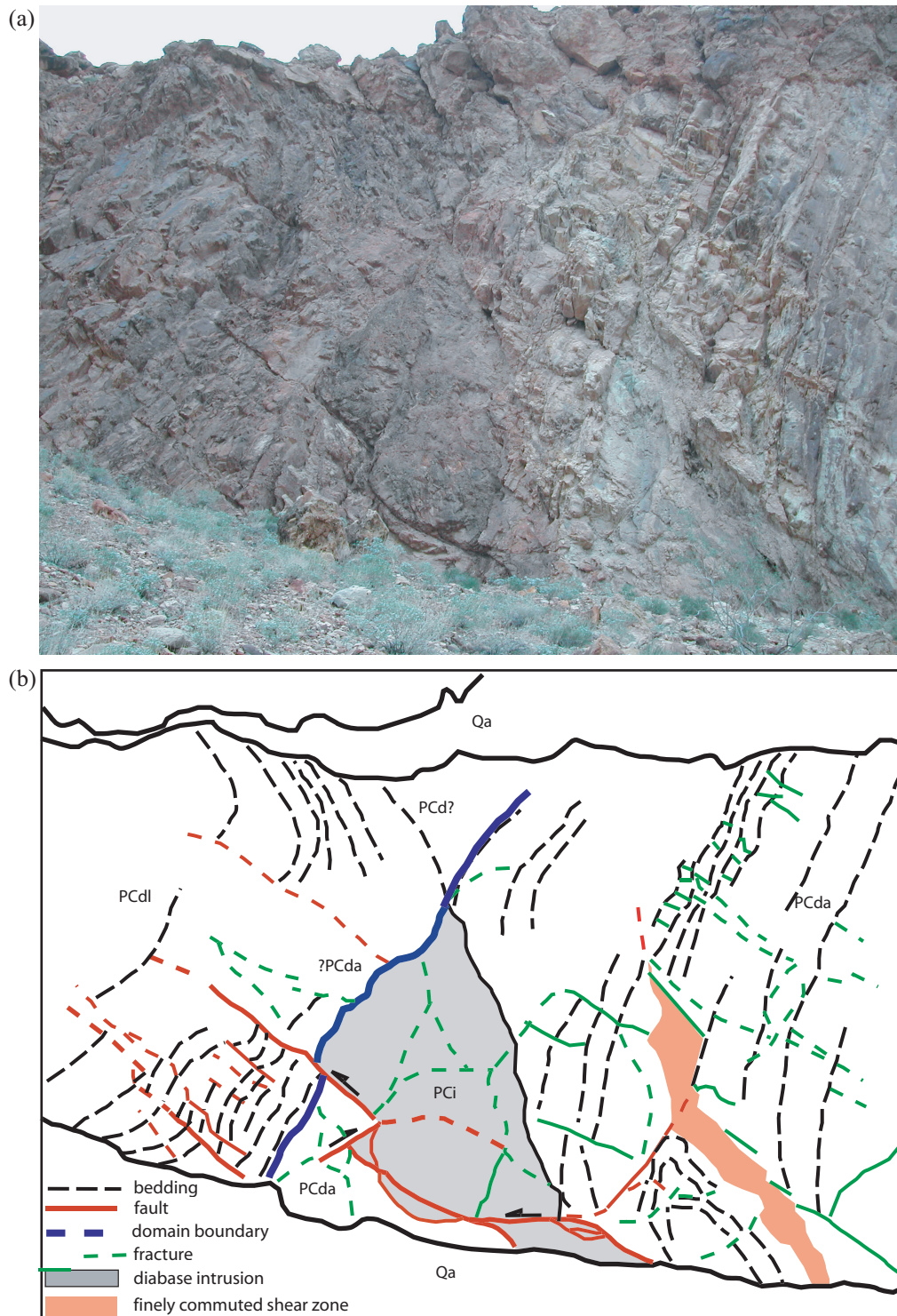
Fig. 24. Detailed map of domain boundary between footwall fold limbs. (a) Photograph and (b) sketch of domain features associated with domain boundary, including diabase instrusion and structural features such as faulting along diabase contacts and tight folding in the region adjacent to the intrusion (sketch by M. Finn).

*2.5 Northeast-Dipping Footwall Fold Limb Domain*

The northeast-dippping footwall fold limb consists of the lower Dox Formation, as identified by Reches (1978). The bedding has a strike of N35W with dips ranging from near vertical at the southwestern domain boundary to near horizontal at the mouth of Palisades Creek (Figs. 25 and 26). The density of mesoscale joints, faults and fractures appears to grade into background levels at over 50 m from the fault zone, or approximately where bed dips are less than 10°.

Structural data were collected from this domain at stations 6 and 19, sections 1, 2, 3 and 4, and F-17, F-18, F-19, F-20 and F-21 (Fig. 26). There is a set of joints with a preferred orientation of N23E 72W, and a possible secondary set of joints with preferred orientation of N62W 34S (Fig. 26). Due to the dramatic change in bedding dip throughout the domain, the joint set orientations display scatter. There are very few veins in this domain, but seven vein measurements indicate an orientation of N80W with dips ranging from 65S to 30S (Fig. 26). There are prominent low angle fractures and reverse faults of both synthetic and antithetic nature. Thirteen faults were measured without consistent orientation or cross-cutting relationships, although 4 displayed oblique reverse slip (Fig. 26). Three well defined, background fracture sets exist in the lower Dox Formation at over 50 m from the fault zone: N15W 78W, N71E 78S and N60W 65S (Fig. 26).

**3. Data Analysis**

The identification of positive inversion and Laramide-induced contractional folding at the Palisades Monocline provides the basis for interpreting field observations (Reches, 1978). Because the Precambrian formations of the Palisades Monocline have undergone two phases of deformation, Laramide footwall folding must first be removed from the Precambrian strata prior to interpretation of Precambrian deformation (Table 1). Precambrian extension and normal faulting caused hanging wall rotation towards the fault zone, which must be removed in order to interpret the initial stage of deformation
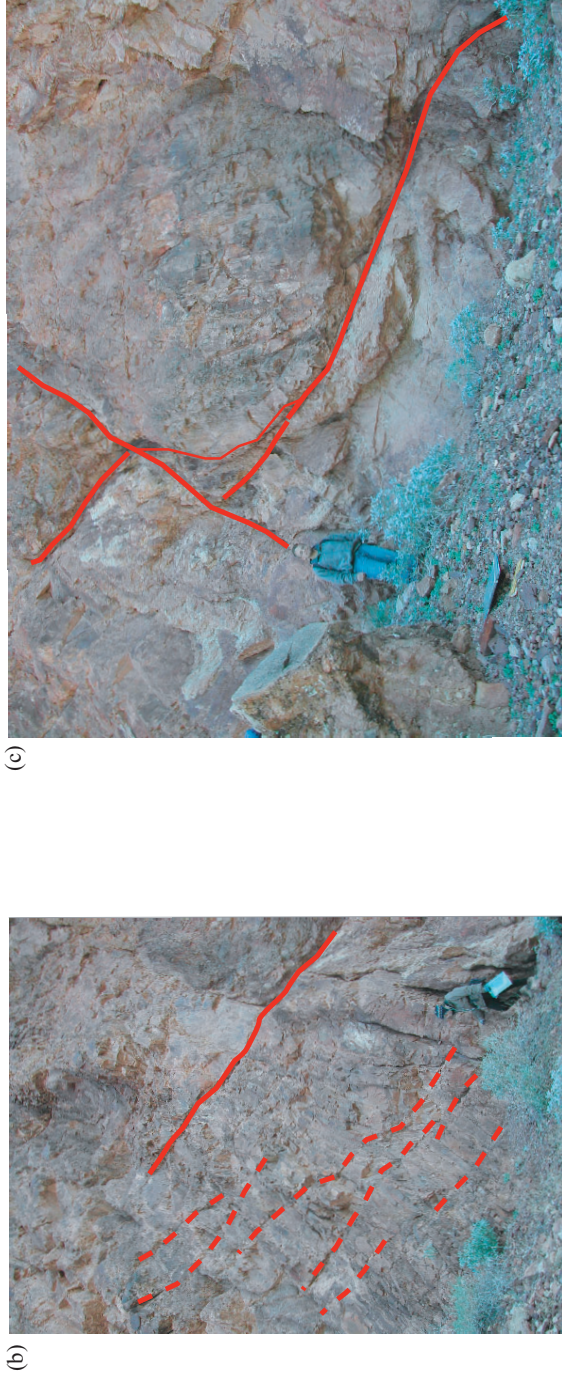
Fig. 25. Photographs of footwall features. (a) Entire footwall outcrop (sketch map shown in Fig. 21). (b) Synthetic faults and fractures common in the footwall fold at locations 1, 2, 3 and 4. (c) Antithetic fault cross-cutting synthetic fault and diabase contact near locations 5 and 6 (see Figs. 8 and 16). Faults shown as solid red lines, and fractures as dashed red lines.
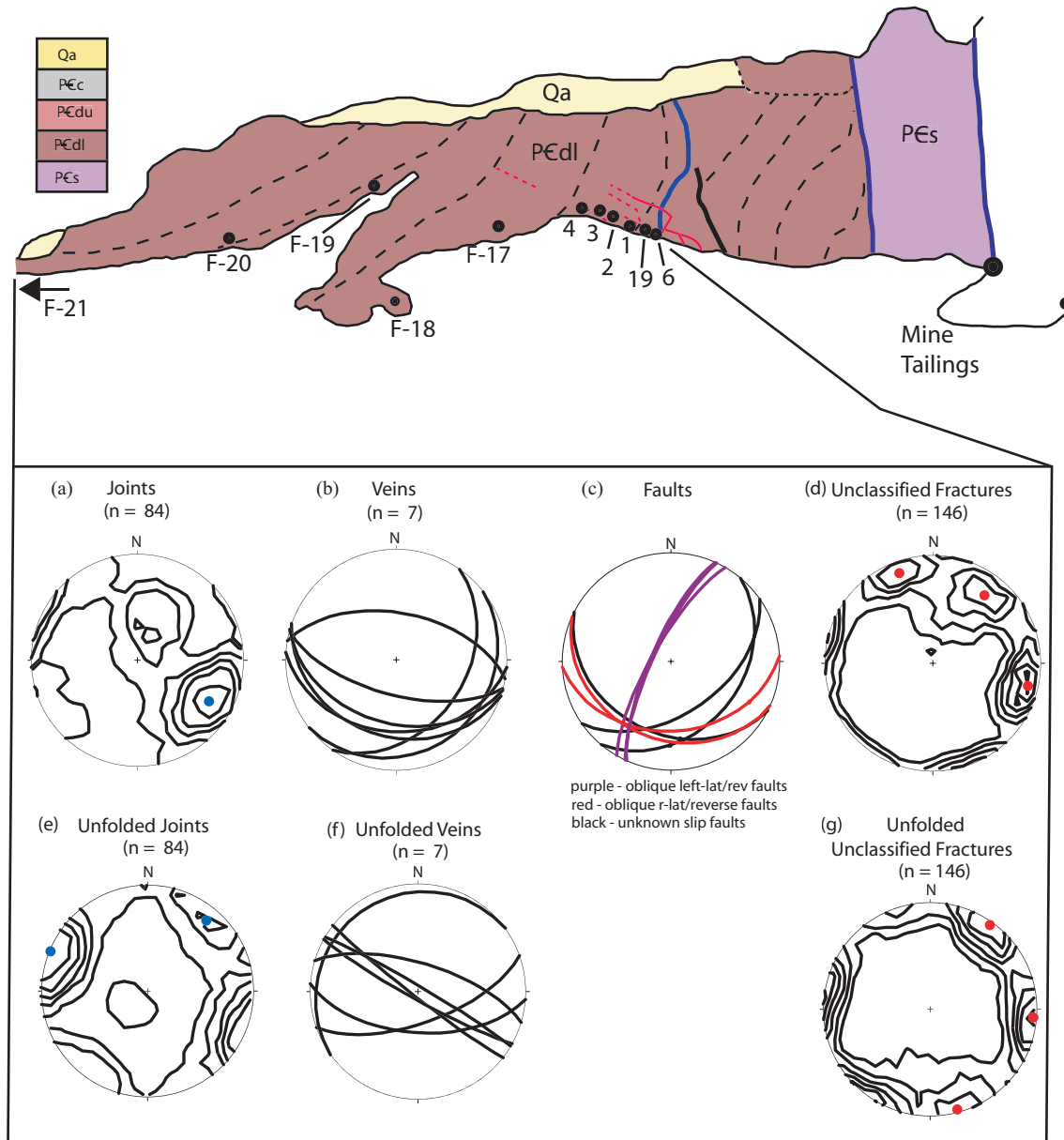
Fig. 26. Structural features of the northeast dipping footwall fold limb. Sketch map indicates structural featues of the footwall and and data collection locations for small structures. Stereonet plots display best fit pole orientations of (a) joints, (b) veins, (c) faults, (d) unclassified fractures, (e) joint orientation with bedding horizontal reference frame, (f) vein orientation with bedding horizontal reference frame, and (g) unclassified fractures with bedding horizontal reference frame. Stereonet plots are equal area, lower hemisphere projections, Kamb contouring with contour interval of $2\sigma$.

Table 1. Rotation data for bedding horizontal reference frame for each data collection location across the Palisades fault zone.

|  | Location | Rotation angle (clockwise) | Rotation axis (trend, RHR) |
|---|---|---|---|
| **Footwall** | Station 1 | 67 | 135 |
|  | Station 2, 2A | 75 | 142 |
|  | Station 3 | 104 | 128 |
|  | Station 4 | 101 | 135 |
|  | Station 5, 6 | 49 | 110 |
|  | Sections 1, 2, 3 | 60 | 146 |
|  | Section 4 | 80 | 130 |
|  | F - 17 | 57 | 130 |
|  | F - 18 | 58 | 097 |
|  | F - 19 | 20 | 104 |
|  | F - 20 | 07 | 164 |
|  | F - 21 | 09 | 095 |
| **Hanging Wall** | Scans AA', BB' CC', DD' | 15 | 132 |
|  | Section 6 | 13 | 096 |
|  | Section 5 | 08 | 250 |
|  | Section 4 | 07 | 216 |
|  | Section 3 | 03 | 137 |
|  | Section 2 | 05 | 159 |
|  | Section 1 | 14 | 147 |

(Reches, 1978; Huntoon, 1993; 2003; Table 1).  Due to the uncertainty of bedding within the Shinumo domains of the fault zone, all structural features within those domains are interpreted in their present orientation.

The deformation features chosen for rotation into a bedding horizontal reference frame are veins, joints and fracture sets that have a consistent orientation with respect to bedding (e.g. bedding perpendicular joints) and independent of bedding attitude (Table 2).  These features are often offset across, or abut against, bedding layers and could predate bedding rotation and possible flexural-slip folding along bedding.  Additionally, all features that are indicative of extension are analyzed and compared in both their current and bedding horizontal reference frame orientations.  Deformation features of that cut across bedding and folds or are indicative of contraction are analyzed in their current orientation.

After rotation into a bedding horizontal reference frame, there is one preferred vein orientation (N58W 90), and two preferred joint orientations (N51W 90 and N45E 90) throughout the entire study area (Table 2, Fig 27).  The similarity of joint and vein orientations with the unclassified fracture orientations suggests that many of these fractures are joints (Fig. 27).  The preferred orientations of the two joint sets are approximately orthogonal, with a set parallel to the Palisades fault, consistent with northeast-southwest Precambrian extension, and a set perpendicular to the Palisades fault, consistent with northeast-southwest Laramide contraction. The relative concentrations of fault parallel and fault perpendicular joints and fractures differ between the footwall and hanging wall.  The footwall has a stronger concentration of fault perpendicular joints and fractures, suggesting more contraction deformation in the footwall.  The hanging wall displays a stronger relative concentration of fault parallel features, suggesting extensional deformation is concentrated within the hanging wall.

 The observed northwest-southeast, fault-parallel orientation of joints, veins, and fractures, and hanging wall normal faults suggest northeast-southwest extension normal to the Palisades fault.  The Palisades structures do not require separate structural

Table 2. Summary of preferred orientations for structural features within each domain of the Palisades fault zone.

| | Joints Preferred Orientations | | Veins Preferred Orientation | | Faults Preferred Orientation | Unclassified Fractures Preferred Orientation | |
| --- | --- | --- | --- | --- | --- | --- | --- |
| | Present horizontal orientation frame | Bedding reference | Present horizontal orientation frame | Bedding reference | (all faults) | Present horizontal orientation frame | Bedding reference |
| **Hanging wall** 86 joints 56 veins 44 faults 89 fractures | N56W, 90 N64E, 90 | N51W, 90 N45E, 90 | N57W, 90 | N58W, 90 | N50W, 76S N50W, 80N (mostly normal) | N47W, 90 N15E, 78W | N/A |
| **Fault zone (Shinumo)** 57 veins 10 faults 10 fractures | N/A | N/A | N50W, 90 (dip range ± 30°) | N/A | no preferred orientation | no preferred orientation | N/A |
| **Vertical Footwall Limb** 7 veins 17 faults 2 fractures | N/A | N/A | N70W, 60S | N75W, 72N | N42W, 34S (synthetic) N35W, 28N (antithetic) (mostly reverse) | N/A | N/A |
| **Northeast – Dipping Footwall Limb** 84 joints 7 veins 8 faults 146 fractures | N23E, 72W N62W, 34S | N20E, 90 N55W, 82S | N80W, 47S (dip range ± 17°) | N70W, 90 | no preferred orientation | N15E, 78W N71E, 78S N60W, 65S | N5E, 90 N75E, 90 N55W, 90 |
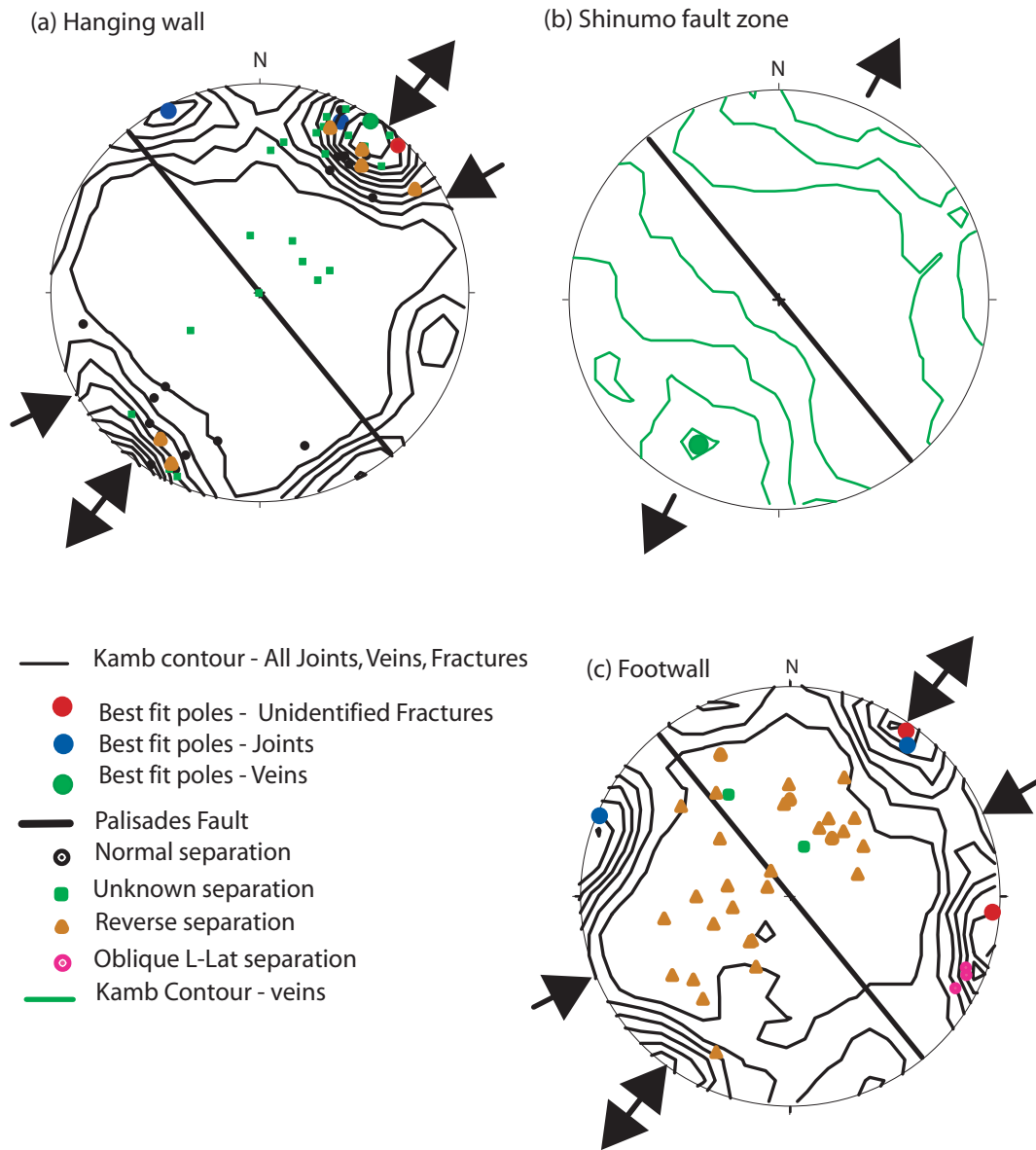
Fig. 27. Stereonet plot summary of the structural fabric across the Palisades fault. (a) Hanging wall fabric. (b) Shinumo fault zone. (c) Entire footwall. Poles to all measured joints, veins and fractures are contoured, with the best-fit poles for prominent sets of each. Both the hanging wall and footwall, have a dominant set of joints, veins, and fractures parallel the Palisades fault suggestiing NE-SW extension (black arrows), which is consistent with Timmons et al. (2003). Reverse faults in both the hanging wall and footwall and the secondary joint set suggest a horizontal NE-SW contraction axis (black arrows), which is generally consistent with N67W contraction axis (grey arrows) suggested by Reches (1978). Stereonet plots are equal area, lower hemisphere projections, Kamb contour with contour interval of 2σ.

signatures for the multiple extension phases as suggested for regional deformation by Timmons et al. (2001).  The consistent northwest orientation of joints, faults, veins and fractures implies concurrent formation during the early 1.1 b.y. extension episode.  It is possible that the later, more east-west 0.8 b.y. extension episode did not locally overprint a new structural fabric, but opened or sealed existing fractures and may explain the parallel orientation of joints and veins.  While parallel veins and joints do exist at the same locations, the concentration of veins decreases with increasing distance from the fault zone, possibly indicating fault zone controlled fluids could only seal joints within and immediately adjacent to the fault (Fig. 28).

There is consistent and similar orientation of faults with both normal and reverse separation within the hanging wall (Fig. 27).  The high angle, northwest striking normal faults are consistent with formation during northeast-southwest Precambrian extension.  The high angle reverse faults suggest contraction, but are not consistent with low angle thrust faults found elsewhere in the Precambrian and Paleozoic formations of the Grand Canyon (Huntoon, 2003).  Mohr-Coulomb failure criterion does not predict formation of high angle reverse faults in response to the sub-horizontal Laramide contraction axis determined by Reches (1978) or Anderson and Barnhard (1986), but the criterion does suggest that reverse slip could be induced on existing high angle faults, joints or fractures during horizontal contraction (e.g. Handin, 1969; Jaeger and Cook, 1976, Sibson, 1985).  These high angle faults with reverse separation are interpreted to be Precambrian normal faults that have been reverse-reactivated during Laramide deformation.  The northwest strike of reverse-reactivated hanging wall faults and northeast strike of the secondary joint set are consistent with horizontal, N67W contraction suggested by Reches (1978).  The low angle thrust faults in the footwall may represent a conjugate pair (Fig. 27), which would indicate a horizontal, northeast-southwest contraction axis consistent with that of Reches (1978).

The structural fabric within the Precambrian formations of the Palisades Monocline is consistent with northeast-southwest Precambrian extension suggested by

Fig. 28. Histogram plot of the distribution of open fractures and veins in the Palisades fault zone and hanging wall domain.

Timmons et al. (2001) and northeast-southwest Laramide contraction suggested both locally (Reches, 1978) and regionally (Fig. 27; Anderson and Barnhard, 1986). The Precambrian formations of the Palisades Monocline have been deformed during the two distinct phases of nearly co-axial, positive inversion.

CHAPTER IV

DISCUSSION

**1. Kinematic Model**

The juxtaposition of the Comanche Point member of the Dox Formation in the hanging wall with the Shinumo ore body consisting of the clay-rich, brown, quartz sandstone unit indicates 850 to 1000 m of normal separation (Fig. 7). This estimate is consistent with the 950 m of Precambrian normal displacement suggested by Reches (1978), and implies minimal Laramide reverse-reactivation of the hanging wall boundary fault. The structural offset of the clay-rich, brown, quartz sandstone of the Shinumo ore body across the central fault surface from the top Shinumo "quartzite" unit indicates less than 250 m reverse displacement (Fig. 7). The footwall boundary fault juxtaposes the Shinumo "quartzite" unit in the hanging wall against the Escalante Creek member of the Dox Formation in the footwall, and indicates less than 300 m of reverse offset (Fig. 7). The 80 to 88 m of reverse fault displacement of the entire fault zone reported by Reches (1978) falls under the 550 m maximum estimate of reverse fault displacement, but it is not possible to better constrain fault displacement on either domain boundary fault without more detailed study of the stratigraphy of the Shinumo and Dox Formations. Even without such information, it is possible to infer that the majority of the reverse fault displacement occurred along the central and footwall boundary faults.

This interpretation suggests that the Shinumo blocks in the fault zone were in the footwall during Precambrian normal faulting, and then incorporated into the hanging wall during Laramide reverse faulting. Most of the 80 to 88 m of Laramide reverse slip was accommodated along the central and footwall faults (Fig. 29). The Shinumo block acted as a relatively rigid block pushing into and concentrating deformation in the footwall, as indicated by footwall folding and thrust faulting. The hanging wall boundary fault primarily indicates normal shear sense of secondary, Z-shaped foliation
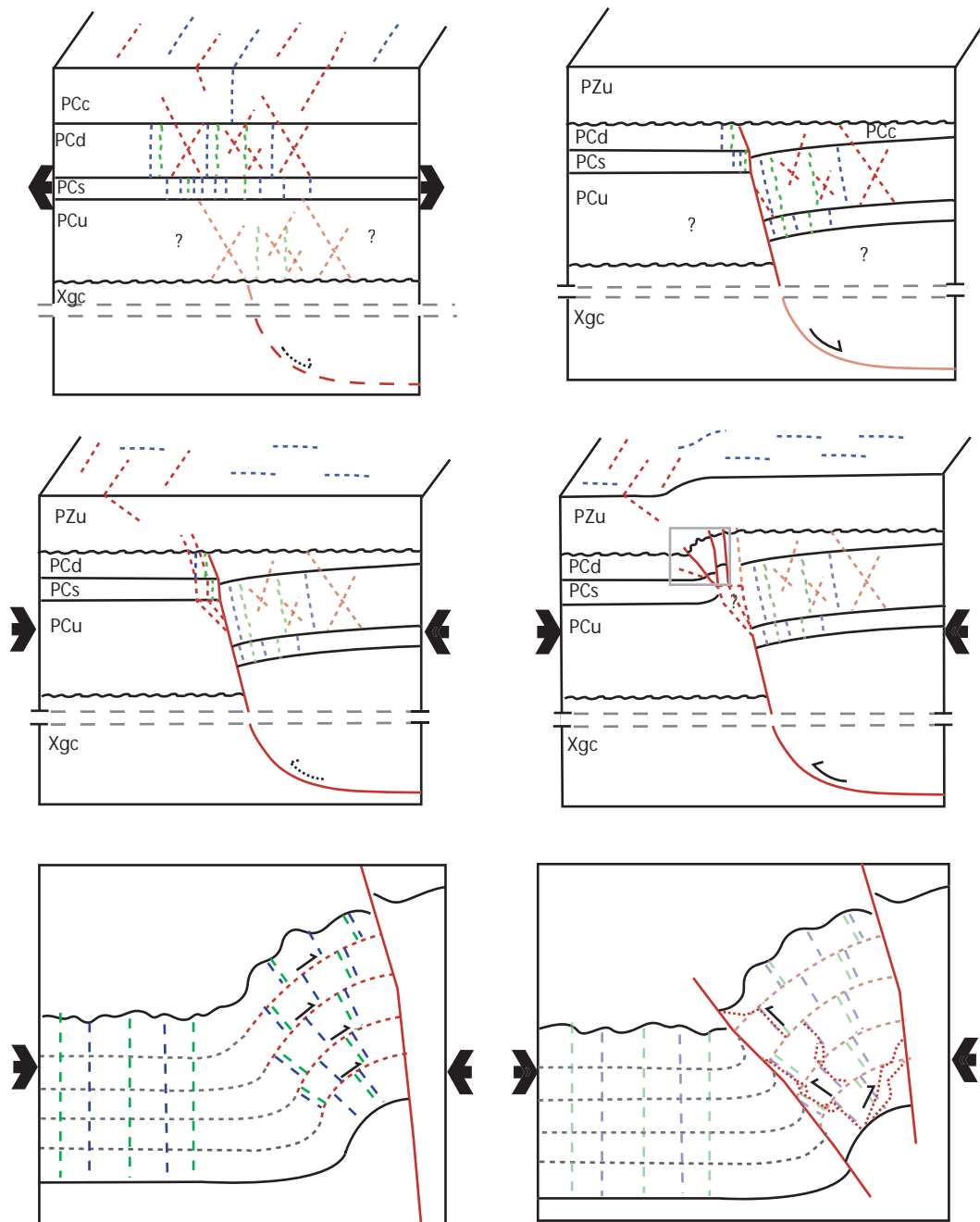
Fig. 29. Schematic interpretation of the development of the Palisades Monocline. (a) Precambrian extension induced normal faulting and opening mode deformtation such as veins and joints. (b) Extensional deformation is concentrated within the hanging wall and master normal fault rotated the hanging wall. (c) and (d) Laramide contraction caused reverse movement along basement fault, near vertical uplift of the hanging wall and reverse, short-cut faults in the footwall. (e) and (f) Detailed interpretation of deformation withing the Dox formation: contraction induced flexural slip folding which offset bedding perpendicular joints and veins. As fold tightened, synthetic and antithetic thrust faults reactivate joint, vein and bedding sufaces.

folds (Fig. 16), although Reches' (1978) geologic map displays reverse separation across the fault to the southeast (Fig. 9).

The relationship between thrust faults and folds was partially controlled by the previously formed joints and veins.  In the northeast-dipping limb of the footwall fold, there is right lateral offset across bedding layers as a consequence of flexural-slip (Fig. 30; e.g. Donath and Parker, 1964; Ramsay, 1967; Chapple and Spang, 1974; Tanner, 1989).  The folding rotated the bedding perpendicular joints and veins into a favorable orientation for reactivation as reverse faults during horizontal contraction (e.g. Segall and Pollard, 1983; Wilkins et al., 2001; Silliphant et al., 2002; Bergbauer and Pollard, 2004), but the surfaces are discontinuous and terminate into bedding.  Footwall cross-cutting relationships suggests bedding parallel slip offset joints and veins, although there are no slip lineations to support this inference.  Southwest-dipping thrust faults, most of which were reactivated joints and veins (Figs. 22 and 23), do not terminate against bedding surfaces and post-date the inferred bedding parallel slip.  Although the southwest-dipping reverse faults may have propagated through bedding surfaces, they often linked into and transferred shear displacement to other faulted joints and veins. With continued strain, the linked faults may have developed into a shear zone of intense deformation as seen along the syncline-anticline boundary (Fig. 24; Martel et al., 1988). It is possible that increased localization of shear in this area may have been influenced by the presence of the intrusion.

In addition to synthetic, southwest-dipping thrusts reactivating joints and veins, northeast dipping antithetic thrusts are also common, especially within the lower, tightly folded layers of the footwall anticline (Fig. 21).  These antithetic thrusts offset veins and reduction bands, and cut through bedding layers implying post-fold faulting.  Existing joint and vein features did not control the northeast-dipping, antithetic faults, because most are located within the northeast-dipping limb of the anticline fold where existing joints and veins have southwest dip.  Instead, the northeast-dipping antithetic thrusts often propagated through, and occasionally along, northeast-dipping bedding surfaces.

Outcrop investigation found only three specific examples to study cross-cutting relationships between synthetic and antithetic thrusts, and these examples suggest concurrent formation of thrusts.  It is unclear whether the footwall thrust faults were the result of far-field, horizontal Laramide compression, localized stress due to flexural slip folding, or some combination of both.  Concurrent formation of the thrusts might indicate tightening of the footwall syncline fold as it began to bind and inhibit flexural-slip, which resulted in intrabed faulting from horizontal Laramide compression (e.g. Ramsay, 1967; Gutierrez-Alonso and Gross, 1999).  Analysis of the synthetic and antithetic thrusts indicates a possible conjugate pair with a horizontal, northeast-southwest, maximum compressive stress that is consistent with the Laramide deformation (Fig. 30; Reches, 1978; Anderson and Barnhard, 1986).  Numerical investigation of single layer folding suggests maximum compressive stress trajectories that could cause the antithetic thrust orientation, and may explain the increased density of antithetic thrusts at stations 1, 2, 2A and 3 in the steeply dipping and overturned section of the fold limb (Figs. 13 and 20; Chapple and Spang, 1974).  It is most likely that some combination of both far-field compression and localized folding were responsible for the footwall thrusts.  The synthetic faults only occurred along reactivated joints and veins that were optimally oriented for shear under Laramide compression, whereas layer folding may have been responsible for antithetic thrusts.

In conclusion, Precambrian extension at 1.1 b.y. (and possibly 0.8 b.y.) caused the formation of the Palisades fault and 950 m of normal slip, along with distributed vertical joints and veins perpendicular to the northeast-southwest extension axis. Concurrent northeast trending contraction features suggested by Timmons et al. (2001) are not present, and there was minimal subsequent deformation until Laramide contraction.  Contractional deformation within the Precambrian formations supports co-axial inversion with northeast-southwest contraction as identified within the overlying Paleozoic formations (Reches, 1978).  During contraction there was widespread vertical jointing parallel to the contraction direction and concentrated deformation in the footwall
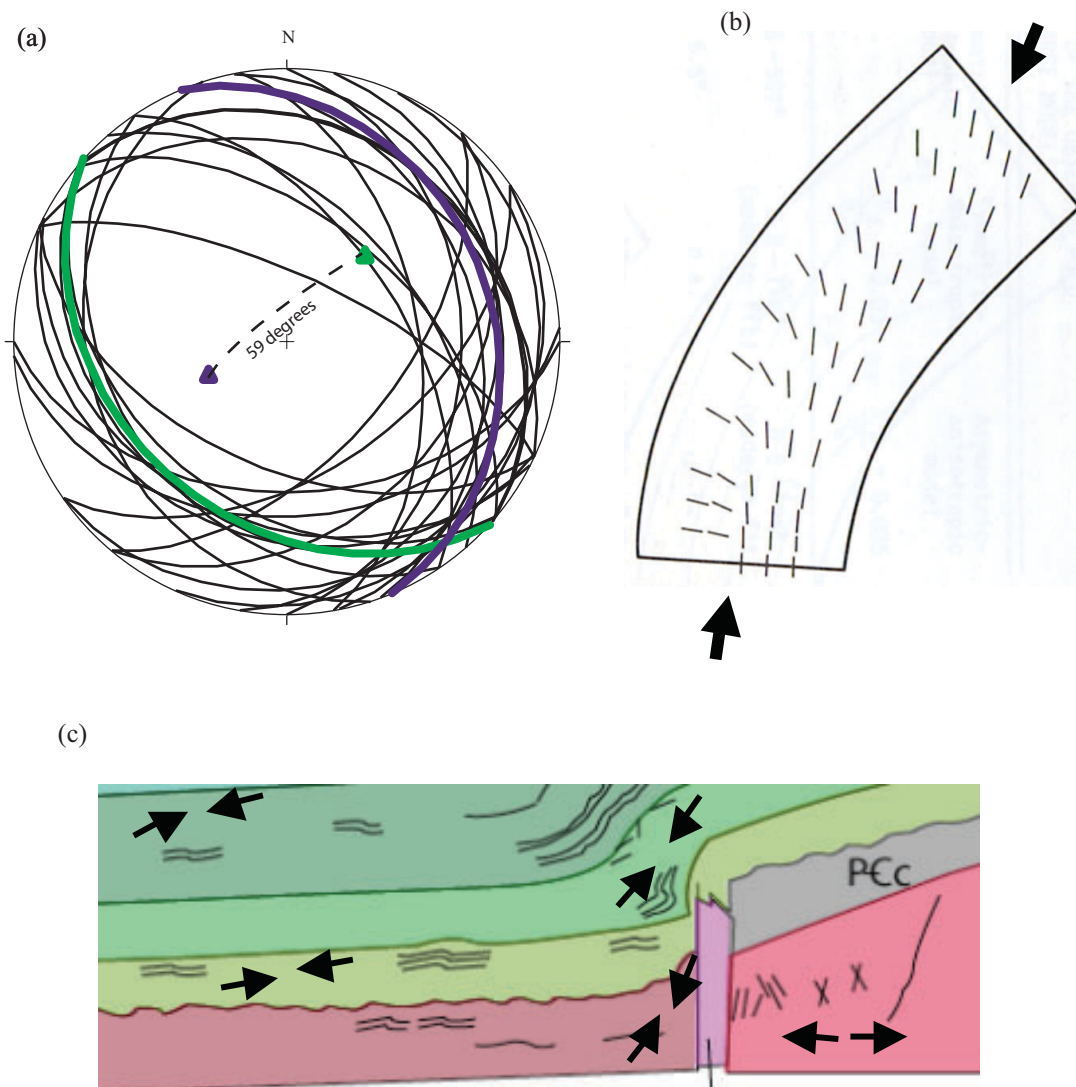
Fig. 30. Comparison of Palisades footwall reverse faults with stress field induced from single layer folding. (a) Stereonet plot of all footwall reverse faults suggests conjugate set and may imply a NE-SW horizontal greatest compressive stress during Laramide formation. (b) Stress field induced from single layer folding may have controlled reverse fault formation as suggested by Chapple and Spang (1974). (c) Local stress field in the footwall of the Palisades fault zone determined by Reches (1978) is consistent with fold induced faulting. Green great circles represents synthetic thrusts, blue represents antithetic thrusts. Stereonet plot is lower hemisphere projection.

including folding, reverse faulting and reverse reactivation of existing structures. Flexural-slip folding rotated bedding and existing joints and veins, while offsetting the joints and veins across bedding. As folding tightened and inhibited flexural-slip, thrust faulting cut through folded bedding, veins, reduction bands and deformation bands. Synthetic thrusts often formed along existing joint surfaces and veins that had been rotated into optimal shear orientation, while fold-induced antithetic thrusts were less controlled by existing structures, but occasionally followed bedding surfaces. The last, and only partially or locally developed, stage of deformation was through going, synthetic reverse faults and shear zones within the footwall, as seen along the boundary between the vertical and northeast dipping footwall fold limbs (Fig. 24).

## 2. Comparison to Physical Models

Comparison of a natural example of positive inversion with physical models of positive inversion provides insight into inversion development and kinematic processes. During northeast-southwest directed Precambrian extension, the Palisades fault underwent approximately 950 m of normal offset, followed by 250 m of Larmide reverse uplift (which includes faulting, flexure and tilt), or approximately 25% inversion recovery based on total vertical throw across the monocline (Reches, 1978). The inversion recovery achieved by reverse slip along the Palisades fault zone was 88 m of the original 950 m of normal slip, or less than 10% inversion. Because throw across the vertical Palisades fault zone does not accommodate horizontal shortening, it is difficult to compare with physical models (e.g. Buchanan and McClay, 1991; Mitra, 1993; Eisenstadt and Withjack, 1995; Kuhle, 2001) that identify strain and percent inversion recovery from horizontal displacement of forcing blocks along pre-cut faults. Additionally, Reches (1978) describes layer thickness changes of the Bright Angel shale and Redwall limestone, and compactive cataclastic flow features within the Redwall limestone that indicate horizontal shortening during vertical movement along the Palisades fault. The difficulties in resolving horizontal strain in the Palisades Monocline

encourages comparison with a range of model recovery percentages and to different stages of kinematic development. Model inversion values are helpful to understand the relative kinematic development of different physical models, but caution must be used when comparing percent inversion recovery with the estimated values from the vertical throw of the Palisades monocline.

Reches (1978) concludes a Laramide shortening axis of 08$^o$ N67E, which is nearly co-axial to the northeast-southwest extension axis suggested by Timmons et al. (2003) and is 20$^o$ from normal to the Palisades fault. Both Reches (1978) and this study did not find significant evidence of strike-slip faulting or other out of plane deformation at the Palisades Monocline, as indicated by reverse slip on small faults and Palisades fault parallel axial planes for the overlying monocline flexure. Although other regional studies of Laramide monoclines suggest out of plane strain is significant (e.g. Tindall and Davis, 1999; Bump and Davis, 2003), the Palisades Monocline appears to accommodate mostly in plane deformation and provides a valid comparison with physical models of co-axial inversion.

Ideally, models chosen for direct comparison would be defined by co-axial inversion of a near vertical fault normal fault (at the surface), model materials that display a similar mechanical response to the Dox Formation interbedded sandstones and shales at approximately 3 km of burial, and allow for footwall and hanging wall deformation. Due to experimental set-up constraints, and the specific goals of the modeler, many models do not include all of these features, but do provide for investigation of at least one feature consistent with the Palisades area. Specific models chosen for comparison are the sand models of Buchanan and McClay (1991), the clay layer models of both Eisenstadt and Withjack (1995) and Mitra (1993), and the solid rock models of Kuhle (2001). Some models use a non-deformable, or rigid, footwall below a predetermined fault surface (e.g. Keller and McClay, 1995; Buchanan and McClay, 1991; Mitra and Islam, 1994; McClay, 1995), which is not consistent with the folded and fractured Dox formation in the footwall of the Palisades fault. Other

conditions to consider when comparing models include the geometry of the fault or forcing blocks (e.g. listric or ramp, dip angle), model material and cohesiveness, confining pressure, and extensional structures that may control subsequent contractional features (e.g. Koopman et al., 1991).

*2.1 Comparison to Sandbox Models*

The sandbox models of Buchanan and McClay (1991) use layers of sand and mica against a rigid footwall to investigate hanging wall deformation throughout the inversion process. After 35% extension, the models display roll-over similar to the Palisades hanging wall and the formation of normal faults and grabens (Fig. 3). During contraction, some of the hanging wall faults are reactivated in a reverse sense as inferred at the Palisades Monocline (Fig. 3). The sandbox models display low angle reverse faults along rotated hanging wall bedding planes that suggest deformation processes similar to the reactivation of rotated joints and veins in the Palisades footwall, and imply that rotation of existing planar features is an important factor during contractional deformation. The inconsistencies between the sandbox models and the Palisades study area include: 1) reverse reactivation of normal faults, including the master normal fault, appears to accommodate more contractional strain in the models than seen at the Palisades study area; and 2) the Palisades hanging wall does not display low angle, back-thrusts as suggested by the models. These inconsistencies are possibly explained by the rigid footwall of the models, which require all contractional strain to be accommodated along the fault surface and within the hanging wall.

*2.2 Comparison to Clay Models*

Mitra (1993) and Eisenstadt and Withjack (1995) use layered clay to model inversion. The specific difference between the models includes the use of a pre-cut fault during both extension and contraction (Fig. 4; Mitra, 1993) in contrast to unassisted development of extensional and contractional features (Fig. 31; Eisenstadt and Withjack,

(a)



1 cm

(b)



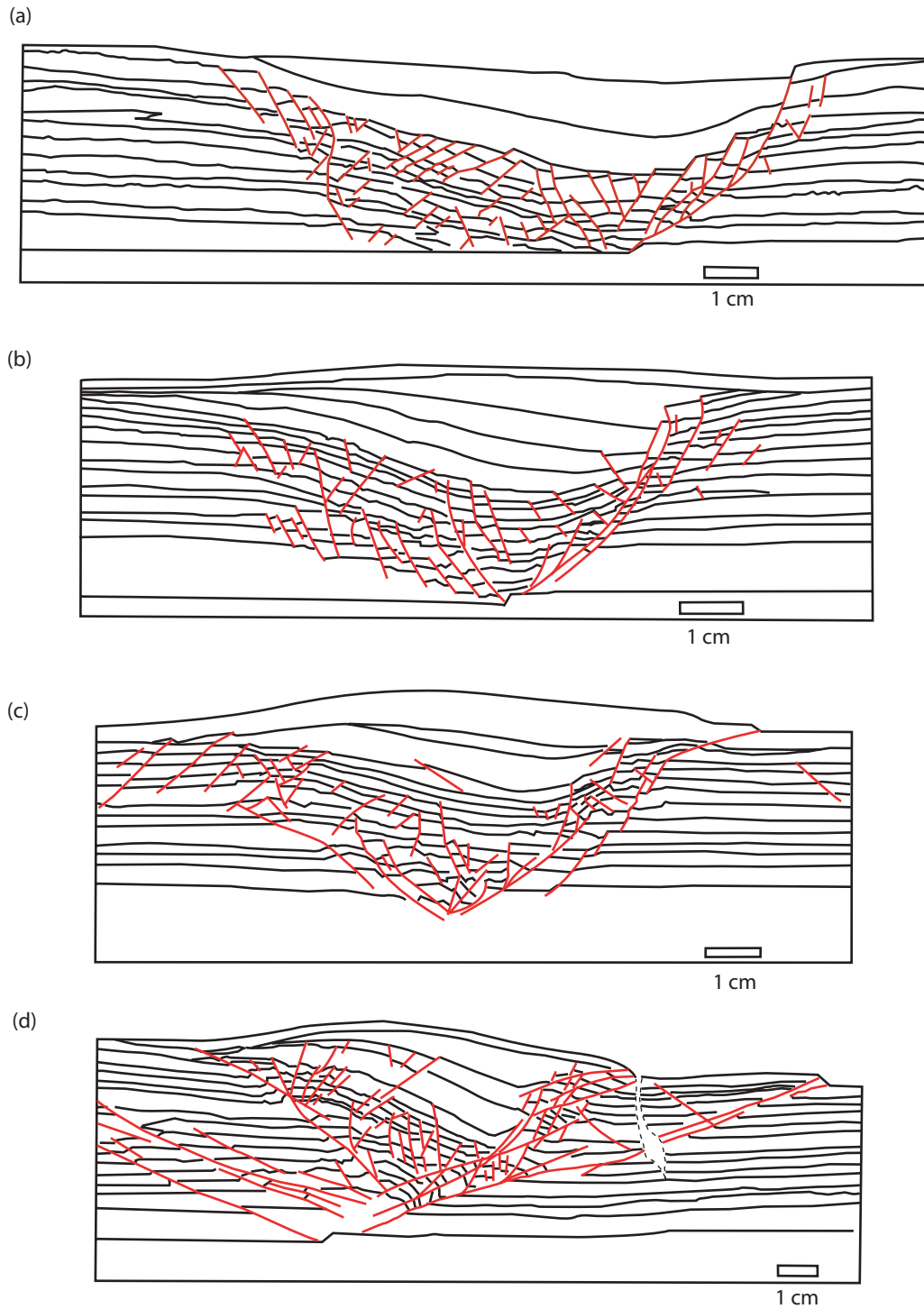1 cm

(c)



1 cm

(d)



1 cm

Fig. 31. Line drawing interpretation of a clay model of positive inversion without a pre-cut fault. (a) Post-extension geometry (4 cm extension) including syn-extension deposition. (b), (c), and (d) Geometry after 50%, 100% and 200% inversion. Red lines indicate faults (from Eisenstadt and Withjack, 1995).

1995).  The fault break-through model of Mitra (1993) requires sufficient extension that a master normal fault develops which offsets the entire layered sequence, as seen at the Palisades Monocline.  Extension features that are similar to the Palisades Monocline include hanging wall rotation towards the footwall, and localization of all normal faults in the hanging wall.  During contraction, there is both reverse reactivation of existing faults and formation of low angle footwall reverse faults that break-through the entire sequence and localize slip.   Mitra (1993) defines three zones of distinct movement that compare favorable with the Palisades fault zone: 1) the hanging wall which moves parallel to the fault plane; 2) the footwall which moves horizontally; and 3) a wedge-shaped fault zone where individual particles move in a concave down, arcuate path.  The final model geometry (Fig. 4) is strikingly similar to Reches' (1978) Palisades Monocline cross-section interpretation, although there is more master fault reactivation. The development of the model parallels the inferred kinematic development of the Palisades Monocline, even though many of the deformation processes within the model take place at magnitudes of inversion over 100%.

Although it is difficult to compare the amount of strain and recovery between the models and the Palisades monocline, it appears that model development of inversion structures requires more inversion recovery than at the Palisades monocline.  The models of Eisenstadt and Withjack (1995) develop footwall folding and thrust faulting similar to the Palisades study area, but at 100% to 200% recovery (Fig. 31).  Eisenstadt and Withjack (1995) suggest their clay models are more likely to reactivate existing faults than produce new reverse faults when compared to cohesionless sand models, which would delay development of new contractional features until larger recovery is achieved. But if the cohesion of the clay encourages fault reactivation, there would not be the significant contractional hanging wall deformation described in the clay models that is not described in the sand box models.

*2.3 Comparison to Rock Models Deformed at Confining Pressure*

Kuhle (2001) deforms solid rock material at confining pressure in a tri-axial deformation apparatus.  In order to maintain a mechanical response consistent with constant burial depth during both phases of inversion, Kuhle (2001) deforms a single layer (1 x 2 x 5.6 cm) of Indiana limestone at a 100 MPa during extension (18% axial strain), and 25 MPa during contractional inversion of up to 165% recovery (Fig. 5).  The use of solid rock material allows for petrofabric study of microfractures in addition to faulting and folding (Fig. 6).

The extensional features compare well with the inferred Palisades extensional geometry, including the formation of a slightly listric, 70° dipping, normal fault (master fault) that offsets the limestone layer by 3 mm and an antithetic, graben forming normal fault in the hanging wall (Fig. 5).  Microfracture dip orientations within the models indicate sub-horizontal extension in both the hanging wall and footwall domains as inferred across the Palisades fault (Fig. 6).  During contraction, the rock models develop three domains of deformation compatible with the Palisades fault zone: 1) the hanging wall, 2) the footwall, and 3) an uplifted wedge bounded between the master normal fault on the hanging wall side and a new system of footwall reverse faults.  Similar contraction and inversion features include minimal hanging wall deformation, and new, low angle, synthetic footwall reverse faults that accommodate contraction. Microfracture study indicates a horizontal compressive in the footwall identical to that inferred from faults in the Palisades footwall.  At 38% recovery, footwall microfractures display the co-existent extension and contraction orientations, which may parallel the co-existence of extensional joints and veins with contractional folding and low angle reverse faults in the footwall of the Palisades fault.  Model features that are inconsistent with the Palisades study area include: 1) lack of footwall folding, although the footwall in the model is not layered with weak layers that would enhance flexural slip; 2) lack of footwall antithetic reverse faults, which without folding, were not able to reactivate

rotated bedding planes; and 3) more reverse reactivation of the master normal fault than at Palisades study area.

*2.4 Comparison Summary*

There are many similarities between the structures and inferred kinematic model of the Palisades Monocline and the kinematic development of physical models, regardless of physical and mechanical properties of model materials. In general, the hanging wall is dominated by extensional deformation with limited contractional deformation (assuming non-rigid footwall), although some sandbox and clay layered models display hanging wall back-thrusts. Common hanging wall features in both settings include high angle, conjugate normal faults, near vertical opening mode fractures and hanging wall rollover towards the fault zone. Footwall domain comparisons are more difficult, as many models incorporate a rigid, non-deformable footwall, and/or focus attention to the hangingwall growth stratigraphy. In general, the footwall displays more distributed deformation with contractional features such as synclinal folding and low angle thrust faults that 'short-cut' the upper footwall corner. The most striking geometrical similarity between models of all materials and the Palisades fault is an uplifted, central wedge bounded by the hanging wall, master normal fault, and lower angle, footwall, 'short-cut' reverse faults. At the Palisades fault, the blocks of Shinumo Formation may be approximated as the uplifted wedge or 'pop-up' structure, bounded by the hangingwall normal fault, and footwall thrust faults.

Extension is accommodated mostly by normal slip on a master fault and is accompanied by high angle normal faulting or near vertical opening mode fracture, depending on the model material properties. The evolution of inversion is more difficult to constrain, but the kinematic interpretation of the Palisades fault zone corresponds well with physical models, especially those deformed at confining pressure (e.g. Kuhle, 2001) or with model material capable of folding (e.g. Eisenstadt and Withjack, 1995). This similarity suggests increased mean stress or temperature during inversion did not allow

for reactivation of the master normal fault, and promoted flexural-slip folding of the footwall. However, the cause of increased mean stress or temperature is not known, and multiple possibilities exist: 1) The effect of 3000 m of overburden, 2) thermal increase also associated with hydrothermal activity, and 3) increased footwall stress due to relatively rigid, hanging wall Shinumo blocks thrusting over (or into) the footwall Dox Formation. Physical models also support the sequential formation of synthetic, footwall thrust faults, each one forming farther from the master fault and widening the fault zone in the footwall direction.

While the physical models compare favorably with the Palisades Monocline, there are some discrepancies between them, many of which may be related to the mechanical properties of the deforming model materials as compared to the Palisades stratigraphic sequence. Most notably, the differences are most often found in the hanging wall domain, where the Palisades Monocline does not display antithetic back-thrusts and there is minimal to no reactivation of the master normal fault during contraction. This implies kinematic developement of the fault zone and Shinumo domains that is consistent with the solid rock models of Kuhle (2000), and is inconsistent with 'pop-up' structures or inverted grabens as identified by McClay (1995) that require reactivation of the master normal fault. Also common in many of the sandbox models is a large, hanging wall graben bounded between the master normal fault and a large antithetic normal fault. Many hanging wall conjugate normal faults form grabens in the Dox Formation, but are orders of magnitude smaller than the Palisades fault. Finally, the development of recognized inversion features at the Palisades Monocline occurs at relatively lower magnitudes of inversion than suggested by physical models of all materials.

**3. Comparison to Numerical Models**

Mathematical and physical models have investigated the stress field and potential failure of rock layers above a non-deformable, basement-block fault of varying dip

angles (Patton and Fletcher, 1995; Gangi et al., 1977). The models considered here do not investigate the two-phase process of inversion, but these single-phase models provide insight into deformation during horizontal contraction and vertical block motion for the Palisades fault zone. Patton and Fletcher (1995) use an analytic series solution of incompressible viscous fluid to model a 45° reverse fault and vertical block motion, while Gangi et al. (1977) presents an analytical solution for the stresses at the initiation of failure for an isotropic elastic layer above a 65° dipping reverse fault. The results of both Patton and Fletcher (1995) and Gangi et al. (1977) indicate that the maximum compressive stress trajectories predict upward propagation of the fault along a curved fault trajectory, concave towards the footwall, from a near vertical orientation at the initial fault tip (Fig. 32). The initial, near vertical dip of the expected failure occurs for 45° reverse fault (Patton and Fletcher, 1995), 65° reverse fault (Gangi et al., 1977) and the vertical fault models (Patton and Fletcher, 1995). Due to the upward flattening of the arcuate failure, Gangi et al. (1977) suggest a sequential formation of arcuate faults with increasing strain that emanate from near the tip of the basement fault.

These results agree with stress trajectories inferred through petrofabric study of single-phase physical models with 60° reverse fault (Friedman et al., 1976), and vertical fault (Logan et al., 1978). Inconsistencies are found in the footwall, lateral to the vertical failure zone, where both analytical solutions suggest near horizontal maximum compressive stress, but the physical models indicate high angle to near vertical stress trajectories. Patton and Fletcher (1995) suggest an experimental condition may not have been accounted for in the model, or discrepancies between the stress fields may be due to evolution of the physical models during continuing strain. Important factors that may need to be accounted for in the analytical models include confining pressure and effect of the intermediate stress.

In comparison with the Palisades fault zone, the analytical models are consistent with high angle, reverse basement faulting that results in the sequential formation of sub-vertical faults in the footwall direction. The predicted failures emanate from near the
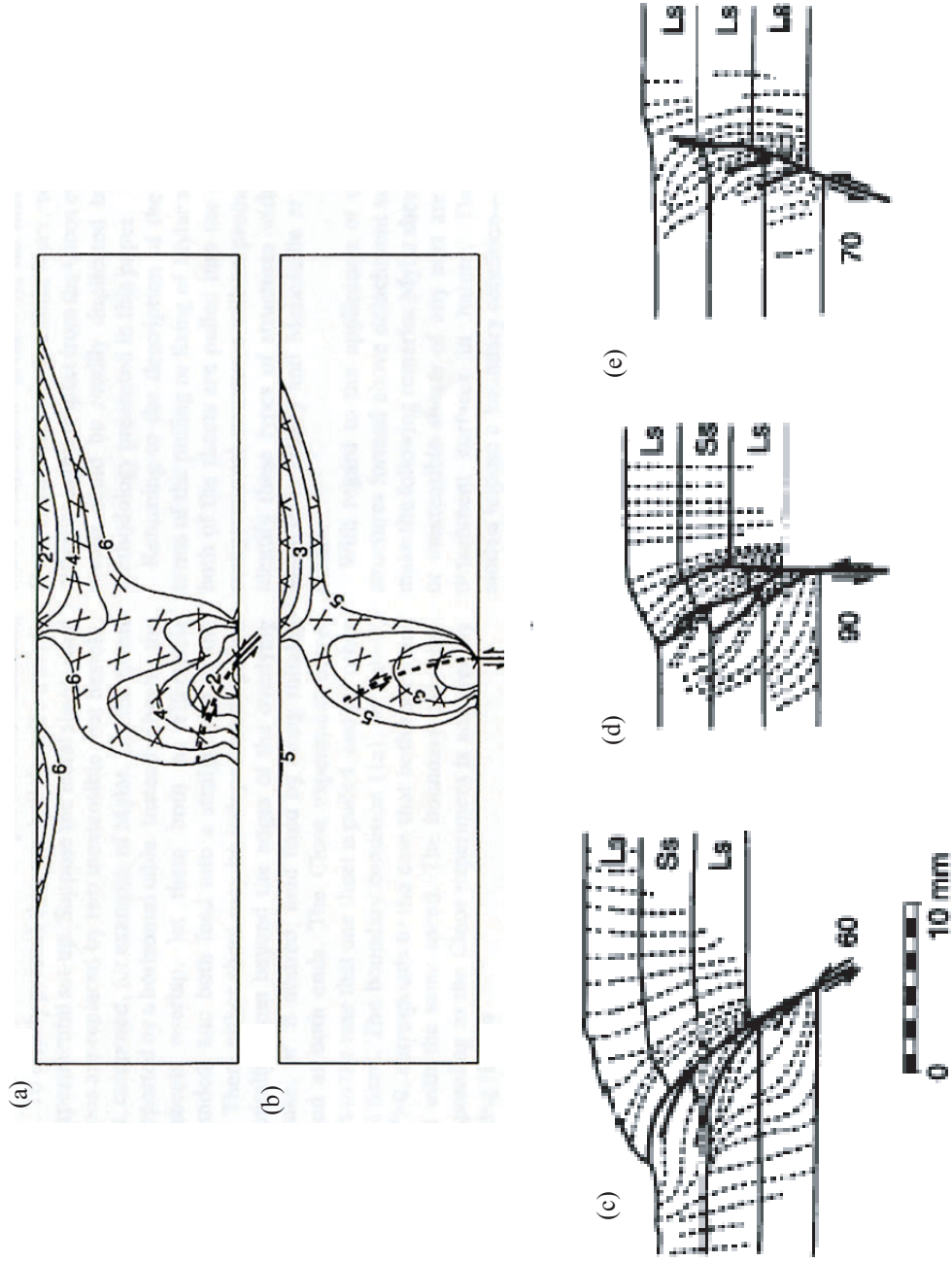
Fig. 32. Comparison of theoretical and experimental failure in rock layer above basement fault. Analytical series solution from Patton and Fletcher (1995) for (a) 45° reverse fault and (b) vertical fault. Physical models of rock material including (c) Friedman et al. (1976), (d) Logan et al. (1978) and (e) Patton (1984) (after Patton and Fletcher, 1995).

uplifting basement block tip, and may correlate with the three fault surfaces of the Palisades fault that bound the two uplifted blocks of Shinumo formation in the interior of the fault zone. The vertical, planar nature of the faults within the Palisades fault zone does not agree with the arcuate nature predicted by the models, but the models only predict initial failure, not the evolution of the failure. In addition, the models do not take into consideration pre-existing extensional structures that may act as perturbations or be reactivated during the contractional state.

**4. Horizontal Compression and Vertical Block Motion**

Reches (1978) concludes a sub-horizontal, Laramide compression axis plunging $8^o$ in the direction of N67E for the Palisades monocline from structural analysis of small faults and folds, calcite twinning, kink bands within the Paleozoic formations. Mohr-Coulomb failure suggests high angle faults, such as the Palisades fault zone, are not optimally oriented for reverse slip during horizontal compression, although experimental studies demonstrate uniaxial contraction can cause slip on an existing plane oriented at a high angle to the contraction axis (e.g. Brun and Nalpas, 1996; Sassi et al., 1993, Kuhle, 2001). Propensity for fault reactivation has been analyzed both experimentally and theoretically using Mohr-Coulomb failure, and these studies suggest the orientation of maximum compressive stress with respect to a pre-existing fracture plane is a critical parameter (e.g. Handin, 1969; Jaeger and Cook, 1976; Sibson, 1985). Existing fractures in the Palisades study area will have a propensity for reactivation if they are oriented at $12^o$ to $42^o$ to the maximum compressive stress direction of the Palisades area (Sibson, 1990), but it has been noted that Precambrian normal faults were not favorably oriented for reverse-reactivation with respect to the Laramide stress state (Reches, 1978). If Mohr-Coloumb failure and two-dimensional strain is assumed, these features should not have been reactivated as reverse faults except under conditions of high pore fluid pressure (Sibson, 1990). Assuming that the least compressive stress was vertical during Laramide compression, then increased pore fluid pressure would reduce or could

effectively offset (effective pressure law) the lithostatic overburden, which Sibson (1990) suggests might result in hydrofracturing and the formation of horizontal veins concurrent with reverse displacement on the fault.  It is difficult to determine the pore fluid pressure during Laramide compression, but there is no indication of the horizontal veins or hydrofracturing suggested by Sibson (1990).  Additionally, physical models deformed at confining pressure (Kuhle, 2001) suggest increased fluid pressure is not necessary to reactivate steeply dipping faults during horizontal contraction.

Thus the question remains: How does horizontal Laramide contraction induce reverse slip on high angle normal faults?  Reches (1978) addresses these issues by suggesting two independent, but simultaneous processes occur: 1) horizontal compression, and 2) vertical uplift along the presumably weak, gouge filled Palisades fault.  Reches (1978) concludes that vertical movement along the fault could not independently create the sub-horizontal, layer parallel shortening indicated by structural analysis of subsidiary features, and that horizontal compression was not large enough to lock the fault through increasing normal stress and shear strength.

The current understanding of Laramide basement fault geometry indicates a listric or flattening fault dip with depth, which implies a more optimal orientation for fault reactivation under horizontal compression (e.g. Brown, 1993).  Assuming the deep but flat, decollment nature of these faults is significantly longer than the near surface, steeply dipping sections, it is possible to consider the near vertical section as a small restraining bend along an otherwise well-oriented fault for horizontal compression.  Other possible insight comes from numerical models, which indicate initial failure is vertical for layers overlying high angle basement faults of (Gangi et al., 1977; Patton and Fletcher, 1995).  Once deformation has begun, the local stress associated vertical block motion may modify or drown the far-field stress, and will also be complicated by perturbations due to existing and presently forming structures (e.g. anisotropic layering, fractures).  In other words, deformation close to or immediately above the fault is indicative of motion along the fault, but deformation laterally outside of that area is

indicative of a more far-field stress (e.g. Chester and Logan, 1987). The consistent orientation, spacing and shear sense of basement-derived deformation in the Colorado Plateau and the Grand Canyon suggests the Palisades monocline is indicative of regional Laramide deformation.

CHAPTER V

CONCLUSIONS

The Palisades Monocline and underlying fault zone demonstrate kinematic evolution and deformation associated with positive inversion. The structural features associated with the Palisades Monocline and underlying fault zone are consistent with physical and numerical models of positive inversion and basement induced fault-propagation folds during horizontal contraction.

1) The structural fabric within the Precambrian formations is consistent with coaxial, positive inversion. The inferred northeast-southwest, horizontal Precambrian extension axis is consistent with regional tectonic events (Timmons et al., 2001), and the inferred northeast-southwest, horizontal contraction axis is consistent with Laramide deformation identified in the overlying Paleozoic units (Reches, 1978).

2) The kinematic history of the Palisades fault zone includes 950 m of Precambrian normal faulting along the hanging wall boundary fault, hanging wall roll-over, vertical joints, veins and high angle normal faults. Subsequently, Laramide inversion induced footwall folding, faulting, and reactivation of existing features. Existing planes of weakness such as bedding horizons and joints were rotated during footwall folding, and then reactivated as low angle reverse faults. Two Laramide reverse faults developed in the footwall and accommodated the majority of the 80 to 88 m of slip reported by Reches (1978). These reverse faults uplifted the relatively oldest rocks, which are bounded within the center of the fault between the hanging wall and footwall.

3) The structural fabrics associated with the different phases of inversion are partitioned into the three deformation domains similar to that seen in previous physical models of inversion. Extensional features, such as hanging wall roll-

over, high angle joints and veins, and conjugate normal faults dominate the hanging wall. Contractional features including folds, reverse-reactivated faults and new thrust faults define footwall deformation. The central, up-lifted domains of relatively oldest rocks display both extension and contraction deformation features such as veins and thrust faults.

4) Although the Palisades fault zone has experienced 25% inversion recovery, there is consistent kinematic development with physical models of co-axial, positive inversion at over 50% recovery. Both the Palisades fault zone and physical models develop three domains of deformation within the fault zone: the hanging wall, the footwall, and interior fault-bounded, uplifted wedge. The fault-bounded wedge is uplifted through the formation of footwall bounding reverse faults that widen the fault zone in the footwall direction.

5) The reverse displacement induced along the vertical Palisades fault zone during horizontal Laramide compression is consistent with both physical and numerical models. Although vertical block motion during horizontal compression is not predicted directly by the Mohr-Coulomb criterion, physical models and analytical solutions (incorporating Mohr-Coulomb criterion) suggest maximum stress trajectories and near vertical failure above high angle basement faults that compare favorably with the Palisades fault zone.

# REFERENCES

Allmendinger, R. W., 2002. Allmendinger's Stereonet for Windows Version 1.1.6. Cornell University, Ithaca, New York.

Allmendinger, R. W. and Jordan, T. E., 1981. Mesozoic evolution, hinterland of the Sevier orogenic belt. Geology 9, 308-313.

Anderson, E. M., 1942. The dynamics of faulting and dyke formation with applications to Britain. Oliver and Boyd, Edinburgh.

Anderson, R. E. and Barnhard, D. P., 1986. Genetic relationship between faults and folds and determination of Laramide and neotectonic paleostress, western Colorado Plateau-transition zone, central Utah. Tectonics 5, 335-357.

Armstrong, R. L., 1968. Sevier orogenic belt in Nevada and Utah. Geological Society of America Bulletin 79, 429-447.

Bergbauer, S. and Pollard, D. D., 2004. A new conceptual fold-fracture model including prefolding joints, based on the Emigrant Gap anticline, Wyoming. Geological Society of America Bulletin 116, 294-307.

Beus, S. S. and Morales, M., 2003. Introducing the Grand Canyon. In: Beus, S. S. and Morales, M. (Eds.), Grand Canyon Geology, 2nd Editon. Oxford University Press, pp. 1-8.

Bowring, S. A. and Karlstrom, K. E., 1990. Growth, stablilization, and reactivation of Proterozoic lithosphere in the southwestern United States. Geology 18, 1203-1206.

Brown, W. G., 1993. Structural style of Laramide basement-cored uplifts and associated folds. In: Snoke, A. W., Steidtmann, J. R., and Roberts, S. M. (Eds.), Geology of Wyoming. Geological Survey of Wyoming Memoir 5, pp. 312-371.

Brun, J.-P. and Nalpas, T., 1996. Graben inversion in nature and experiments. Tectonics 15, 677-687.

Buchanan, P. G. and McClay, K. R., 1991. Sandbox experiments of inverted listric and planar fault systems. Tectonophysics 188, 97-115.

Bump, A. P. and Davis, G. H., 2003. Late Cretaceous-early Tertiary Laramide deformation of the northern Colorado Plateau, Utah and Colorado. Journal of Structural Geology 25, 421-440.

Chapple, W. M. and Spang, J. S., 1974. Significance of layer-parallel slip during folding of layered sedimentary rocks. Geological Society of America Bulletin 85, 1523-1534.

Chester, F. M. and Logan, J. M., 1987. Composite planar fabric of gouge from the Punchbowl fault, California. Journal of Structural Geology 9, 621-634.

Dart, C. J., McClay, K. and Hollings, P. N., 1995. 3D analysis of nverted extensional fault systems, southern Bristol Channel basin, UK. In: Buchanan, J. G. and Buchanan, P. G. (Eds.), Basin Inversion. Geological Society Special Publication 88. Geological Society of London, pp. 393-413.

Davis, G. H., 1978. Monocline fold pattern of the Colorado Plateau. In: Matthews, V., III (Ed.), Laramide Folding Associated with Basement Block Faulting in the Western United States. Geological Society of America Memoir 151, pp. 215-233.

Dickinson, W. G., 1981. Plate tectonic evolution of the southern cordillera. Arizona Geological Society Digest 14, 113-135.

Donath, F. A. and Parker, R. B., 1964. Folds and folding. Geological Society of America Bulletin 75, 45-62.

Dutton, C. E., 1882. The Physical Geology of the Grand Canyon District. United States Geological Survey 2nd Annual Report, 49-166.

Eisenstadt, G. and Withjack, M. O., 1995. Estimating inversion: results from clay models. In: Buchanan, J. G. and Buchanan, P. G. (Eds.), Basin Inversion. Geological Society Special Publication 88. Geological Society of London, pp. 119-136.

Elston, D. P, 1989. Middle and Late Proterozoic Grand Canyon Supergroup, Arizona. In: Elston, D. P., Billingsley, G. H. and Young, R. A. (Eds.), Geology of the Grand Canyon, Northern Arizona. American Geophysical Union, pp. 94-105.

Elston, D. P. and McKee, E. H., 1982. Age and correlation of the late Proterozoic Grand Canyon disturbance, northern Arizona. Geological Society of America Bulletin 93, 681-699.

Ford, T. D. and Dehler, C. M., 2003. Grand Canyon Supergroup: Nankoweap Formation, Chuar Group, and Sixty Mile Formation. In: Beus, S. S. and Morales, M. (Eds.), Grand Canyon Geology 2nd Edition. Oxford University Press, pp. 53-75.

Gangi, A. F., Min, K. D. and Logan, J. M., 1977. Experimental folding of rocks under confining pressure: part IV – theroretical analysis of faulted drape folds. Tectonophysics 42, 227-260.

Gilbert. G. K, 1876. The Colorado Plateau Province as a field for geological study. American Journal of Science 12, 16-24 and 85-103.

Gutierrez-Alonso, G. and Gross, M. R., 1999. Structures and mechanisms associated with development of a fold in the Cantabrian Zone thrust belt, NW Spain. Journal of Structural Geology 21, 653-670.

Handin, J., 1969. On the Coulomb-Mohr Failure Criterion. Journal of Geophysical Research 74, 5343-5348.

Hendricks, J. D., 1989. Petrology and chemisty of igneous rocks of middle Proterozoic Unkar Group, Grand Canyon Supergroup, northern Arizona. In: Elston, D. P., Billingsley, G. H. and Young, R. A. (Eds.), Geology of the Grand Canyon, Northern Arizona. American Geophysical Union, pp. 106-116.

Hendricks, J. D. and Stevenson, G. M., 2003. Grand Canyon Supergroup: Unkar Group. In: Beus, S. S. and Morales, M. (Eds.), Grand Canyon Geology 2nd Edition. Oxford University Press, pp. 39-52.

Holdsworth, R. E., Butler, C. A. and Roberts, A. M., 1997. The recognition of reactivation during continental deformation. Journal of the Geological Society 154, 73-78.

Huntoon, P. W., 2003. Post-Precambrian tectonism in the Grand Canyon region. In: Beus, S. S. and Morales, M. (Eds), Grand Canyon Geology 2nd Edition. Oxford University Press, pp. 222-259.

Huntoon, P. W., 1993. Influence of inherited Precambrian basement structure on the localization and form of Laramide monoclines, Grand Canyon, Arizona. In: Schmidt, C. J., Chase, R. B., and Erslev, E. A. (Eds.), Laramide Basement Deformation in the Rocky Mountain Foreland of the Western United States. Geological Society of America Special Paper 280, pp. 243-256.

Huntoon, P. W., 1981.  Grand Canyon monoclines, vertical uplift or horizontal compression? Contribution to Geology 19, 127-134.

Jaeger, J. C. and Cook, N. G. W., 1976.  Fundamentals of Rock Mechanics. Halted Press, New York.

Karlstrom, K. E., Ilg, B. R., Williams, M. L., Hawkins, D. P., Bowring, S. A. and Seaman, S. J., 2003.  Paleoproterozoic rocks of the granite gorges. In: Beus, S. S. and Morales, M. (Eds.), Grand Canyon Geology 2nd Edition. Oxford University Press, pp. 9-38.

Keller, J. V. A. and McClay, K. R., 1995.  3D sandbox models of positive inversion. In: Buchanan, J. G. and Buchanan, P. G. (Eds.), Basin Inversion. Geological Society Special Publication 88, Geological Society of London, pp. 137-146.

Kelly, V. C., 1955a.  Monoclines of the Colorado Plateau. Geological Society of America Bulletin 66, 789-804.

Kelly, V. C., 1955b.  Regional tectonics of the Colorado Plateau and relationship to the origin and distribution of uranium. University of New Mexico Publications in Geology 5.

Koopman, A., Speksnijder, A. and Horsfield, W. T., 1987.  Sandbox model studies of inversion tectonics. Tectonophysics 137, 379-388.

Kuhle, N. J., 2001. Effects of burial history, rock ductility and recovery magnitude on inversion of normal faulted strata. M. S. Thesis (*Unpublished*), Texas A&M University.

Logan, J. L., Friedman, M. and Stearns, M. T., 1978.  Experimental folding of rocks under confining pressure: part VI – further studies of faulted drape folds. In: Matthews, V., III (Ed.), Laramide folding associated with basement block faulting the Western United States. Geological Society of America Memoir 151, 235-271.

Lowell, J. D., 1995. Mechanics of basin inversion from worldwide examples. In: Buchanan, J. G. and Buchanan, P. G. (Eds.), Basin Inversion. Geological Society Special Publication 88, Geological Society of London, pp. 137-146.

Lucchitta, I., 1974.  Structural evolution of northwest Arizona and its relation to adjacent Basin and Range province structures. In: Eastwood, R. L. et al. (Eds.), Geology of northern Arizona, Part I. Northern Arizona University, pp. 336-354.

Marshak, S., Karlstrom, K. and Timmons, J. M., 2000. Inversion of Proterozoic extensional faults: an explanation for the pattern of Laramide and Ancestral Rockies intracratonic deformation, United States. Geology 28, 735-738.

Martel, S. J., Pollard, D. D. and Segall, P., 1988. Development of simple strike-slip fault zones, Mount Abbot Quadrangle, Sierra Nevada, California. Geological Society of America Bulletin 100, 1451-1465.

Maxson, J. H. and Campbell, I., 1933. Faulting in Bright Angel, Arizona. Pan-American Geologist 59, 303-304.

McClay, K. R., 1995. The geometries and kinematics of inverted fault systems: a review of analogue model studies. In: Buchanan, J. G. and Buchanan, P. G. (Eds.), Basin Inversion. Geological Society Special Publication 88, Geological Society of London, pp. 137-146.

Middleton, L. T. and Elliott, D. K., 2003. Tonto Group. In: Beus, S. S. and Morales, M. (Eds.), Grand Canyon Geology 2nd Edition. Oxford University Press, pp. 90-106.

Mitra, S., 1993. Geometry and kinematic evolution of inversion structures. American Association of Petroleum Geologists Bulletin 77, 1159-1191.

Mitra, S. and Islam, Q. T., 1994. Experimental (clay) models of inversion structures. Tectonophysics 230, 211-222.

Nemcok, M., Gayer, R. and Miliorizos, M., 1995. Structural analysis of the inverted Bristol Channel Basin: implications for the geometry an timing of fracture porosity. In: Buchanan, J. G. and Buchanan, P. G. (Eds.), Basin Inversion. Geological Society Special Publication 88, Geological Society of London, pp. 37-146.

Noble, L. F., 1914. The Shinumo quadrangle, Grand Canyon district, Arizona. U. S. Geological Survey Bulletin 549, 1-96.

Patton, T. L. and Fletcher, R. C., 1995. Mathematical block-motion model for deformation of a layer above a buried fault of arbitrary dip and sense of slip. Journal of Structural Geology 17, 1455-1472.

Powell, J. W., 1873. Some remarks on the geological structure of a district of country lying to the north of the Grand Canyon of the Colorado. American Journal of Science 5, 456-465.

Ramsay, J. G., 1967.  Folding and Fracturing of Rocks. McGraw Hill, New York.

Reches, Z., 1978.  Development of Monoclines: Part I. Structure of the Palisades Creek branch of the East Kaibab monocline, Grand Canyon, Arizona. In: Matthews, V., III (Ed.), Laramide Folding Associated with Basement Block Faulting in the Western United States. Geological Society of America Memoir 151, 273-311.

Sassi, W., Colletta, B., Bale, P., and Paquereau, T., 1993.  Modelling of structural complexity in sedimentary basins: the role of pre-existing faults in thrust tectonics. Tectonophysics 226, 97-112.

Sears, J. W., 1973.  Structural geology of the Precambrian Grand Canyon series, Arizona. Ph. D. Dissertation (*Unpublished*), University of Wyoming.

Segall, P. and Pollard, D. D., 1983.  Nucleation and growth of strike-slip faults in granite. Journal of Geophysical Research 88, 555-568.

Shoemaker, E. M., Squires, R. L. and Abrams, M. J., 1974.  The Bright Angel and Mesa Butte fault systems of northern Arizona. In: Easterwood et al. (Eds.), Geology of Northern Arizona Part I – Regional Studies. Northern Arizona University, pp. 355-391.

Sibson, R. H., 1990.  Rupture nucleation on unfavorably oriented faults. Bulletin of the Seismological Society of America 80, 1580-1604.

Sibson, R. H., 1985.  A note on fault reactivation. Journal of Structural Geology 7, 751-754.

Silliphant, L. J., Engelder, T. and Gross, M. R., 2002.  The state of stress in the limb of the Split Mountain anticline, Utah: constraints placed by transected joints. Journal of Structural Geology 24, 155-172.

Stearns, D. W., 1978.  Fault and forced folding in the Rocky Mountains foreland. In: Matthews, V., III (Ed.), Laramide Folding Associated with Basement Block Faulting in the Western United States, Geological Society of America Memoir 151, 1-38.

Stevenson, G. M. and Beus, S. S., 1982.  Stratigraphy and depositional setting of the upper Precambrian Dox Formation in the Grand Canyon. Geological Society of Americal Bulletin 93, 163-173.

Stone, D. S., 1993.  Basement-involved thrust-generated folds as seismically imaged in the subsurface of the central Rocky Mountain foreland. In: Schmidt, C. J., Chase, R. B., and Erslev, E. A. (Eds.), Laramide Basement Deformation in the Rocky Mountain Foreland of the Western United States. Geological Society of America Special Paper 280, 271-318.

Tanner, P. W. G., 1989.  The flexural-slip mechanism. Journal of Structural Geology 11, 635-655.

Timmons, J. M., Karlstrom, K. E. and Sears, J. W., 2003. Geologic structure of the Grand Canyon Supergroup. In: Beus, S. S. and Morales, M. (Eds.), Grand Canyon Geology 2nd Edition, Oxford University Press, pp.

Timmons, J. M., Karlstrom, K. E., Dehler, M., Geissman, J. W. and Heizler, M. T., 2001. Proterozoic multistage (ca. 1.1 and 0.8 Ga) extension recorded in the Grand Canyon Supergroup and establishment of northwest- and north-trending tectonic grains in the southwestern United States. Geological Society of America Bulletin 113, 163-180.

Tindall, S. E. and Davis, G. H., 1999.  Monocline development by oblique-slip fault-propagation folding: the East Kaibab monocline, Colorado Plateau, Utah. Journal of Structural Geology 21, 1303-1320.

Turner, J. P. and Williams, G. A., 2004.  Sedimentary basin inversion and intra-plate shortening. Earth-Science Reviews 65, 277-304.

Walcott, C. D., 1889.  Study of a line of displacement in the Grand Cañon of the Colorado, in northern Arizona. Geological Society of America Bulletin 1, 49-64.

Wilkins, S. J., Gross, M. R., Wacker, M., Eyal, Y. and Engelder, T., 2001.  Faulted joints: kinematics, displacement-length scaling relations and criteria for their identification.  Journal of Structural Geology 23, 315-327.

# VITA

Name:          James Cory Orofino

Date of Birth:  21 April 1978

Education:      M.S., Geology, Texas A&M University, 2005

               B.A., Physics, The Colorado College, 2000

Address:       2107 SW 86 Terrace, Gainesville, FL 32607
               Tel.: (352) 332-3098